ELECTRONIC PROPERTIES OF NOBLE METALS AND SOME FCC TRANSITION METALS

A THESIS

submitted in fulfilment of the
requirements for the award of the degree
of
DOCTOR OF PHILOSOPHY
in
PHYSICS

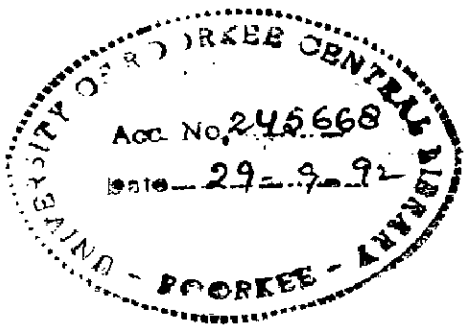

By

RAJEEV AHUJA

DEPARTMENT OF PHYSICS
UNIVERSITY OF ROORKEE
ROORKEE-247 667 (INDIA)

AUGUST, 1991

To

My

Parents

CANDIDATE'S DECLARATION

I hereby certify that the work which is being presented in the thesis entitled **"ELECTRONIC PROPERTIES OF NOBLE METALS AND SOME FCC TRANSITION METALS"** in fulfilment of the requirement for the award of the Degree of Doctor of Philosophy submitted in the Department of **PHYSICS** of the University is an authentic record of my own work carried out during a period from **APRIL 1987 to AUGUST 1991** under the supervision of **Dr. S. AULUCK.**

The matter embodied in this thesis has not been submitted by me for the award of any other Degree.

RAhja

(RAJEEV AHUJA)
Candidate's Signature

This is to certify that the above statement made by the candidate is correct to the best of my knowledge.

S. Auluck

(S. AULUCK)
Signature of Supervisor

Date : August 22, 1991

The Ph.D. Viva-Voce examination of **Shri RAJEEV AHUJA,** Research Scholar, has been held on 8/12/91

S. Auluck

Signature of Guide

8/12/91.

Signature of External Examiner(s)

In this thesis, an attempt has been made to study the electronic properties of noble metals and some fcc transition metals. During the past two decades the techniques for solving the band structure problems have reached a point where, with the aid of large computers, an accurate solution may be obtained. In this work we use the linear-muffin-tin-orbital (LMTO) method in the atomic sphere approximation (ASA) to solve the band structure problem. The variational principle for a one-electron Hamiltonian is used and the trial function is a linear combination of energy independent muffin-tin orbitals (MTO). The secular equation reduces to an eigen value equation . The trial function is defined with respect to a muffin-tin (MT) potential and the energy bands depend on the potential inside the spheres through potential parameters which describe the energy dependence of the logarithmic derivatives. The energy independent MTO is the linear combination which matches on the solution of the Laplace equation in the interstitial region and is regular at infinity. The LMTO method is particularly suited for closely packed structure and it combines the desirable features of the Korringa Kohn Rostoker (KKR), linear combination of atomic orbitals (LCAO) and Cellular methods. The secular matrix is linear in energy, the overlap integrals factorise as potential parameters and structure constants, the later are canonical in the sense that they neither depend on energy nor on the cell volume and they specify the boundary conditions on a single MT or atomic sphere in the most convenient way. This method is very well suited for

self-consistent calculations. In this thesis we are interested in the Fermi surface (FS - a ground state property) of metals which can be calculated within the density functional formalism. This requires that we perform self-consistent electronic struture calculations. The electron density can be utilised as a central quantity and the formulation of a many-particle problem into a single-particle like frame work, is the essence of the density functional theory (DFT). Starting from the Thomas-Fermi method and several modifications, the DFT has been rejuvenated by the pioneering works of Hohenberg, Kohn and Sham who have laid its strict mathematical foundation and thus provided a formal justification for the use of density as a basic quantity. In the DFT, the problem faced is that exchange and correlation energy function can only be approximated. Hence to overcome this problem, we have used the local density approximation (LDA) for exchange-correlation (XC) which is valid when the density varies slowly in space. To check the effect of exchange and correlation potential on our problem, we have used different XC potentials such as von Barth-Hedin (BH), Barth-Hedin modified by Janak (BHJ), Vosko-Wilk and Nussair (VWN) and Slater $X\alpha$. approximated by different workers. We have also included a nonlocal-XC potential in LDA given by Langreth and Mehl.

There are a number of powerful experimental methods for measuring the FS. These methods include de Haas-van Alphen (dHvA), cyclotron resonance, magneto-resistance etc. The dHvA effect has proved to be most accurate and reliable tool for probing the electronic struture near the fermi energy. There exists voluminous data on FS and cyclotron masses. We have

compared our results with these data. Hence in the first chapter we review briefly the LMTO theory, DFT as well as some of the experimental methods for measuring FS.

Chapter 2 is devoted to the FS of noble metals. The main reason for choosing the noble metals is that their FS is easy to study as it consists of single sheet and has already been studied experimentally and theoretically in great detail so that a study of these metals can be used to debug the programs. Another reason for choosing these metals is that spin-orbit effects vary from negligible to predominent as we move from copper (Cu) to gold (Au). We have calculated extremal areas for four orbits in the noble metals and studied the effect of (i) various XC potentials (ii) increasing the number of $\vec{k}$ points in the Brillouin-zone (BZ) summations (iii) including angular momentum expansion up to ℓ=3 and (iv) inclusion of relativistic effects. We observe that in the case of noble metals the choice of XC potential plays an important role while the other effects are not significant. Here we have adopted a different criterion to determine the agreement between the computed FS extremal areas and the experimentally measured areas. This is done by calculating the shift in the Fermi energy ΔE_F required to bring the calculated FS area in agreement with the experiment. Our results show that in case of copper and silver the extreme ΔE_F is 4.1 and 0.9 mRyd, respectively, with the Slater Xα (α=0.77) XC potential while for gold ΔE_F is around 3.5 mRyd with Slater Xα (α=0.693) XC potential. Here α has been treated as an adjustable parameter and the values reported are for the best agreement with the experimental data.

The success with which the LMTO method gives the FS topology of noble metals prompted us to perform similar calculations for the transition metals palladium and platinum. These metals possess a complicated FS and we believe that the accuracy with which the LMTO method can give FS topologies will be born out by our results. Interest in palladium and platinum has kept alive because of their fascinating electronic properties such as high density of states, large paramagnetic susceptibilities with unique temperature dependence, alloying, catalysis etc. The FS of palladium consists of four sheets i.e. a closed electronic surface centred at Γ, a sheet of hole centred at X, an open hole surface and a sheet of L pocket hole. However platinum has only the first three sheets and has no L pocket hole. The study of palladium and platinum also involves the study of same effects as we have studied for noble metals. We observe that in case of palladium and platinum the relativistic effects play important role while these effects are found to be negligible in noble metals. Similar to the case of the noble metals, the increase of number of $\vec{k}$ points and including angular momentum expansion up to ℓ=3 does not affect FS areas for palladium but in case of platinum these effects are significant. The results of this phase of investigation are compiled in chapter 3. We found that the inclusion of relativistic effects, in case of palladium and platinum, brings forth a dramatic improvement in results. The ΔE_F reduces to 4.0 mRyd with Slater Xα (α=0.75) for palladium and 2.7 mRyd for platinum with Slater Xα (α=0.815) XC potential from ΔE_F of 16.0 and 40.0 mRyd, respectively.

The many-body interactions (such as electron-electron, electron-phonon and electron-paramagnon) renormalise the dynamic properties of bare electrons. We have calculated the enhancement factor λ (λ=0 in absence of many-body interactions) and Fermi velocities for these metals. These are compared with other theoretical results.

All the metals discussed so far are paramagnetic. As an example of a ferromagnetic metal, we have chosen nickel because here the effect of exchange interaction and spin-orbit interaction has to be included. In chapter 4 , we have discussed FS of nickel. We have calculated various FS orbit areas for magnetic field along [001], [110] and [111] directions. We have calculated ΔE_F with different XC potentials,. Our results for nickel are in agreement with the experiment and other theoretical results.

The interpretation of pressure effects on both, electron transport and crystallographic properties of metals, usually requires some knowledge of the way in which the FS is affected by pressure. We have studied the effect of hydrostatic pressure on the FS of noble metals, palladium, platinum and nickel. The effect of pressure on the FS provides a valuable check on the reliability of band-structure calculations. We have calculated pressure derivatives of extremal areas [d(lnA)/dP] by performing self- consistent band-structure calculations at two different radii. Our results are compared with the experimental results. Thus chapter 5 is devoted to the effect of hydrostatic pressure on the FS.

The effect of uniaxial strain on the FS is discussed in chapter 6. When a metal is strained, the electron energy-bands shift by amount ΔE which depends on the tensor component of strain ϵ as well as the electron wave vector $\vec{k}$. As a result the fermi surface of a strained metal will differ slightly from that of the unstrained. Accurate prediction of the difference is a severe test of an energy band calculation. We have applied the uniaxial tension along [001] and [111] directions in case of noble metals and dependence of FS extremal cross-section areas $[d(\ln A)/d(\ln A_s)]$ is calculated. Our results are consistent with the results obtained by other workers.

The seventh chapter provides the summary and concluding remarks about the present work reported in earlier chapters.

ACKNOWLEDGMENTS

I wish to express my deepfelt gratitude to my research supervisor Dr. S. Arluck for his impeccable guidance, invaluable suggestions, keen interest and constant encouragement throughout the course of the present study.

I gratefully acknowledge the help and co-operation rendered by Dr. T. Nautiyal to facilitate the smooth progress of this work. I offer my special and sincere thanks to Drs. K. S. Baliyan and Kiran Jain for their kind help in reading and checking manuscript. They were always available readily for any type of help and advice.

I am thankful to Prof. M.K. Srivastava and Prof. S.N. Gupta for providing me all the facilities in the department to carryout this work.

The financial support from University Grants Commission and Council of Scientific and Industrial Research are thankfully acknowledged.

My grateful thanks are due to my parents and brother who inspired me to go in for higher studies and research. Behind every study there stands a myraid of people whose help and contribution make it successful. Since such a list will be prohibitively long, I may be excused for important omissions.

Rajeev Ahuja

CHAPTER PAGE

CHAPTER I

THE LINEAR MUFFIN-TIN ORBITAL METHOD, DENSITY FUNCTIONAL THEORY, EXCHANGE-CORRELATION POTENTIALS, FERMI SURFACE EXPERIMENTS AND CALCULATION OF FERMI SURFACE

1.1 *INTRODUCTION*

It is impossible to understand the behaviour of metal semiconductor, or insulator without a good knowledge of its electronic band structure. The properties of matter under normal conditions are governed by the behaviour of electrons that are moving around the heavier nuclei. The stationary states of a system of electrons moving in the mean electrostatic field of the electrons themselves and nuclei can be revealed by electronic structure calculations.

A field such as this has its own history and its own philosophies. To many of its practitioners, the calculation of band structure is a problem of computational technique. It is simply a matter of finding a workable procedure that will generate solutions of the equations to any desired degree of numerical accuracy. The determination of electronic band structure came to be regarded as an art, where one tried to build up a model of the energy surface represented by some parameters but consistent both with experiment and with some rough algebraic approximation to the solution of the Schrodinger equation. The success of this procedure has revolutionized the whole theory of metals in recent years. To make further progress, however, it was essential to combine technique and art into a science. So, we have learned to treat this problem as one where algebric

analysis, numerical computation, and physical intuition all have their part.

Energy levels in atoms are discrete and they are designated by orbital and spin quantum numbers. A particular energy level of an atom becomes N-fold degenerate for a system of N atoms, each atom being isolated from the others. When these atoms are brought closer together to form a solid, the degeneracy is split and N levels spread into a band. One electron states in a solid are called Bloch states. The direct computation of these, or their investigation by inference from experiment, is therefore one of major industries of solid state physics. Each Bloch state is identified by two quantum numbers, a band index indicating the band the state belongs to and a wave vector representing its crystal momentum. There are many methods to calculate the energy bands of solids. Among the different methods, the linear methods which have been used for over ten years, are often more trickey to setup and to use but they treat uranium as well as sodium. They can be more accurate and need smaller basis sets. These methods are computationally very fast and hence are widely preferred.

1.1.1 Band Structure Methods :

The electronic structure problem is solved within two approximations :

1. The Born-Oppenheimer approximation.
2. The one electron approximation.

The band structure problem is many body problem. In order to solve this we have to resort to numerous approximations of which the first is the Born-Oppenheimer approximation [38] in

which the motion of electrons is assumed to be independent of the motion of nuclei. This reduces the problem to that of an interacting electron system in the potential field of nuclei for a particular configuration of them. Next comes the one-electron approximation [173] which allows us to reduce the problem to that of an independent electron moving in an effective crystal potential- an average perodic potential due to all other electrons and nuclei. The continual development and advent of fast electronic computers have provided us with the capability of solving the one-electron Schrodinger equation to any accuracy we desire. Thus the problem ultimately boils down to the construction of an effective one-electron crystal potential. So in this picture one has to solve the one electron Schrodingr equation.

$$[-\nabla^2 + V(r)]\,\psi_{jk}(r) = E_{jk}\,\psi_{jk}(r) \qquad (1.1)$$

where V(r) is total mean field, in order to find the one electron energies E_{jk} and wave function $\psi_{jk}(r)$. For a supposed total field V(r) one solves the Schrodinger equation and the electronic charge density is constructed as

$$n(r) = \sum_{j,k}^{occ} |\psi_{jk}(r)|^2 \qquad (1.2)$$

and then a new field is constructed by solving Poisson's equation

$$\nabla^2 u(r) = -8\pi\, n(r) \qquad (1.3)$$

for the electronic contribution u(r), to which is added the field from the nuclear point charges and exchange-correlation corrections. With a weighted average of new and old fields, the calculation is repeated and cycle iterated until the two fields

are consistent. When self consistently has been reached the potential and total electronic energy of the electrons and nuclei are obtained in the Born-Oppenheimer approximation.

Before presenting the LMTO method, let us briefly review how the energy band-problem has been tackled in the past. In this context we note that traditional methods may be divided into two categories depending whether they use wave function expansions in some set of fixed basic function like atomic orbitals, Gaussians and plane waves or they expand the wave functions in a set of energy and potential dependent partial waves as done in the Korringa-Kohn-Rostoker (KKR) and the Augmented plane wave (APW) methods. The KKR and APW methods require a computational effort which, despite recent attempts to improve the efficiency, is barely feasible in truely self-consistent calculations. This is particularly so in the calculation of ground state proporties of compounds and magnetic crystals, where self-consistency is imperative and in the calculation of excitation spectra, where matrix elements are needed. The linear combination of atomic orbitals method, when used as a first principle method, is cumbersome and when parametrised, it has either too many parameters or the wave functions are ill defined. The linear combination of Gaussian orbitals (LCGO) has some computational advantage but it needs at least twice as many basic functions as, say, the KKR method. The modern first-principles peeudopotential method meets the requirements but it is limited to treating the sp-like valence and conduction electrons. Computationally this can be remedied by the addition of localized orbitals to the plane wave basis set. But such a hybrid scheme is neither elegant

nor in accordance with the chemical and physical intuition based upon the smooth trends observed through the perodic table. It is necessary to use the self-consistent methods for computing one-electron eigen values and eigen states with speed and accuracy. The so called linear methods of band theory satisfy the requirements rather well. This is true for the Linear Muffin Tin Orbital(LMTO) method [11, 12, 13, 196]. This method is linearized version of the Korringa-Kohn-Rostoker(KKR) method. Almost identical with the solid state LMTO method is the augment-spherical wave (ASW)method of Williams, Kubler and Gelatt [241]. In later years the LMTO method has been extended to treat impurities in the crystal with the Green's function technique by Koeing et al [130] and by Gunnarsson et al [93] and it has been used for both metal and semiconductor hosts. Recently Harris [100], Casula and Herman [49] and Springborg et al [208, 209] have developed the LMTO for clusters and molecules. For plane, crystal line surfaces thin-film LMTO techniques have been devised by Fujiwara [85] and by Fernondo et al [80]. It was recently dicovered that the conventional solid state LMTO basis set can be transformed exactly into orthogonal [14, 15] tight-binding (TB) [16] and minimal [135] basis-sets and this simplifies and generalizes the solid-state LMTO method considerably. This chapter describes the formalism of the LMTO method. Density functional theory as well as some of the experimental methods of measuring Fermi surface.

1.1.2 The LMTO Method :

The basic problem of the band theory is to obtain one-electron energies and wave functions by solving the

Schrodinger equation. So in this picture the energy band problem may be separated into two parts : one which depends on the one electron potential and atomic volume, and the other which depends on the crystal symmetry. It is therefore natural first to study the one-electron states in a single sphere, then to place such spheres on a regular lattice and establish the boundry conditions which follow from the crystal symmetry, and finally to introduce the approximations leading to the LMTO method. To solve the one-electron problem, one has to construct a crystal potential. Let us consider a crystal with one atom per primitive cell. Let us approximate the crystal potential V(r) by a muffin-tin potential which is spherically symmetric within the sphere of radius say S_{MT} centred at the atom and to have a constant value V_{MTZ} outside the sphere, i.e. in the interstitial region between the spheres. V_{MTZ} is known as muffin tin zero. This kind of potential is designed to facilitate matching of wave functions from the cell to cell through the assumption that the electron propagates freely between spheres with a constant wave number $\kappa = \sqrt{E - V_{MTZ}}$. The justification behind this is that the wave length $2\pi/\kappa$ is large when compared with the thickness of interstitial region. Since in most applications we are interested only in those electrons which barely move from cell to cell, the kinetic energy κ^2 that is at the level of the potential in the interstitial region between the atoms, ± 1/2 Rydberg, and, hence, 1 to 2 Ryd below the vaccum level.

Let us, for simplicity, consider one atom per primitive cell and within a single muffin-tin well (Fig.1.1) we define the potential as

$$V_{MT}(r) = \begin{cases} V(r) - V_{MTZ} & r \leq S_{MT} \\ 0 & r \geq S_{MT} \end{cases} \qquad (1.4)$$

so the hamiltonian for the muffin tin wells

$$H = -\nabla^2 + V_{MT}(r) \qquad (1.5)$$

and the energy of this system

$$E = \kappa^2 + V_{MTZ}(r) \qquad (1.6)$$

so we can write

$$H - E = -\nabla^2 + \sum_{R} V_{MT}(|r - R|) - \kappa^2 \qquad (1.7)$$

where sum extends over the crystal. We now seek the solution of the Schrodinger equation

$$\left[-\nabla^2 + V_{MT}(r) - \kappa^2\right] \psi_L(E,r) = 0 \qquad (1.8)$$

for all values of κ^2, for an electron moving in the potential from an isolated muffin tin well embedded in the flat potential V_{MTZ}. In this case, the spherical symmetry spreads throughout and the wave functions are

$$\psi_L(E,r) = i^{\ell} Y_{\ell}^{m}(\hat{r})\ \psi_{\ell}(E,r) \qquad (1.9)$$

where L denotes the quantum numnber ℓ and m, i^{ℓ}, is a phase factor and $Y_{\ell}^{m}(\hat{r})$ is a spherical harmonic. Inside the MT sphere and radial part $\psi_{\ell}(E,r)$ has to be regular at the origin in order to be normalisable. It is obtained by numerical integration of radial Schrodinger equation i.e.,

$$\left[-\frac{d^2}{dr^2} + \frac{\ell(\ell+1)}{r^2} + V(r) - E\right] r\psi(E,r) = 0 \qquad (1.10)$$

for muffin tin potential it should be

$$\left[- \frac{d^2}{dr^2} + \frac{\ell(\ell + 1)}{r^2} + V_{MT}(r) - \kappa^2 \right] r\psi_\ell(E,r) = 0 \qquad (1.11)$$

In the region of constant potential the solutions of (1.8) are spherical waves with wave number κ, and they satisfy (1.11) with

$$\left[- \frac{d^2}{dr^2} + \frac{\ell(\ell + 1)}{r^2} - \kappa^2 \right] r y_\ell(\kappa r) = 0 \qquad (1.12)$$

This is well-known Helmholtz wave equationm. We may take the two linearly independent solutions to be the sperical Bessel function i.e. $j_\ell(\kappa r)$ and Neumann $n_\ell(\kappa r)$ function. i.e. $j_\ell(\kappa r)$ is regular at origin as well as infinity while $n_\ell(\kappa r)$ is regular at infinity. In the small κr limits

$$\left.\begin{aligned} j_\ell(\kappa r) &\longrightarrow (\kappa r)^\ell/(2\ell + 1)!! \\ n_\ell(\kappa r) &\longrightarrow -(2\ell - 1)!!/(\kappa r) \end{aligned}\right\} \quad \kappa r \longrightarrow 0 \qquad (1.13)$$

where the double factorial is defined by $!! = 1\cdot3\cdot5\cdot$ and $-1!! = 1$. The asymptotic forms are

$$\left.\begin{aligned} j_\ell(\kappa r) &\longrightarrow \frac{\sin(\kappa r - \ell\pi/2)}{\kappa r} \\ n_\ell(\kappa r) &\longrightarrow \frac{\cos(\kappa r - \ell\pi/2)}{\kappa r} \end{aligned}\right\} \quad \kappa r \longrightarrow \infty \qquad (1.14)$$

1.1.3 Muffin Tin Orbitals :

The muffin tin orbitals (MTO) constitute a popular and efficient basis set first principles electronic structure calculations in solids. Its advantages are the following : 1. It is applicable to atoms from any part of the periodic table. 2. It is minimal in the sense that per site only one s-orbital, three p-orbitals, five d-orbitals and seven f-orbitals are needed.3. The linear MTOs which constitute an energy independent set are

correct to first order in energy. 4. The set is complete for the MT potential used for its generation but is not restricted to treating MT potentials alone. 5. The MTOs may be expand about other sites in terms of numerically evaluated radial functions, spherical harmonics and cononical structure constants. This together with the atomic sphere approximation (ASA), according to which the MT spheres are replaced by overlapping (space filling) Wigner Seitz (WS) spheres, leads to a factorization of matrix elements of nearly an operator into a product of structure constants and radial integrals. 6. The MTOs are automatically orthogonal to the core states.

To obtain the MTO we start from the wave function

$$\psi_L(E,\kappa,r) = i^{\ell} Y_\ell^m(\hat{r}) \begin{cases} \psi_\ell(E,r) + \kappa \cot(n_\ell) j_\ell(\kappa r) & r \le S_{MT} \\ \kappa\, n_\ell(\kappa r) & r \ge S_{MT} \end{cases} \quad (1.15)$$

where $\psi_L(E,\kappa,r)$ is the solution of (1.8) at energy E in the entire space and the constant of integration $\cot(n_\ell)$ is obtained by applying the boundary condition that the function should be continuous and differentiable at the sphere boundary $r=S_{MT}$. This requires that

$$\cot(n_\ell(E,\kappa)) = \frac{n_\ell(\kappa r)}{j_\ell(\kappa r)} \cdot \left. \frac{D_\ell(E) - \kappa r n'_\ell(\kappa r)/n_\ell(\kappa r)}{D_\ell(E) - \kappa r j'_\ell(\kappa r)/j_\ell(\kappa r)} \right|_{r=S_{MT}} \quad (1.16)$$

where the logorithmic derivative $D_\ell(E)$ is defined as

$$D_\ell(E) = \frac{S}{\psi_\ell(E,S)} \left. \frac{\partial \psi_\ell(E,r)}{\partial r} \right|_{r=S} \quad (1.17)$$

This is monotonically decreasing function of energy except at its

singularities. The other function of energy known as potential function depends only on the potential inside the atomic sphere, can be defined as

$$P_\ell(E) = 2(2\ell + 1)\,\frac{D_\ell(E) + \ell + 1}{D_\ell(E) - \ell} \qquad (1.18)$$

and it is an increasing function of energy and the two functions have the forms shown schematically in Fig 1.2. For each ℓ they consist of periods in energy labelled by the principal quantum number n, and separated by the energies $V_{n\ell}$ defind by (1.19) below. The advatage of working with $P_\ell(E)$ rather then $D_\ell(E)$ is that the poles of the former function are outside the range of the ℓ band.

The energies $V_{n\ell}$ separating the periods are defined by

$$D_\ell(V_{n\ell}) = 0 \qquad (1.19)$$

and, within each period, we further define the tree parameters B_ℓ, C_ℓ, and A_ℓ through

$$\begin{aligned} D_\ell(B_\ell) &= 0 \\ D_\ell(C_\ell) &= -\ell-1 \\ D_\ell(A_\ell) &= \infty\,. \end{aligned} \qquad (1.20)$$

So one may call the energies B_ℓ and A_ℓ the bottom and the top, respectively, of the ℓ band. Similarlarly the potential function evaluated at $D_\ell(C_\ell) = -\ell-1$ is zero lead us to call C_ℓ the centre of ℓ band. It may be shown that the energy derivatives $\dot{D}$ and $\dot{P}$ are related to the amplitudes of the MTOs at the sphere boundary.

The important feature of the orbital (1.15) is that the functions inside the well are regular at the origin, while the tail $\kappa n_\ell(\kappa r)$ is regular at infinity. If we approximate the

crystal potential by an array of non-overlapping muffin-tin wells as in (1.7) may be used in conjunction with the tail-cancellation theorem to obtain so called KKR equations. These have the form which is given below and provide exact solutions for muffin-tin geometry.

$$\underline{M}(E)\cdot b = 0 \qquad (1.21)$$

Computationally, however, they are rather inefficient and it is therefore desirable to develop a method based upon the variationl principle and a fixed basis set, which leads to the computatinally efficient eigen value problem

$$(\underline{H} - E\underline{O})\cdot a = 0 \qquad (1.22)$$

1.1.4 Expansion Theorem for MTO Tails

One reason for choosing the tails of the MTO as solutions of the translationally invariant Helmholtz wave equation is the extremely simple expansion theorem

$$n_L(\kappa, r - R) = 4\pi \sum_{L'} \sum_{L''} C_{LL'L''}\, j_{L'}(\kappa, r - R')\, n^{*}_{L''}(\kappa, R - R') \qquad (1.23)$$

where

$$C_{LL'L''} = \int Y^{m}_{\ell}(\hat{\kappa})\, Y^{m'}_{\ell'}(\hat{\kappa})^{*}\, Y^{m''}_{\ell''}(\hat{\kappa})\, d\hat{\kappa} \qquad (1.24)$$

$$= \left(\frac{2\ell'' + 1}{4\pi}\right)^{1/2} c^{\ell''}(\ell' m'; \ell m) \qquad (1.25)$$

are the Gaunt coefficients. This expansion is valid inside the sphere centred at R' and passing through R, i.e. for $|r - R| < |R - R'|$. The coefficients $c^{\ell''}(\ell' m'; \ell m)$ are tabulated by Condon and Shortly [63].

The expansion theorm means that the tail of the muffin-tin orbital i.e a spherical Neumann function including the

angular part $i^{\ell}Y_{\ell}^{m}(\hat{r})$ as in (1.9), positioned at R may be expanded in terms of spherical Bessel functions centred at R'. The reason for the expansion is that the Neumann functions centred at R' are regular at the origin and therefore is expanded in the regular solutions of the wave equation only. Consequently, inside any muffin-tin sphere the tails from the others spheres will have the same functional form as the term proportional to $\cot(n_{\ell})$.

1.1.5 Basic Formalism :

In the LMTO method, attention is focussed upon an energy range centred around some energy E which we are free to choose to suit the problem at hand. For each value of ℓ we parametrize the energy dependence of the radial wave functions, its logarithrnic derivatives and potential functions.

So as radial basis functions, for each value of ℓ,

$$\phi_{\nu\ell}(r) = \phi_{\ell}(E_{\nu}, r) \tag{1.26}$$

and its energy derivative

$$\dot{\phi}_{\nu\ell}(r) = \left.\frac{\partial\phi_{\ell}(E_{\nu}, r)}{\partial E}\right|_{E_{\nu}} \tag{1.27}$$

where $\phi_{\ell}(E,r)$ = is the radial function normalised to unity in the sphere.

$$\phi_{\ell}(E,r) = \langle\psi_{\ell}^{2}(E,r)\rangle^{-1/2}\psi_{\ell}(E,r) \tag{1.28}$$

where the normalisation integral is

$$\langle\psi_{\ell}^{2}(E,r)\rangle = \int\psi_{\ell m}^{*}(E,r)\ \psi_{\ell m}(E,r)\ dr \tag{1.29}$$

using the well known normalisation of spherical harmonic

$$\langle\psi_{\ell}^{2}(E,r)\rangle = \int_{0}^{s}\psi_{\ell}^{2}(E,r)\ r^{2}dr \tag{1.30}$$

Consequently, $\phi_{\nu\ell}(r)$ and $\dot{\phi}_{\nu\ell}(r)$ are orthogonal and it may be shown that they are both orthogonal to the core states. It can be shown that an accurate description of the logarithmic derivatives function D(E) and its inverse E(D) around a region $(D_{\nu\ell}, E_{\nu\ell})$ can be obtained trough four parameters $D_{\nu\ell}$, $\phi_{\nu\ell}$, $\dot{\phi}_{\nu\ell}$ and $\langle\dot{\phi}^2_{\nu\ell}\rangle$.

The corresponding radial logarithmic derivatives at the sphere boundry are

$$D_{\nu\ell} = S\phi'_{\nu\ell}(S)/\phi_{\nu\ell}(S) \tag{1.31}$$

$$D_{\dot{\nu}\ell} = S\dot{\phi}'_{\nu\ell}(S)/\dot{\phi}_{\nu\ell}(S) \tag{1.32}$$

where $' \equiv \frac{\partial}{\partial r}$

1.1.6 Potential parameters

For each value of ℓ quantum number, we use the four parameters $\omega(-\ell - 1)$, $S\phi^2(-\ell - 1)$, $\phi(-\ell - 1)/\phi(\ell)$ and $\langle\dot{\phi}^2\rangle^{-1/2}$, where

$$\omega(-) \equiv \omega(-\ell - 1)$$

$$S\phi^2(-) \equiv S\phi^2(-\ell - 1)$$

$$\phi(-)/\phi(+) \equiv \phi(-\ell - 1)/\phi(\ell) \tag{1.33}$$

here + and - refer to boundry conditions $D = \ell$ and $D = -\ell-1$, which are the logarithmic derivatives of the spherical Bessel and Neumann functions in atomic-sphere approximation (ASA). ASA is common label given by O.K. Andersen to the combination of essentially two approximations, one being that the kinetic energy κ^2 of the tail of the partial wave may be fixed independently of E, the other that the atomic polyhedron of Wigner and Seitz may be aproximated by an atomic sphere. In such a procedure the basic

unit in space is the atomic sphere which by construction has the same volume as the atomic polyhedron. The interstitial region vanishes and kinetic energy κ^2 consistent with (1.16) may be chosen. In the ASA we choose $\kappa^2=0$.

Since the logarithmic derivatives form the link between the atomic sphere potential and the crystal structure, so it is convenient to consider the radial functions which satisfy the boundray condition specified by the logrithmic derivatives.

A trial function of arbitrary logarithmic derivative D is therfore the linear combination

$$\Phi\ (D,\ r) = \phi_{\nu}(r) + \omega(D)\ \dot{\phi}_{\nu}(r) \qquad (1.34)$$

The influence of each sphere on the energy spectrum will then be given as a set of potential parameters (1.33) which are the parameters $\langle\dot{\phi}^2_{\nu\ell}\rangle$, plus the parameters of the energy function $\omega_{\ell}(D)$ and the amplitude functions $\phi_{\ell}(D,S)\equiv\phi_{\ell}(D)$. From equation (1.34)

$$\omega\ (D) = -\ \frac{\phi_{\nu}(r)}{\dot{\phi}_{\nu}(r)}\ \frac{D - D_{\nu}}{D - \dot{D}_{\nu}} \qquad (1.35)$$

Witin the basis (1.32) we obtain the expectational value of the Hamiltonian, i.e. the energy as

$$E_{\ell}(D) = E_{\nu\ell} + \omega_{\ell}(D)/\ [\ 1 + \langle\dot{\phi}^2_{\nu\ell}\rangle\ \omega^2_{\ell}(D)\ ]\ + 0\ (\varepsilon^3) \qquad (1.36)$$

The variational estimate is correct to the third order in $\varepsilon(E - E_{\nu})$. If the small parameter $\langle\dot{\phi}^2_{\nu\ell}\rangle$ is neglected and we get

$$E(D) = E_{\nu} + \omega_{\ell}(D) + 0\ (\varepsilon^2) \qquad (1.37)$$

These expressons are much more general and these are around the energy E_{ν} which may be chosen to suit the the particular problem at hand.

The first parameter $\omega_\ell(-)$, according to equation (1.35) represents the second order estimate of the position of the band centre relative to $E_{\nu\ell}$ i.e.

$$\hat{C}_\ell = E_{\nu\ell} + \omega_\ell(-) \tag{1.38}$$

Similarly, for the square-well pseudopotential

$$\hat{V}_\ell = E_{\nu\ell} + \omega_\ell(+) \tag{1.39}$$

The function $\omega(D)$ and $\phi(D)$ are thus related by

$$S\,\phi^2(D) = -\,d\omega/dD \tag{1.40}$$

The parameter $S\phi^2(-)$ is proportional to the bandwidth of the ℓ band.

$$\hat{W}_\ell = S\phi^2(-)\,\frac{(2\ell+1)^2}{\ell} \qquad \ell \neq 0 \tag{1.41}$$

$$\hat{W}_s = S\phi^2(-)\left[\frac{\phi(+)}{\phi(-)}\right]^2\left[\frac{\phi(+)}{\phi(-)} - 1\right]^{-1} \qquad \ell = 0 \tag{1.42}$$

If we evaluate the estimates (1.40), $\phi(-)/\phi(+) \simeq 0.8$ for free s electrons, we find that $\hat{W}_\ell = (6, 9, 13, 16) \times S\phi^2(-)$ for s, p, d, and f elecrons respectively. Hence the width of the ℓ band is of the order of $10\ S\phi^2(-)$.

The $\langle\dot{\phi}_\nu^2\rangle^{-1/2}$ determines the width of the energy window, i.e. the energy range over which the variational estimate (1.36) is valid. The variation expressons depends on the E_ν, which may be chosen to suit the particular problem. The enegy $E_{\nu\ell}$ around which the expansion is performed is taken to be the centre of gravity of the occupied part of ℓ band. Of other possible choices of $E_{\nu\ell}$, the choice $E_{\nu\ell} = C_\ell$ results in best overall energy bands, while $E_{\nu\ell} = E_F$ gives the correct Fermi surface and correct Fermi velocities.

To see the signifiance of $\phi(+)/\phi(-)$, without going into mathematice involved we find that

$$\omega(-) - \omega(+) = (2\ell + 1)\, S\phi(-)/\phi(+) \qquad (1.43)$$

this shows that $\phi(-)/\phi(+)$ governs the distortion contained in the scaling from canonical bands to energy bands.

The structure constant matrix $S^{k}_{\ell m\ \ell' m'}$ is hermition and can be transformed for the ℓm representation where the each subblock is diagonalised. The $(2\ell+1)$ digonal elements $S^{k}_{\ell i}$ if each subblock are the unhybridised or pure, canonical ℓ bands. The pure n_ℓ energy band $E_{n\ell i}(k)$ obtain by n'th solution of $P_\ell(E) = S^{k}_{\ell i}$, which is merely a monoatomic mapping of the canonical bands on to an energy scale specified by n'th branch of the potential function. The canonical bands have a number of properties such as (i) A pure canonical s band diverges at the centre of the Brillouin zone. (ii). The longitudinal branch of the canonical p band is discontinuous at the centre of the zone. (iii). The centre of gravity of a canonical band with $\ell > 0$ is zero at each value of the Bloch vector k. (iv). The width of a canonical band may be estimated from the second moment which depends only upon the radial destribution of the atoms in the crystal. (v). The second moment of the canonical s band diverges etc.

1.1.7 Energy Independent MTO

In this section we will discusse the energy independence of the MTO. The amplitude $\kappa n_\ell(\kappa S)$ and logarithmic derivative $\kappa S n'_\ell(\kappa S)/n_\ell(\kappa S)$ at the sphere, as well as its tail, depend on energy only through κ. If we fix κ at some suitable value, the

energy dependence of the tail would be suppressed and this make the amplitude and slope of the MTO at the sphere energy independent. So now we shall keep the energy E of the orbital and wave number κ of the tail as completly separate entities, fix κ and using linear combinations of MTOs in a variational procedure.

We shall now augment the MTO and show that the augmented MTO

$$\chi_L(E, \kappa, r) = i^{\ell} Y_\ell^m(\hat{r}) \begin{cases} \psi_\ell(E, r) + \kappa\cot(n_\ell) J_\ell(\kappa r) & r \leq S_{MT} \\ \kappa N_\ell(\kappa r) & r \geq S_{MT} \end{cases} \quad (1.44)$$

for a particular choice of the augmented spherical Bessel and Neumann function $J_\ell(\kappa r)$ and $N_\ell(\kappa r)$ may be made energy independent around a fixed energy E_ν to first order in $(E - E_\nu)$. At the same time, the muffin-tin orbital becomes orthogonal to core states, ensuring that the LMTO method does not converge to core eigenvalues. In connection with the augmentation one should realise that once κ has been fixed, the spherical Bessel and Neumann funtions lose their special significance as exact solutions of the Schrodinger equation in the region of constant potential. Hence, if desired, they may be replaced, i.e. augmented, by more appropriate functions which are attached to them at the sphere in a continuous and differentiable fashion.

To arrive at suitable definitions of J_ℓ and N_ℓ we simply disregard $\kappa^2 \equiv E - V_{MTZ}$, fix κ, and demand that the energy derivatives of the muffin-tin orbital (1.44)

$$\dot{\chi}_L(E, \kappa, r) = \dot{\psi}_\ell(E, r) + \kappa\dot{\cot}(n_\ell(E)) J_\ell(\kappa r) \quad (1.45)$$

be zero at $E = E_\nu$. Thus the augmented spherical Bessel function

$$J_\ell(\kappa r) = \begin{cases} -\dot{\psi}_\ell(E_\nu, r) \,/\, \kappa\dot{\cot}(n_\ell(E_\nu)) & r \le S_{MT} \\ j_\ell(\kappa r) & r \ge S_{MT} \end{cases} \qquad (1.46)$$

This will make the muffin-tin orbital (1.44) energy independent, i.e. $\dot{\chi}(E_\nu, \kappa, r) = 0$, to first order in $(E - E_\nu)$. The MTO (1.15) is continuous and differentiable, we get

$$n_\ell(\kappa r) = \psi_\ell(E, r) + \kappa\dot{\cot}(n_\ell(E))j_\ell(\kappa r) \qquad (1.47)$$

near the sphere boundary. Therefore

$$0 = \dot{\psi}_\ell(E_\nu, r) + \kappa\dot{\cot}(n_\ell(E_\nu))j_\ell(\kappa r) \qquad (1.48)$$

holds to first order in $(r - S_{MT})$, showing that (1.46) is continous and differentiable at $r = S_{MT}$. This result is a direct consequence of normalisation which is implied in definition (1.44) and which is characterised by an energy-independent amplitude $n(\kappa S_{MT})$ and an energy-independent logarithmic derivative $D\{n_\ell\}$ at the sphere.

From the defination of normalised partial wave ϕ (1.28) and the trial function Φ (1.34), the energy derivative $\dot{\psi}_\ell(E_\nu, r)$ is given by

$$\dot{\psi}_\ell(E_\nu, r) = \langle\dot{\psi}^2_\ell(E_\nu)\rangle^{1/2}\phi_{\nu\ell}(r) + \langle\psi^2_\ell(E_\nu)\rangle^{1/2}\dot{\phi}_{\nu\ell}(r) \qquad (1.49)$$

$$= \langle\dot{\psi}^2_\ell(E_\nu)\rangle^{1/2}\Phi(D\{\dot{\psi}_\ell\}, r) \qquad (1.50)$$

From eq.(1.48) we can see that $\dot{\psi}_\ell(E_\nu)$ and $j_\ell(\kappa r)$ will have the same logarithmic derivative at S_{MT} and consequently

$$\dot{\psi}_\ell(E_\nu, r) = \langle\dot{\psi}^2_\ell(E_\nu)\rangle^{1/2}\Phi(D\{j_\ell\}, r) \qquad (1.51)$$

In the same manner as in (1.23), we define that tail $N_\ell(\kappa r)$ as

$N_L(\kappa, r-R)$

$$= \begin{cases} 4\pi \sum_{L'} \sum_{L''} C_{LL'L''} J_{L'}(\kappa, r - R') \, n^{*}_{L''}(\kappa, R - R') & \begin{cases} |r - R| \le S_M \\ \forall\, R' \neq R \end{cases} \\ n_L(\kappa, r - R) & \text{otherwise} \end{cases} \tag{1.52}$$

$N_L(\kappa, r-R)$ is everywhere continuous and differentiable, furthermore orthogonal to the core states of all muffin-tin wells except that centred at R.

So the simplified MTO is

$$\chi_L(\kappa, r) = i^{\ell} Y^m_{\ell}(\hat{r}) \begin{cases} \dfrac{\kappa n_{\ell}(\kappa S)}{\Phi_{\ell}(D\{n_{\ell}\}, S)} \Phi_{\ell}(D\{n_{\ell}\}, r) & r \le S_{MT} \\ \\ \kappa N_{\ell}(\kappa r) & r \ge S_{MT} \end{cases} \tag{1.53}$$

and the augmented spherical bessel function by

$$J_{\ell}(\kappa r) \approx \begin{cases} \dfrac{j_{\ell}(\kappa S)}{\Phi(D\{j_{\ell}\}, S)} \Phi(D\{j_{\ell}\}, r) & r \le S_{MT} \\ \\ j_{\ell}(\kappa r) & r \ge S_{MT} \end{cases} \tag{1.54}$$

So we see that χ is linear combination of ϕ and $\dot{\phi}$ which has the logarithmic derivative D{n} and the augmented muffin-tin orbital is also continous and differentiable, and orthogonal to the core states of all muffin tins. Hence these orbitals are well suited for use in connecton with variational principle.

1.1.8 One-centre Expansion and Structure Constants

A wave function for a MT potential of non-overlapping array of MT wells, $V_{MT}(|r-R|)$, centred at sites R of a three-dimensional perodic lattice and embedded in a flat potential may be written as the linear combination of MTO's

$$\psi(E,r) = \sum_L \alpha_L^k \chi_L^k(E, \kappa, r) \tag{1.55}$$

where we introduced the Bloch sum of MTO's

$$\chi_L^k(E, \kappa, r) = \sum e^{ik\cdot R} \chi_L(E, \kappa, r-R) \tag{1.56}$$

It can be shown, using the expansion theorem (1.23) or (1.52) that the wave function may be written in terms of a one centre expansion of the form

$$\chi_L^k(E, \kappa, r) = \chi_L(E, \kappa, r) + \sum J_{L'}(\kappa, r) \mathcal{B}_{L',L}^k(\kappa) \tag{1.57}$$

where $\mathcal{B}_{L',L}^k$ is the KKR structure constant defind by

$$\mathcal{B}_{L',L}^k = 4\pi \sum_{R\neq 0} C_{LL'L''} \sum e^{ik\cdot R} \kappa n_{L''}^*(\kappa,R) \tag{1.58}$$

Equation (1.57) will converge inside the MT sphere at the origin and in the interstitial region, outside the neighbouring MT spheres but inside the sphere centred at the origin and passing through the nearest-neighbour sites. The region of convergence stated above follows from the fact that the expansion theorem (1.22) is valid iside the sphere passing through the nearest-neighbour sites while the tails are defind only oustide their own MT spheres. The structure constants are independent of the potential, and the matrix $\mathcal{B}_{\ell' m;\ell m}^k$ is Hermitian.

1.1.9 Secular Matrix

Use of the linear combination of muffin-tin orbitals in a variational method has the advantage that it leads directly to an

eigenvalue problem and it is possible to include non-muffin-tin perturbations to the potential. According to the Rayleigh-Ritz variational principle, one varies ψ to make the energy functional stationery i.e.

$$\delta\langle \psi|H - E|\psi \rangle = 0 \qquad (1.59)$$

Here E is the Lagrange multiplier. Eqation (1.59) has solutions when

$$\det \{\langle \chi^{k}_{L'}|H - E|\chi^{k}_{L''}\rangle\} = 0 \qquad (1.60)$$

using the Bloch condition (1.56) and rearrangement of the lattice sums we obtain

$$N^{-1}\langle \chi^{k}_{L'}|H - E|\chi^{k}_{L}\rangle = \langle \chi^{k}_{L'}|H - E|\chi^{k}_{L}\rangle_{O} \qquad (1.61)$$

The LCMTO secular matrix is obtained by inserting the one centre expansion in equation (1.61). We obtain

$$\begin{aligned}\langle \chi^{k}_{L'}|H - E|\chi^{k}_{L}\rangle_{O} = {} & \langle \chi_{L'}|H - E|\chi_{L}\rangle_{O} \\ & + \sum_{L''} \{\langle \chi_{L'}|H - E|J_{L''}\rangle_{O} \mathcal{B}^{k}_{L''L} + \langle J_{L''}|H - E|\chi_{L}\rangle_{O} \mathcal{B}^{k}_{L',L''}\} \\ & + \sum_{L''L'''} \mathcal{B}^{k}_{L',L''} \langle J_{L''}|H - E|J_{L',''}\rangle_{O} \mathcal{B}^{k}_{L',''L}\end{aligned}$$

...(1.62)

The subscript O means that the integral is only over the sphere at the origin. The one-centre term is the one that is zeroth order in $\mathcal{B}$, the two-centre terms are the ones that are first order in $\mathcal{B}$, and the three-centre or crystal-field term is the one that is second order in $\mathcal{B}$.

To turn the LCMTO method into an efficient calculational technique, we introduce the atomic-sphere approximation and paramerise the energy dependence of the one, two and three centre or overlap integrals. The resulting procedure constitutes the so

called linear muffin-tin orbital (LMTO) method. Now the LMTO secular matrix may be written in the form $\underline{\underline{H}} - E\underline{\underline{O}}$, which corresponds to the generalised eigenvalue problem.

$$\sum_{L} (H^{k}_{L',L} - E^{jk} O^{k}_{L',L}) \alpha^{jk}_{L} = 0 \qquad (1.63)$$

and this may be solved by efficient numerical techniques to give the eigenvalues E^{jk} and eigenvectors α^{jk}_{L} .Here $H_{L',L}$ is the hamiltonian matrix and $O_{L',L}$ is the overlap matrix.

1.1.10 The Combined Correction Term

The atomic sphere approximation introduces errors which are unimportant for many applications, e.g. self-consistency procedures, there are cases where energy bands of high accuracy are needed and where one should include the combined corrections terms. These terms arises due to the differences between the atomic sphere and the atomic polyhedron, the $\kappa^2 = o$ used in the ASA and the correct kinetic energy, and because of the neglect of higher partial waves. The extra terms added to the LMTO matrices that accomplish corrections to these errors are called the combined correction terms. The correction terms are obtained by including the perturbation

$$V(r) = (V_{MTZ} - E + \kappa^2) \left[\theta_{WS}(r) - \theta_{MT}(r) \right] \qquad (1.64)$$

to the potential, where $\theta_{WS}(r)$ and $\theta_{MT}(r)$ are step functions which select out the region between the muffin-tin sphere and the atomic polyhedron. With the combined correction terms included in an LMTO calculation, one corrects the errors of the ASA to first order in $\left[E - V_{MTZ} - \kappa^2\right]$.

1.2 SIMULATION OF RELATIVISTIC EFFECTS

The relativistic effects in 5d transition series and even the 4d series, are quite large. It is therefore desirable to make some provision for their inclusion in our method. The relativistic Hamiltonian in the absence of any external field takes the form [71]

$$H = -\frac{\hbar^2}{2m_o}\nabla^2 + V(r) - \frac{\hbar^4}{8m_o^3c^2}\nabla^4 + \frac{\hbar}{4m_o^2c^2}\vec{\sigma}\cdot(\nabla V(r)\times p) + \frac{\hbar^2}{8m_o^2c^2}\nabla^2 V(r) \qquad (1.65)$$

where $V(r)$ is the crystal potential, $\vec{\sigma}$ is the Pauli spin operator, and p is the linear momentum operator. The first two terms in (1.65) correspond to the non-relativistic Hamiltonian. The third term is a correction to the kinetic energy operator arising from the change of electron mass with velocity (mass-velocity term). The fourth term $\vec{\sigma}\cdot(\nabla V \times p)$ is the so-called spin-orbit interaction operator. The last term, referred to as the Darwin term, has no simple classical analogue.

The principal qualitative effect of spin-orbit interaction is to produce additional splittings in the d bands. The remaining effect of this term and the effect of other relativistic terms (mass velocity and Darwin terms) are quantitative in nature as they produce shifts and distortion of the bands. It is reasonable to include the Spin-orbit interaction term only between d functions, where degeneracy effects are important. The inclusion of the spin-orbit interaction doubles the dimension of the total Hamiltonian, since the Hamiltonian now refers to both spin-up and spin down electrons.

1.3 DENSITY FUNCTIONAL FORMALISM

A great deal of attention has been devoted to using electron density as basic variable in applied quantum mechanics. The basic variable is better alternative to quantum mechanical wave function mainly in three ways :

Firstly, the electron density describes the three dimensional distribution of electron in a system, and hence is a function of only the three corrdinates and independent of the number of coordinates of the electrons present. The density-based formalisms offer great simplification over the usual wave function approach because, difficulty in solving the Schrodinger equation increases very rapidly as the number of electrons increases. Secondly, the electron density being a physically observable quantity, the accuracy of the quantum mechanical calculations and approximations can be tested directly. Thirdly, it provides a classical picture of quantum phenomena, since the electron density is a function of three spatial coordinates and enables one to build up various interpretive models.

The electron density can be utilized as a central quantity and the formulation of many particle problem with in a single particle like framework, is the essence of the Density Functional Theory. Starting from the Thorms Fermi method and several modifications, Density functional theory (DFT) has been rejuvenated by the pioneering work of Hohenberg, Kohn and Sham [105, 132] who have laid its strict mathematical foundation and thus provided a formal justification for the use of density as basic quantity. Since then, a significant body of work has been done to carry out various modifcations and extensive applications

to a wide variety of problems in atomic, molecular and solid state physics with remarkable partical success.

1.3.1 Hohenberg-Kohn Theorem :

Hohenberg and Kohn [105] have proved two theorems. The first one establishes that the nondegenerate ground state of an interacting N-particle system under a static external single particle potential V(r), which is completely characterised by the single particle density, n(r). The second theorem states that, for a given external potential, V(r), the energy is a unique functional of the particle density, n(r), and the ground state energy corresponds to a minimum of the energy functional with respect to the variation of density function. The variation of the particle density is performed under a constraint of conservation of particles as given below :

$$\int n(r)dr = N \qquad (1.66)$$

where N is the total number of particles in the system. The stationary condition

$$\partial\left\{E\,[n] - \mu \int n(r)\, dr\right\} = 0 \qquad (1.67)$$

where μ is the lagrangian multiplier, has been used to obtain

$$\frac{\partial E\,[n]}{\partial n(r)} - \mu = 0 \qquad (1.68)$$

where $\left[\frac{\partial E\,[n]}{\partial n\,(r)}\right]$ is a functional derivative of energy functioal E, with respect to the charge density n(r). The equation (1.68) forms a key equation of density functional theory and provides a deterministic equation for n(r). If one considers a collection of an arbitrary number of electrons moving in a system under the influence at am extermal potential V(r) and the mutual coulomb

repulsion, then the Hamiltonian can be constructed as a sum of kinetic energy, T, potential energy, V, and coulomb repulsion energy, U, as

$$H = T + V + U \tag{1.69}$$

where one writes T, V, and U as

$$T = \frac{1}{2} \int \nabla\psi^*(\mathbf{r})\ \nabla\psi\ (\mathbf{r})\ d\mathbf{r} \tag{1.70}$$

$$V = \int V(\mathbf{r})\ \psi^*(\mathbf{r})\ \psi(\mathbf{r})\ d\mathbf{r} \tag{1.71}$$

$$U = \frac{1}{2} \int \frac{1}{|\mathbf{r} - \mathbf{r}'|}\ \psi^*(\mathbf{r})\ \psi^*(\mathbf{r})\ \psi\ (\mathbf{r}')\ \psi\ (\mathbf{r}')\ d\mathbf{r}\ d\mathbf{r}' \tag{1.72}$$

where ψ and ψ^* are the field operator and its conjugate respectively.

It has been assumed, for simplicity, that the ground state is non degenerate. Thus, the electron density, n(r) for the ground state ϕ, can be written as

$$n\ (\mathbf{r}) = \left\langle \phi,\ \psi^*(\mathbf{r})\ \psi\ (\mathbf{r})\ \phi \right\rangle \tag{1.73}$$

which is clearly a functional of external potential V(r), through ϕ.

In order to write an expression for energy, in the terms of density, one requires a knowledge about its functional form. The energy functional E [n], has been written by Hohenberg and Sham [105] as

$$E\ [n] = \int V(\mathbf{r})\ n(\mathbf{r})\ d\mathbf{r} + F\ [n] \tag{1.74}$$

where F [n] is a universal functional valid for any number of particles and any external potential, viz.,

$$F\,[n] = \langle \psi |\ T + U\ | \psi \rangle \qquad (1.75)$$

assumes its minimum value for the correct n(r), if the admissible functions are restricted by the condition of eq (1.66). If F [n] is a known functional of n, the problem of determining the ground state energy and density for a given extermal potential would be just a problem of the minimization of a functional of the three dimensional density function. However, the determination of F [n], poses a major complexity in the many electron electron system, because of the long range of coulumb repulsion. It is convenient to write F [n] as

$$F\,[n] = \frac{1}{2}\int\int \frac{n(r)\ n(r')}{|r - r'|}\ dr\ dr' \ + G\,[n] \qquad (1.76)$$

where G [n] is a universal functional like F [n] and it includes kinetic T[n], exchange and correlation E_{xc}[n], energy functionals and can be written as

$$G\,[n] = T\,[n] \ + E_{xc}[n] \qquad (1.77)$$

The final expression for E [n] is

$$E\,[n] = \int V\,(r)\ n(r)\ dr + \frac{1}{2}\int\int \frac{n(r)\ n(r')}{|r - r'|}\ dr\ dr' + T\,[n] + E_{xc}[n] \qquad \ldots(1.78)$$

1.4 LOCAL DENSITY APPROXIMATION

Here, the basic idea is to assume the local density to be uniform in an infinitesimal volume element of the space coordinates. The kinetic, exchange and correlation energies for uniform electron gas have been taken within that volume element and added to the gradient expansion of the energy functional.

Such an approximation might work well only when one assumes the density slowly varying in space.

1.5 EXCHANGE AND CORRELATION POTENTIALS

To check the effect of exchange and correlation (XC) potential on our problem, we have used different XC potentials approximated by different workers such as von Barth-Hedin (BH) [28], Barth-Hedin modified by Janak (BHJ) [112], Vosko-Wilk and Nussair (VWN) [231] Slater Xα [198] and Langreth and Mehl (LM) [137].

1.5.1 BH-XC Potential [28]

In our calculations we have used the BH-XC potential given by Barth and Hedin. We have disscussed it very briefly.

The exchange and correlation energy can be defind as

$$\varepsilon_{xc} = \varepsilon_x + \varepsilon_c \qquad (1.79)$$

where x as subscript means exchange, c as subscript means correlation. Here ε_x is the ordinary Hartree-Fock contribution

$$\varepsilon_x = -6 \left[\frac{3}{4\pi}\right]^{\frac{1}{3}} \frac{1}{\rho} \left(\rho^{(+)4/3} + \rho^{(-)4/3} \right) \qquad (1.80)$$

The μ_x and μ_c are the contributions to the chemical potential from the exchange and correlation energy. μ_x and μ_c are given by the formulae [187]

$$\mu_x = \varepsilon_x - \frac{r_s}{3}\frac{\partial \varepsilon_x}{\partial r_s} \quad \& \quad \mu_c = \varepsilon_c - \frac{r_s}{3}\frac{\partial \varepsilon_c}{\partial r_s} \qquad (1.81)$$

From eq.(1.80) and eq.(1.81)

$$\mu_x^P = \gamma \, (\varepsilon_x^F - \varepsilon_x^P) \qquad (1.82)$$

where γ = 4/3 a/ (1-a) and a = $2^{-1/3}$and the P superscript means

the paramagnetic state x=1/2, and F superscript means the ferromagnetic state x=0. Now a new function f(x) can defind as

$$f(x) = (1-a)^{-1} \{ x^{4/3} + (1-x)^{4/3} - a \} \tag{1.83}$$

The exchange energy ε_x from (1.80) can be written as

$$\varepsilon_x = \varepsilon_x^P + \gamma^{-1} \mu_x^P f(x) \tag{1.84}$$

Similarly the the correlation energy can be shown as

$$\varepsilon_c = \varepsilon_x^P + \gamma^{-1} \nu_c f(x) \tag{1.85}$$

and the ν_c can be written as

$$\nu_c = \gamma (\varepsilon_c^F - \varepsilon_c^P) \tag{1.86}$$

The r_s dependence of of the ε_x^P and μ_x^P is given by

$$\varepsilon_x^P(r_s) = - \frac{\varepsilon_x^0}{r_s} \tag{1.87}$$

$$\mu_x^P(r_s) = 4/3 \, \varepsilon_x^P(r_s) \tag{1.88}$$

where

$$\varepsilon_x^0 = - \frac{3}{2\pi\alpha_0} \simeq 0.9163 \text{ (Ryd)} \tag{1.89}$$

The r_s dependence of the quantities ε_c^P and ε_c^F can be represented as [101]

$$\varepsilon_c^P = -c^P F\left[\frac{r_s}{r^P}\right] \qquad \varepsilon_c^F = -c^F F\left[\frac{r_s}{r^F}\right] \tag{1.90}$$

where

$$F(z) = (1 + z^3) \ln\left[1 + \frac{1}{z}\right] + \frac{z}{2} - z^2 - \frac{1}{3} \tag{1.91}$$

and

$$c^P = 0.0504, \qquad c^F = 0.0254$$
$$r^P = 30 \qquad r^F = 75 \tag{1.92}$$

They have chose these numerical values in order to reproduce the correlation energy ε_c as function of r_s which are calculated using a 'two-bubble' approximation for the exchange and correlation energy as discussed in detail by Barth and Hedin [28].

1.5.2 BHJ-XC Potential [112]

Janak [112] has made some modification to XC potential given by Barth and Hedin. There is small change in the numerical value of the four parameters as disscussed in BH-XC potential. This due to fact that they have chosen these four parmeters to reproduce the correlation energies calculated by Singwi et al [195]. Now the new values of these four parameters are

$$c^P = 0.045 \qquad c^F = 0.0225$$
$$r^P = 21.0 \qquad r^F = 53.0 \tag{1.93}$$

1.5.3 SLATER Xα XC Potential [198]

Starting from the Fock term of Hartree equation Slater has given a exchange potential which include the adjustable parameter α as compare to earlier approximation given by him. So making this Fock term into a form containing the electron gas density as

$$v^{ex} = -\frac{4k_F}{\pi} F\left(\frac{k_i}{k_F}\right) \tag{1.94}$$

where k_i is the coordinate axes in k-space which will point in the z-direction and k_F is the Fermi wave vector and function F(x) is given by

$$F(x) = \frac{1}{2} + \frac{1 - x^2}{4x} \ln\left|\frac{1 + x}{1 - x}\right| \tag{1.95}$$

The first that comes to mind is simply to average v^{ex} over all occupied states (i.e., over the Fermi sphere) .As a result, we come to Slater approximation for the exchange potential

$$v_{Sl}^{ex} = - 3 \frac{k_F}{\pi} \qquad (1.96)$$

If the potential is only averaged over the Fermi surface (i.e., the exchange interaction over the whole zone is assumed to be equal to that of the FS electrons) we obtain the Gaspar-Kohn-Sham exchange potential

$$v_{GKS}^{ex} = \frac{2}{3} v_{Sl}^{ex} = -2 \frac{k_F}{\pi} \qquad (1.97)$$

Since the other averaging procedures are also possible, it seems reasonable to take this into account by introducing an adjustable parameter α

$$v_{\alpha}^{ex} = -3 \alpha \frac{k_F}{\pi} \qquad (1.98)$$

For α=1 we retrieve the Slater exchange potential an at α = 2/3 we obtain the Gaspar-Kohn-Sham potential. The "correct" value of α lies somewhere in-between.

1.5.4 VWN-XC Potential [231]

Vosko et al [231] have assessed various approximate forms for the correlation energy per particle of the spin-polarized homogenous electron gas using the Pade approximant technique. According to this approximation the correlation energy can be written as

$$\varepsilon_c^P(r_s) = A^P\left\{\ln\frac{x^2}{X^P(x)} + \frac{2b^P}{Q^P}\tan^{-1}\frac{Q^P}{2x + b^P}\right.$$

$$\left. - \frac{b^P x_o}{X^P(x_o)}\left[\ln\frac{(x - x_o)^2}{X^P(x)} + \frac{2(b^P + 2x_o)}{Q^P}\tan^{-1}\frac{Q^P}{2x + b^P}\right]\right\} \quad (1.99)$$

and

$$\varepsilon_c^F(r_s) = A^F\left\{\ln\frac{x^2}{X^F(x)} + \frac{2b^F}{Q^F}\tan^{-1}\frac{Q^F}{2x + b^F}\right.$$

$$\left. - \frac{b^F x_o}{X^F(x_o)}\left[\ln\frac{(x - x_o)^2}{X^F(x)} + \frac{2(b^F + 2x_o)}{Q^F}\tan^{-1}\frac{Q^F}{2x + b^F}\right]\right\} \quad (1.100)$$

Where

$$X^P(x) = x^2 + b^P x + c^P, \qquad Q^P = (4c^P - (b^P))^{1/2}$$

$$X^P(x_o) = x_o^2 + b^P x_o + c^P \quad (1.101)$$

and

$$X^F(x) = x^2 + b^F x + c^F, \qquad Q^F = (4c^F - (b^F))^{1/2}$$

$$X^F(x_o) = x_o^2 + b^F x_o + c^F \quad (1.102)$$

The values of A, x_o, b and c for the best fit are 0.0310907, -0.409286, 13.0720 and 42.7198 for the paramagnetic case and 0.0621814, -0.743294, 20.1231 and 101.578 for the ferromagnetic case. These values reproduced the spin-dependent Random Phase Approximation correlation energy. Thus the correlation energy is given by

$$\varepsilon_c(r_s) = \varepsilon_c^P(r_s) + (\varepsilon_c^F - \varepsilon_c^P)\, F\,(1 + \beta D) \quad (1.103)$$

where

$$x = (r_s)^{1/2}, \qquad S = (\rho^{(+)} - \rho^{(-)})/\rho$$

$$S^P = 1 + S, \qquad S^F = 1 - S, \qquad D = S^4 - 1$$

$$F = ((S^P)^{4/3} + (S^F)^{4/3} - 2)/(2^{4/3} - 2)$$

$$\beta = 1/(2.74208 + 3.182x + 0.09873x^2 + 0.18268x^3) \qquad (1.104)$$

Now the exchange energy can be defind as

$$\varepsilon_x(r_s) = -0.91633059/r_s \ (1 + 4/3 \ F/5.1297628) \qquad (1.105)$$

So

$$\varepsilon_{xc}(r_s) = \varepsilon_x(r_s) + \varepsilon_c(r_s) \qquad (1.106)$$

by adding eq.(1.200) and (1.202) we get the exchange correlation energy

1.5.5 Langreth and Mehl CLMD XC potential [137]

So far we have discussed different local XC potentials approximated by different workers. In order to check the effect of a non-local XC potential in our calculations, we have included the gradient corrections to the local density potential proposed by Langreth and Mehl. For a numbers of years Langreth and Mehl [137] have proposed a workable calculation scheme for including the effects of exchange and correlation beyond the local-density approximation [132] in nonuniform systems such as atoms, solids, molecules, surfaces, etc. This was based on a mode of approximation introduced to such systems by Langreth and Perdew [139 - 142] and by others [166, 176 - 178]]. The work of Langreth and Mehl [137] was based to large extent on the work of Langreth and Perdew [142] and the type of approximation scheme introduced there. This earlier scheme and its relation to the work of other authors such as Gunnarssson, Jonson and Lundqvist [94 - 96],

Alonso and Girifalco [10], Gunnarsson and Jones [97], and Kohn and Hanke [131] have been aptly reviewed by Williams and von Barth [243]. Perdew and collaborators [162, 165, 249] have revived and elaborated on methods for correcting for self-interactions. Later Langreth and Mehl [138] and Hu and Langreth [107], as well as Perdew [163] and Perdew and Wang [164], have proposed modified gradient expansions for the exchange-correlation energy.

Langreth and Mehl [137] analyzed the dynamic density fluctuation wave-vector decomposition of the exact exchange-correlation energy. From their analysis, they derived a gradient correction to LDA for the exchange-correlation functional which satisfied the correct limits at large and small wavelength. In so doing, they were able to aviod the pathologies that plagued the previous gradient expansions based on straightforward expansion techniques. Langreth and Mehl (LM) developed the following functional form for this correction :

$$V_{LM}(r)=8.56 \times 10^{-3} n^{-1/3}\left\{\frac{7}{9}\left[\frac{\vec{\nabla}\cdot K}{n} - \frac{2K^2}{3n^2}\right] - 2e^{-F}\left[\frac{(1-F/2)\vec{\nabla}\cdot K}{n} - \left[\frac{2}{3} - \frac{11F}{6} + \frac{7F^2}{12}\right]\frac{K^2}{n^2} + \frac{F\,(F-3)\,K\cdot\vec{\nabla}\,K}{2nK}\right]\right\} \quad \ldots(1.107)$$

where $K = \vec{\nabla}\, n(r)$

and

$F = 0.262 \left| \vec{\nabla}\, n(r) \right| / [n(r)]^{7/6}$ in terms of the total electron density n or n(r).

As LM correction involves gradients of the density, it is extermely convenient to make the sperical approximation such that one avoids gradients of the spherical harmonics. It does, of course, limit the precision and may obscure important physical consequences. So we feel, however, that the muffin-tin approximation gives a useful first view. For consistency, the correlation function decribed earlier by von Barth and Hedin (BH) is used in this study as the basic exchange-correlation (XC) functional to which we have added the LM corrections.

1.6 FERMI SURFACE EXPERIMENTS

The commonly used experimental methods to obtain information on electronic structure of metals can be classified into two categories :

(i) The Fermi surface experiments which determine the Fermi-surface dimensions and the dynamical properties of quasi particles.

(ii) Spectroscopic experiments which monitor the band structure far off from the Fermi level.

Here we shall consider some experiments which give information on fermi surface topology. In Table 1.1 we give a list of experiments or methods and respective Fermi surface related quantities that each of them yields information on. The summary of methods for the Fermi surface determination as applied to copper are also given in Fig. 2.1. Most of these experiments are based on the behaviour of a metal in presence of magnetic field $\vec{H}$ and are performed at low temperature. The necessary condition to observe these experiments is $\omega_c \tau \gg 1$ where $\omega_c = \frac{eH}{m_c c}$ is the cyclotron frequency, m_c the cyclotron mass and τ is

some appropriate average of scattering time. The higher is the value of $\omega_c\tau$, the more accurately can the experimental parameters be measured. As the magnetic field strength can not be increased beyond a certain limit, τ should be quite large so as to satisfy above condition. Therefore, the sample should be very pure and very low temperature should be maintained during the experiment so that phonon scattering becomes unimportant and electron is not appreciably scattered during one orbit of its motion. In the de Haas-van Alphen effect experiment there is additional requirement that K_BT (K_B = Boltzmann constant) should be small as compared to the energy separation $\hbar\omega_c$ of the quantum levels. This is more stringent condition requiring temperatures as low as 1 and 2°K during the experiment. Here we shall describe only a couple of the Fermi surface experiments which are relevant to the present study.

1.6.1 de Haas-Van Alphen effect [89, 190, 192] :

The de Hass-van Alphen (dHvA) effect has proved to be the most accurate and reliable tool for investigating the electronic structure of metals in the vicinity of the Fermi surface. Experimentally the magnetization M (or susceptibility χ) of a single crystal is measured at very low temperature (~ 4°K) in presence of magnetic field $\vec{H}$ as a function of field strength H $= |\vec{H}|$ and its orientation with respect to crystal axes. For a fixed direction of crystal and $\vec{H}$, M exhibits oscillations which are periodic in H^{-1}. These oscillations arise essentially from quantization of electron orbits in presence of magnetic field. The frequency f of these oscillations is related with the extremal Fermi surface cross section A_{FS} (i.e. section with plane

perpendicular to $\vec{H}$ which has extremal value) by

$$A_{FS} = \frac{2\pi e}{\hbar c} f \qquad (1.108)$$

or

$$A_{FS} \text{ (atomic units)} = 2.673 \times 10^{-9} f \text{ (Gauss)} \ldots\ldots (1.109)$$

from a knowledge of A_{FS} for every extremal cross section as a function of orientations, one can determine the Fermi surface topology. In some special cases when a sheet of surface is known to be closed, radius vectors can be obtaied from the areas by using some inversion theorems [127, 154]. This makes considerable simplification in building up the picture of the Fermi surface, since the building a surface from a knowledge of its cross sectional areas is a difficult job even for simple cases. Alternatively, if the band structure of metals is known extremal cross sectional areas can be calculated from the knowledge of radius vectors of the Fermi surface orbits and direct comparison with experiment can be made.

The amplitude of the dHvA oscillations has an essentially negative exponential dependence on H^{-1}, the exponent being proportional to $m_c (T + T_D)/H$. Here T is the temperature and T_D is the Dingle temperature which is related to an orbital average of scattering probability. If the magnetic breakdown can take place, there is a further reduction in amplitude which depends on H_o/H where H_o is the breakdown field. Thus m_c, T_D and H_o can be obtaied from the studies of the temperature and field dependence of the amplitude.

1.6.2 Azbel - Kaner Cyclotron Resonance [23]

The cyclotron resonance is the simplest Fermi-surface

dependent phenomenon in metals and corresponds to microwave transitions between the quantized k-space orbits, called Landau levels. In order to describe this phenomenon we recall that the effect of a magnetic field on an electron in state $\vec{k}$ with the velocity $\vec{v}(\vec{k})$ is given by the Lorentz force equation [246]

$$\hbar\vec{k} = (e/c)\,\vec{v} \times \vec{H}, \qquad (1.110)$$

where e is the electronic charge and c is the velocity of light.

This Lorentz force causes the wave vector to describe an orbit on a surface of constant energy. If $\vec{k}$ happens to be the Fermi wave vector, the orbit is given by the intersection of the Fermi surface with a plane normal to $\vec{H}$. If the electron is not scattered, it makes a circuit with cyclotron frequency

$$\omega_c = \frac{|e|\,H}{m_c c} \qquad (1.111)$$

where m_c is the cyclotron effective mass and is given by

$$m_c = \frac{\hbar}{2\pi} \oint \frac{dk}{v_\perp(\vec{k})} \qquad (1.112)$$

or

$$m_c = \frac{\hbar^2}{2\pi} \frac{\partial A}{\partial E} \qquad (1.113)$$

Here $v_\perp(\vec{k})$ is the velocity component normal to, and in the plane of, the orbit; A is the extremal cross sectional area of the fermi surface in the plane of the Fermi surface in the plane of the orbit and E is the energy of the orbiting electron.

To measure ω_c a radio frequency (r.f.) field oscillating with frequency ω is applied. As ω is varied, there will be large energy absorption when ω coincides with the cyclotron frequency,

since then the acceleration produced by the electric field along orbit is always in phase with the velocity of the electron at that point. Therefore it adds coherently to produce a large effect.

In case of metals, if the magnetic field is applied in a direction normal to the surface, this scheme is not effective as the skin-depth phenomenon prevents the penetration of the r.f. field. But if the magnetic field be applied parallel to the surface of the sample, an electron in general follows the helical path in real space with axis parallel to H. In each cycle it comes within the skin-depth and sees the r.f. field. If the frequency of the r.f. field coincides with the cyclotron frequency, we again obsere the resonance known as the Azbel'-Kaner cyclotron resonance (AKCR). Thus knowing ω_c , m_c can be calculated from eq. (1.111).

In addition to above methods size effect, Kohn anomalies in the phenon spectrum and positron annihidation etc. are used to gain informations about the Fermi surface of metals. Since we have not used information from these experiments in this thesis, we shall not discuss them further.

1.7 CALCULATION OF FERMI SURFACES

The LMTO method offers a convenient method for Fermi surface studies because of the rapidity with which it calculates the energy eigenvalues. As mentioned in earlier, the extremal croos-sections of the Fermi surface can be measured through dHvA experiments. The extremal cross-sectional area perpendicular to a particular direction (θ,ϕ) of the magnetic field can be

calculated in three steps :-(1) For the case of ferromagnetic metals, the LMTO is set up with spin qantization along the direction (θ,ϕ) of the applied external field. This is necessary, since the energy bands and the size and shape of of the Fermi surface will depend on (θ,ϕ) because of the presence of the spin-orbit and the exchange interaction. In the absence of either effect, there would be no (θ,ϕ) dependence of the energy bands and in that case (θ,ϕ) can be neglected in the energy band calculation. (2) Constant energy surface for energy equal to ΔE_F is generated. For this one has to calculate energy eigenvalues at large number of points throughout the Brillouin zone. (3) Several cross-sectional areas are measured and compared to obtain extremal cross-sectional areas. The areas are found by numerical integration of the radii calculated at a fixed interval of rotation in the plane normal to the direction (θ,ϕ). The following integration formula has been used by Lee [144]

$$\delta A = \left[\frac{1}{2} \left(r_1^2 + r_2^2 \right) \right] \frac{1}{2} (\delta\psi) \qquad (1.114)$$

where δA is the area of a sector bounded by radii r_1 and r_2 and $\delta\psi$ is the vertex angle of the sector.

1.8 PLAN OF THE THESIS

The material embodied in this thesis is organized in following manner. Chapter II is devoted to the study of Fermi surface of the noble metals using LMTO method. In chapter III, we present the results of Fermi surface and related properties of palladium and platinum. The Fermi surface of the ferromagnetic nickel is discussed in chapter IV. Chapter V is devoted to study

of the effect of hydrostatic pressure on the Fermi surface of the noble metals and transition metals Pd, Pt and Ni. The effect of uniaxial tension on the Fermi surface of the noble metals is discussed in chapter VI. Finally, in chapter VII we summarize the results obtained in this thesis.

TABLE - 1.1

A list of various Fermi surface related experiments and the quantities about which they provide information.

Experimental method or effect	Yields information on
1. Radio frequency size effect	$k_{extremal}$
2. Magnetoacoustic effect	$k_{extremal}$
3. Magnetic induced size effect	$\vec{v}_{\vec{k}}$
4. Kohn anomaly	$\vec{k}_F$
5. Compton effect	$\vec{k}_F$
6. Positron Annihilation	$\vec{k}_F$
7. Galvanomagnetic effect	FS topology
8. dHvA effect	A_{ext}, masses
9. Azbel'-Kaner cyclotron resonance	masses
10. Anomalous skin effect	surface area
11. Tomasch Oscillation and related effects	$\vec{v}_F$

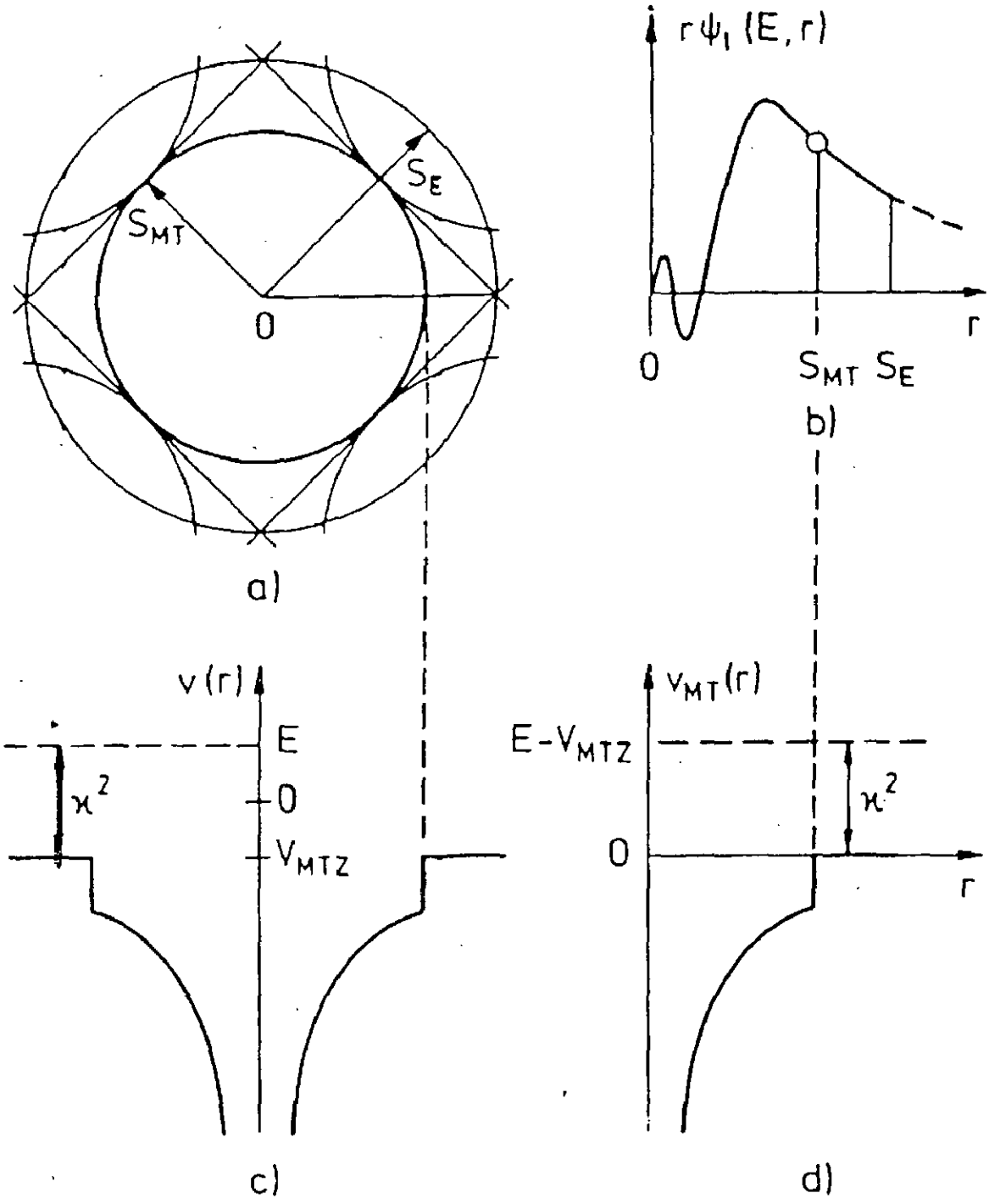

Fig. 1.1 The muffin-tin approximation. a) : the unit cell, the muffin-tin sphere of radius S_{MT}, and the escribed sphere of radius S_E. b) : the radial wave function. c) : the muffin-tin part of the crystal potential V (r). d) : the muffin-tin potential V_{MT} (r).

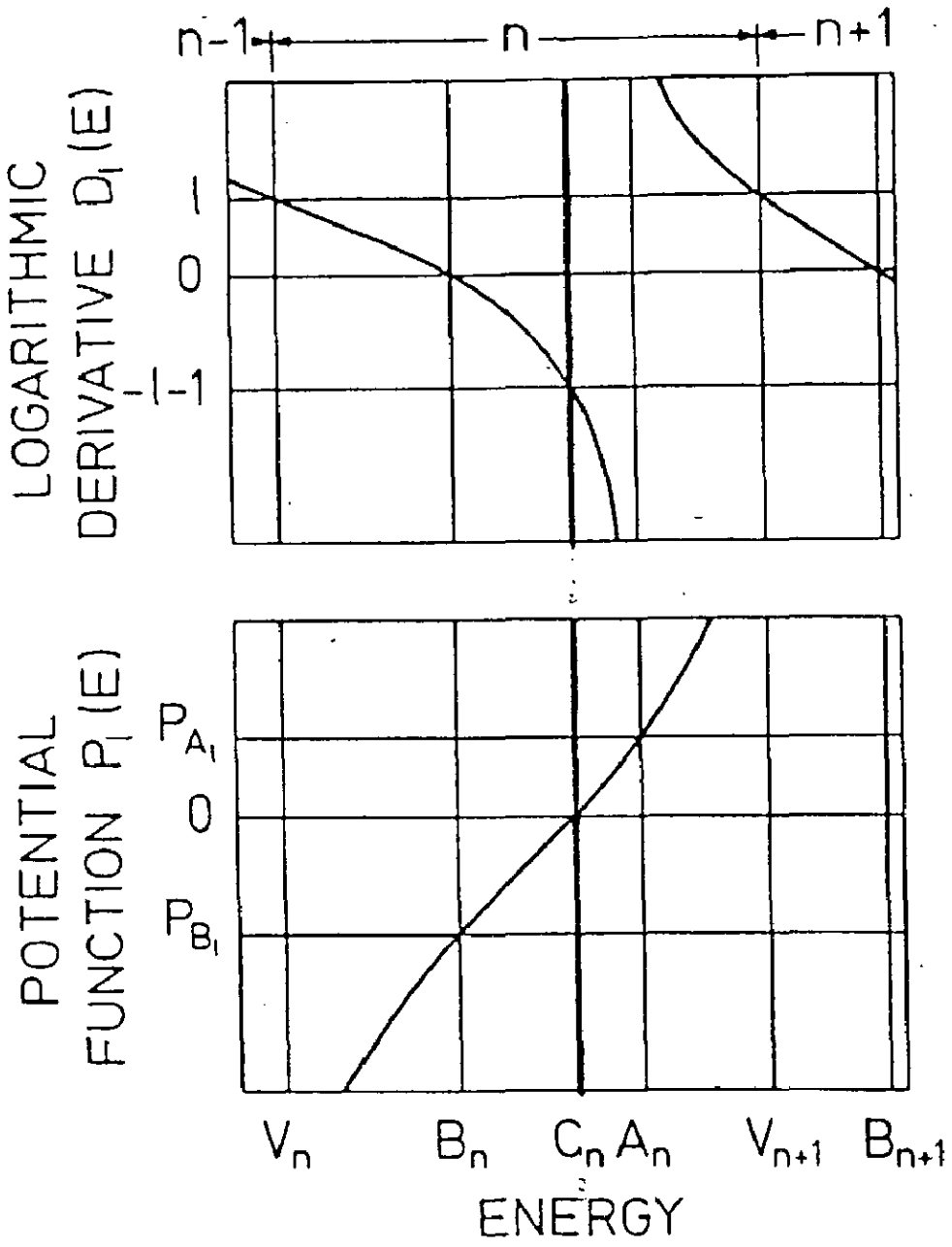

Fig. 1.2 The n'th period of the logarithmic-derivative function $D_\ell(E)$, and the corresponding potential function $P_\ell(E)$. The values P_{A_ℓ} and P_{B_ℓ} equal ℓ and $-2(2\ell + 1)(\ell + 1)/\ell$, respectively.

CHAPTER II

The understanding of the electronic structure of noble metals is a classic problem in solid state physics. The physical properties of transition metal and noble metals are determined largely by the outermost d electrons in the atoms. As this d-shell is progressively filled through a group of transition metals, the physical properties vary drastically [82]. The noble metals follow right after the transition metals and have filled d-shells. Although the energies for the d band lie below the Fermi level, these d-bands in noble metals strongly influence the band-structure and related physical properties. For the last many years noble metals have provided a testing ground for our theoretical understanding of the electronic structure of transition metals. The main reasons for this are (i) Their f.c.c structure is tightly packed. Therefore the muffin-tin approximation made in most band structure calculations is justifiable and (ii) They have been studied experimentally and theoretically in great detail so that these metals can be used to debug our programs. Another reason for choosing noble metals is that spin-orbit effects vary from negligible to predominant as we move from copper to gold.

2.1 BAND STRUCTURE AND FERMI SURFACE

We briefly review the various investigations (experimental and theoretical) of the electronic properties of noble metals. The noble metals crystallise in the fcc structure. The first Brillouin zone for this lattice structure is the truncated octahedran as shown in Fig.2.1. The Fermi surface (FS)

of noble metals would be spherical and would lie entirely within the first Brillouin zone (BZ), if the periodic lattice potential felt by an electron were negligible. The bulging of FS along <100> and <111> direction as shown schematically in Fig.2.2 is due to the lattice potential. With the magnetic field along the <111> direction in the de Haas-van Alphen (dHvA) experiment, a "Belly" (B111) and a "Neck" (N111) orbits are observed. With the field in the <110> direction, a hole orbit resembling a "Dogbone" (D110) is seen and in the <100> direction another Belly orbit (B100) about the spherical body of the surface is observed [192].

The study of the anomalous skin effect by Pippard [168] was the first indication of the presence of necks in copper and was latter confirmed in all the noble metals from dHvA studies by Shoenberg [191]. With the subsequent improvement of experimenal techniques it was possible to determine [40, 98, 111, 119 - 121, 210, 216 - 218] the Fermi surface to substantially higher accuracy than the earlier measurements of Shoenberg [191], Jan and Templeton [111], O'Sullivan and Schirber [217, 218] and Coleridge et al [62] have made high precision ($\sim$ 1 in 10^5)dHvA measurements for various symmetry direction orbits in all the noble metals.

On the other hand calculations of band structure of noble metals can be divided into two categories ; one is the parametrization schemes and the other is first principles calculations. We briefly discuss them. Roaf [180] proposed an analytic expression to represent the Fermi surfaces of the noble metals in the form of a 3-dimensional fourier sum on the basis of Shoenberg's [191] results in which the coefficients were adjusted

to bring the computed cross-sectional areas into agreement with measured values. Zornberg and Mueller [247] have proposed another approach which was applied to the experimental results of Joseph et al [119 - 121] using Mueller's inversion scheme [154]. They obtained radius vectors for the copper Fermi surface to an accuracy of ~ 1 percent using an eleven-term cubic inversion scheme. A considerable advance was made by Halse [98], who used the best available experimental results and the method of Roaf to specify the Fermi surfaces of Cu, Ag and Au to an estimated accuracy of 0.1 percent in the Fermi radii. Coleridge and Templeton [62] have been able to reproduce the cross-sectional areas to within experimental error in all the noble metals using Halse's scheme.

In recent years much effort has been devoted to a deeper understanding of the electronic structure by first-principles energy band calculations in Cu [25, 43, 78, 110, 150, 185, 207, 235] Ag [32, 51, 56, 58, 110, 186, 206] and Au [26, 57, 60, 61, 110, 134, 174, 199]. We will not discuss the merits and demerits of individual calculations as most of them have been reviewed by Dimmock [72]. These studies include both the relativistic and non-relativistic calculations using the augmented plane wave (APW) and the Korringa-Kohn-Rostoker (KKR) methods. Although these calculations are in qualitative agreement with the experimental results, the band gaps in general vary appreciably from one band calculation to another. These variations in band gaps may be attributed to approximations made in the construction of the one electron crystal potential. It has been shown by Williams et al [240] that the band calculations in Cu derived

from Chodorw potential yield energies (for above the Fermi level) which are in error by as much as 10 percent. Janak et al [115] have reported the band structure calculations of copper using KKR method with the exchange coefficient α appearing in Stater's $X\alpha$ theory as a adjustable parameter so that the ground state energy bands generate the measured Fermi surface. The theory treats all electrons identically and provides a more accurage unified interpretation of Fermi surface than previously obtained. On the basis of detailed comparison of the various calculations, particularly the non-relativistic ones, Dimmock [72] concluded that "it appears that the accuracy of the order $\pm$ (0.1 to 0.2) Ryd is the best one can hope to expect from the first principle calculations in silver". Christensen has constructed several potentials in Ag [56] and it was shown that the band structure in particular the d band width and position responded sensitively to changes in the crystal potential. However it was possible to select rather unambiguously the appropriate potential by comparing with experiments. Using the relativistic augmented plane wave (RAPW) calculation [61] he found that the relativistic shifts and the spin-orbit splittings, are essential even in Ag. Similar calculation have also been done for Au [55, 61]. The comparison of these calculations with the non relattivistic one has demonstrated [61] that the shifts and splittings due to relativisitic effects are quite large for gold.

We had previously used Mueller's [155] (and modifications of it [200]) interpolation scheme for calculating Fermi surface and optical properties of the noble and some transition metals [1, 34]. Our reasons for choosing the interpolation scheme were

(i) it is very fast (ii) it gives the band structure and (iii) it can be used to calculate Fermi surface geometry. The Korringa-Kohn-Rostoker (KKR)method of parametrizing, which has now been made very fast has been used either for Fermi surface geometry [189] or for band structure [52] but not for both. Since calculations of extremal areas take a lot of computer time, it would be nice to have an *ab-initio* band structure method which satisfies our three requirements. The LMTO method seems to fit this bill.

Recently Jepsen et al [117] calculated the band structure and FS of the noble metals using the Linear augmented plane wave (LAPW) method with potentials constructed using the local approximation to the density functional formalism and calculated self-consistently by the atomic sphere approximation (ASA) to the linear Muffin tin Orbital (LMTO) method. Relativistic bands shifts (i.e. all relativistic corrections) were included but spin-orbit coupling was neglected. Jepsen et al [117] have shown that their potentials give the Fermi surface comparatively satisfactorily although it is not possible to obtain a satisfactory account of optical excitation energies if these are interpreted as single particle energy differences. In order to place the d-bands correctly, many-body corrections would be needed [117].

We would like to take the cue from the work of Jepsen et al and address ourselves to the question: can a first principle band calculation give an accurate representation of the Fermi surface (FS) geometry ? This is a valid question because the density functional formalism should give the correct Fermi

surface which is a ground state property. In fact the de Haas-Van Alphen experiments measure extremal area. It would therefore be meaningful to calculate the extremal areas. Jepesn et al have suggested that the Fermi surface of noble metals can be well represented by (i) the neck radius and (ii) the ratio A = $k_F[100]/k_F[110]$. We argue that FS geometry means extremal areas which inclues many $\vec{k}$-vectors and not just two or three radii. One of our aims is to ascertain if Jespen et al criterion is indeed correct i.e. that the two quantities above mentioned are sufficient to characterize the Fermi surface geometry of the noble metals.

The calculations discussed so far are in the local density functional approach. In order to check wheather the nonlocal density functional approach could improve the results or not, people have gone beyond the local density approximation. Langreth and his group have done a lot in this direction. The nonlocal corrections given by Langreth and Mehl [137] are also discussed in detail in chapter I and has been successfully tested in non-uniform systems as surfaces and atoms where it has been found to be a significant improvement over the LDA. Langreth and Mehl [138] have applied it for metallic surface energies, as well as to self-consistent atomic calculations which include the ground-state energies of a number of atoms, plus the removal energies. In all cases tried a substantial improvement was found. Mali et al [149] have reported the calculation of electronic properties of some solids using non local density approximation as suggested by Langreth and Mehl in conjunction with atom-in-jellium model and compared their results with LDA. They

find an improvement in the orbital eigenvalues and total energies. Bagno et al [24] have calculated the ground state properties (such as cohesive energy, lattice parameters and bulk modulus) of the third row elements using the Langreth-Mehl-Hu (LMH) [107], the Perdew-Wang (PW) [164] and gradient expansion functionals. Both the PW and LMH functional are found to remove half the errors in the local spin density approximation.

All the nonlocal calculations discussed above do not talk about the Fermi surface calculations which are of course, of our interest. In later years Norman and Koelling [160] have tested the LM gradient correction to LDA for exchange and correlation functional with the use of band structure of copper and vanadium. They have performed band calculations using LAPW method and a warped-muffin-tin (WMT) potential. For copper they have reported the selected eigen value and the Fermi-surface calipers : two on the belly structure (the <100> and <110> direction) to give its anisotropy and a neck radius to characterize the size of necks. These calculations are compared with the previous local work and the characterization of the experimental measurements. They have shown that LM corrections have degraded the agreement with experiment. The anisotropy of the belly is increased when it is already too large. This is in contradiction to the prediction that nonlocality in the mass operator should yield reduced anistropy. As that prediction was made for simple metals where one does not have a relative s-d shift entering and so highlights the significance of the s-d shift. The neck radius is increased where it is already too large, as well. They have concluded that the upward shift of the d-bands is not beneficial in case of the

copper but in case of vanadium it results in an improvement in the calculated Fermi surface.

Recently Barbiellini et al [27] have studied the gradient corrections to the LD potential proposed by Perdew and Wang and to some extent by Langreth, Mehl and Hu in a self-consistent LMTO band calculation in order to determine groundstate and band properties in some 3d, 4d and 5d transition metals, and in the alkali metal Li and Ce. In the case of copper they have shown that the small changes in the Fermi surface from PW calculations go in the correct direction, but are not sufficiently strong and the PW and local density bands are almost identical. The results using LM potentials are still small but opposite. They have concluded that the overall results obtained via gradient-corrected potentials are not yet suffciently good to replace the LD potential.

2.2 CALCULATIONS AND RESULTS

In this part we report calculations of extremal areas for the noble metals using the LMTO method in ASA. We have studied the effects of (i) varying the number of $\vec{k}$ points in the irreducible-Brillouin Zone (BZ) summations (ii) including the f-band parameters and (iii) varying the exchange-correlation (XC) potentials with the view of ascertaining which one is most appropriate for Fermi surface work. The effects of relativistic shifts have also been studied.

We have used the LMTO method in ASA to calculate the energy eigenvalues and eigenvectors. Our primary reason for choosing this method is that it is very fast; as fast as the

empirical methods with the advantage of being an *ab-initio* method. The calculations are done to self-consistency which we take to be that the change in the potential parameters is in the fifth decimal place. We believe that this will converge the energy eigen values to within 10^{-4} Ryd. Starting from the parameters given in Skriver's book [196], this takes about half a dozen more iterations. Using these self-consistent parameters, we have calculated Fermi surface orbital areas and masses using Stark's [212] area mass routine. The area/masses of the computed surfaces in a plane normal to direction (i.e. the magnetic field) were found by numerical integration of radii calculated at a fixed interval of rotation in that plane. In calculation reported here the stepping angle $\delta\theta$ is taken to be 5°. Making this $2\frac{1}{2}^{\circ}$ changed the calculated areas by less than $\frac{1}{2}$%.

In the past, authors have taken percentage error [114, 115] in the Fermi surface area as a meaningful index of the success of the fit to the Fermi surface. We take the view that in a band calculation, since we are calculating energy eigen values, we would like to know the error in the eigenvalues. It would be, therefore meaningful to talk of error in terms of the shift in the Fermi energy ΔE_F required to bring the calculated Fermi surface area in agreement with experiment. ΔE_F can be calculated using following formula [145].

$$\Delta E_F = \frac{1}{n} \frac{A_{expt.} - A_{calc.}}{m_b} \qquad (2.1)$$

where $A_{expt.}$ and $A_{calc.}$ are experimental and calculated areas and m_b is the band mass of the orbit. For a band structure the value of the maximum spread in ΔE_F will be called the 'extreme error'.

We would also like to stress that the area-mass codes calculate eigenvalues at each $\vec{k}$ point on the Fermi surfaces and use no fitting procedures (as used in APW and KKR methods). There is no need to do the fitting as LMTO is very fast. Our calculations are compared with the very accurate data of Coleridge and Templeton [62].

2.2.1 General Considerations :

Jepsen et al [117] have calculated the band structure and Fermi surface of the noble metals using the LAPW method with the potentials constructed using the local approximation to density functional formalism and calculated self-consistently by the ASA to the LMTO method. Relativistic band shifts were included but spin orbit coupling was neglected. They include the s,p,d and f potential parameters with the BZ summations being performed over 715 points. We would first like to address ourselves to (i) the effect of neglecting the f-potential parameters and the effect of varying the number of $\vec{k}$ points in the BZ summations. These are done for copper.

Consider first the effect of truncating the ℓ-expansion in the potential parameters. We have performed calculations with 240 $\vec{k}$ points in the BZ summation in two ways by including (i) ℓ = 0,1,2 terms and (ii) ℓ = 0,1,2,3 potential parameters for copper. Our results for the four Fermi surface orbits are given in Table 2.1. For these calculations, we have used the Barth-Hedin (BH) exchange correlation (XC) potential [28]. A look at Table 2.1 shows that the results do not change significantly by including the ℓ = 3 terms. The extreme ΔE_F, which is determined by the N111 and B111 orbits reduces from 12.5 mRyd to 11.5 mRyd, which is

within the accuracy of the LMTO eigenvalues. Hence all furthers calculations are performed by angular momentum expansion up to ℓ=2. Calculations were next performed using 240 $\vec{k}$ points, 505 $\vec{k}$ points and 916 $\vec{k}$ points in the BZ summations. These results are also given in Table 2.1. Once again we have used the BH-XC and included the s, p and d potential parameters. We obtain an extreme ΔE_F of 12.5 mRyd (240 $\vec{k}$ points), 11.8 mRyd (505 $\vec{k}$ points) and 12.3 mRyd (916 $\vec{k}$ points). *There is no significant change.* Hence all further calculations are performed with 240 $\vec{k}$ points and including ℓ=0,1,2 term only. We have calculated energy band structure of the noble metals by determining the eigenvalues at each $\vec{k}$ points but confined to the irreducible 1/48 th portion of the BZ. The band structure obtained using Slater Xα-XC potentials along symmetry directions are displayed in Figs. 2.3-2.5.

2.2.2 Copper

A look at Table 2.1 indicates that the BH-XC potential does not give a good representation for the FS of copper. An extreme ΔE_F is around 10 mRyd, larger than an extreme ΔE_F of about 0.1 mRyd obtained with the interpolation scheme [194] or by the KKR parametrization [189]. We have also calculated ΔE_F for parameters of Jepsen et al [117] and obtain 14.5 mRyd. Morever we have to lower E_F by about 15 mRyd from the value given by Jepsen et al [117]. This may be attributed to the fact that they used the LAPW method for calculating eigenvalues. With the view to ascertaining how the various treatments of XC influence the eigenvalues and the Fermi surface, we have repeated the calculations with the Barth-Hedin XC potential using Janak's (BHJ) parameters [112] (which make it same as the Hedin Lundquist

(HL) XC potential [101], Slater $X\alpha$ potential [198] and the recent most accurate Vosko-Wilk-Nussair (VWN) XC potential [231]. Janak et al [114, 115] have shown that the $X\alpha$ method with α = 0.77 gives a good fit to the Fermi surface of copper. We have therefore taken α= 0.77 in the $X\alpha$ method.

The calculated Fermi surface areas for various XC potentials for copper are given in Table 2.1. The values of extreme ΔE_F for the various XC are 4.1 mRyd ($X\alpha$ method with α= 0.77), 13.7 mRyd (BHJ), 5.7 mRyd (VWN) and 12.5 mRyd (BH). The $X\alpha$ method with α= 0.77 gives the best fit to the Fermi surface data. The price we pay is that α is an adjustable parameter so obviously the fit is better. Note the recent XC of VWN is also as good as the $X\alpha$ results. The BH and BHJ do not give a good representation for the Fermi surface of copper.

At this juncture we would like to compare our results with those of Janak et al [114, 115] who have performed self-consistent calculations for copper and silver using the KKR method. They have taken the N111 and B111 orbits to decide the fit to the Fermi surface. Our calculations support this. A look at Table 2.1 indicates that the extreme ΔE_F is indeed governed by the N111 and B111 orbits for all the XC used except for the $X\alpha$ and for the VWN-XC where it is governed by N111 and D110 orbits. Janak et al found that α= 0.77 in the $X\alpha$ method provides the best fit to the Fermi surface. Using their results we obtain the extreme ΔE_F to be 6.7 mRyd (for the four orbits) which is slightly larger than the ΔE_F obtained by us. We have not explored the possibility of varying α any more because we feel that variation with α of the Fermi surface orbits will not be much

different from that obtained by Janak et al. All the extreme ΔE_F are much larger than the ΔE_F of about 0.1 mRyd obtained by the interpotation scheme [194] or by the KKR parameterization [189].

Jepsen et al have determined the goodness of the Fermi surface geometry by calculating only two parameters (i) neck radius k_N/k_S where k_S is the radius of the free-electron sphere and (ii) an anisotropy parameter $A = k_F[100]/k_F[110]$. We have also calculated these and are given in Table 2.1 for the various XC potentials. Although the change in these parameters is small for the various XC potentials nevertheless the $X\alpha$ ($\alpha = 0.77$) gives the values that are closest to the experimental values. We are surprised that Jepsen et al contention that two parameters characterize the copper Fermi surface has been well borne out by our calculations. It is surprising to note the difference in the values of k_N/k_S and A obtained by Jepsen et al and by us using their potential parameters. This could be due to the fact that they used the LAPW method

We have calculated Fermi surface calipers and Fermi surface areas using the nonlocal Langreth and Mehl correction terms. These correction are added to the local exchange-correlation functions described by von Barth-Hedin. All the calculations are done with 240 $\vec{k}$ points and taking the angular momentum expansion up to $\ell = 2$. The calculations are compared with the results of the local exchange-correlation potential of BH to ascertain the effect of the nonlocal corrections. We also compare our results with those of other workers. Norman and Koelling [160] and Barbiellini et al [27] have characterized their results for the Fermi surface of copper

in terms of a few critical calipers : two belly radii and one neck radii. We have also reported the Fermi surface caliper for copper in Table 2.2 and compared it with experimental results [62] and our local potential results. These results show that the nonlocal corrections have degraded the agreement with the experiment in accordance with the results of Norman and Koelling and Barbiellini et al. As these changes are very small, it is not possible to make any comment on the predication that nonlocality should reduce the anisotropy (which is for the simple metals where one does not have relative s-d shift).

In order to get better understanding of the effect of the nonlocal corrections it would be better to calculate the Fermi surface areas (as areas require many more $\vec{k}$ vectors). We have calculated the Fermi surface areas using local (BH) and Langreth and Mehl's nonlocal potential. These are given in Table 2.3. In the case of BH-XC poential ΔE_F for the B111 orbit was 1.1 mRy but for the nonlocal potential, the ΔE_F is 2.0 mRyd. Similarly for the neck area ΔE_F goes from 9.6 to 11.5 mRyd but in case of B100 it is reduced by 0.6 mRy. The overall extreme ΔE_F is increased by 3.0 mRyd in comparison with the local BH-XC. Hence we can say that the Nonlocal potential degraded the agreement of Fermi surface area with experimentaly measured one. This is in agreement with the calculations of Norman and Koelling and Barbiellini et al thus lending credence to our calculations.

2.2.3 Silver

We have performed similar calculations for silver. Results are given in Table 2.4. The extreme ΔE_F using the various XC are 16.4 mRyd(BH), 16.3 mRyd (BH with f band parameter) 25.5

mRyd (Jepsen's parameters), 15.6 mRyd(BHJ), 15.3 mRyd (BH with 505 $\vec{k}$ points), 0.9 mRyd (Xα with α= 0.77) and 3.8 mRyd (VWN). As in case of copper, the extreme ΔE_F is again governed by the N111 and B111 orbits except for the Xα case where it is B111 and B100 orbits. All results are for 240 $\vec{k}$ points and including ℓ = 0,1,2 terms only, unless stated otherwise. Once again, we find that Xα method (wth α= 0.77) gives the best fit to the data. In fact this is the kind of agreement one gets with the KKR parametrization [189] or interpolation scheme [194]. Amongst the other XC potentials, the VWN is the best. We have also calculated the neck radius k_N and anisotropy parameter A. Again we find that the Xα method (α= 0.77) gives values for these in good agreement with the experiment. It is pleasing to note that our k_N/k_S and A agree with the values obtained by Jepsen et al. For copper this was not the case. Calculations by Janak et al [114, 115] give an extreme ΔE_F of 8.5 mRyd. Thus we are led to the conclusion that the LMTO method in ASA gives a better representation to the Fermi surface of copper and silver using the same α in the Xα method. The VWN fares best considering that it has no adjustable parameter. We have also studied the effect of non-local LM-XC potential on the FS of silver and find that it does not lead to any change when compared with local potential (BH-XC).

2.2.4 Gold :

Table 2.5 summarizes our results for gold. The extreme ΔE_F for the various XC potentials are 3.2 mRyd (BH), 3.6 mRyd (BH with *f*-band parameters), 2.8 mRyd (Jepsen's potential parameters), 3.5 mRyd (BH with 505 $\vec{k}$ points), 3.4 mRyd (BHJ), 19.5 mRyd (VWN) and 15.8 mRyd (Xα-XC with α = 0.77). Unlike the

cases of copper and silver the extreme ΔE_F is now not governed by the same two orbits. In fact for various XC potentials used, the orbits always vary. The fact that the Xα-XC does not give a good fit to the Fermi surface of gold suggests the need to vary α. We have performed calculations for various α's and plotted the results in Fig. 2.6. The figure illustrates that even in Xα-XC, different values of α give different orbits which control the extreme ΔE_F. From the figure we find that α= 0.693 would yield an extreme ΔE_F of 3.5 mRyd, which is the same as with BH and BHJ XC potentials. On calculating k_N and A, we find that those XC potentials which give the best fit to the Fermi surface geometry also give values of these parameters in agreement with the experiments. Again the k_N/k_S and A calculated by us do not agree with the values of Jepsen et al . In case of gold also the non local LM-XC does not affect Fermi surface area.

2.2.5 Relativistic Corrections

With the view to determine how relativitic corrections would influence the shape of the Fermi surface, we have decided to study gold because here the relativistic corrections are the largest. We have calculated the relativistic bands along symmetry directions. These results are plotted in Figures 2.7-2.10. Our calculations demonstrate that the neck radius is almost unchanged by relativistic band shifts. However k_F[100] increases by 0.3% amd k_F[110] decreases by 1.4%. This changes A to 1.226. This will tend to reduce the B100 area slightly but will leave the extreme ΔE_F almost unchanged. Hence relativistic corrections are not sufficient to reduce ΔE_F significantly.

2.3 CONCLUSIONS

In this chapter we have reported results of accurate calculations of four FS orbits for the noble metals using the LMTO-ASA method. These calculations have been performed by (i). including or neglecting f-band parameters, (ii) varying the number of $\vec{k}$ points in the BZ summations and (iii) using different XC potentials. Our results indicate that the f-band potential parameters have only a marginal influence on the FS. This is not surprising because f-bands are at least ~ 5eV above E_F. We also find that by changing the number of $\vec{k}$ points in the BZ summation from 240 to 916 does not change the FS significantly. Table 2.6 summarises all our results for the noble metals with various XC potentials. It is obvious that no single XC potential gives a good representation for the FS of the noble metals. The Xα method with a variable α gives the best agreement with the experimental data. The value of α for Au comes to be 0.693 while for Cu and Ag it is 0.77. The BH and BHJ XC potentials work well for Au but not for Cu and Ag. The VWN-XC potential gives the Ag FS satisfactorily but not for Cu and Au. Thus no single XC gives the FS of all the noble metals satisfactorily. We are a bit surprised that the VWN-XC potential which is most reliable (with an estimated maximum error of 1 mRyd) gives such a large extreme ΔE_F. The best agreement works out to be an extreme ΔE_F of 3-4 mRyd (0.9 mRyd for Ag is surprising and stands out from others). It is worth noting that these ΔE_F are smaller by 50% than those from accurate and detailed calculations of Janak et al and hence are the smallest ever obtained by an *ab initio* band calculation. They are still an order of magnitude larger than the ΔE_F=0.1 mRyd

obtained by empirical methods. Clearly the empirical methods with many adjustable parameters can give a better representation for the FS geometry in noble metals and no *ab-initio* method can hope to compete with them. The nonlocal XC by LM does not improve the results. In case of copper it degraded with experiment while in case of silver and gold it does not leave any effect.

We have also studied the suggestion of Jepsen et al that the FS of noble metals could be characterized by k_N/k_S and $A = k_F[100]/k_F[110]$. Here again we find that there is no consistent picture. For Cu and Ag, the XC potentials which give good agreement with experimental areas also give values of k_N/k_S and A in agreement with the experiment. For Au, this was not found to be the case. We find that the values of A and k_N/k_S using Jepsen et al potential parameters do not always agree with the values obtained by Jepsen et al. We feel this may be due to the fact that they used a more accurate LAPW method.

TABLE 2. 1

Calculated extremal areas in a.u. for copper and ΔE_F in Ryd. (in brackets)

γ_s=2.669 a.u., k_s=0.7213 a.u.$^{-1}$

Name of the orbit			B111	N111	B100	D110	$A=\frac{k_F[100]}{k_F[110]}$	$\frac{k_N}{k_s}$
Experimental Area[a]			1.5523	0.0581	1.6026	0.6707	1.11	0.189
pts. in BZ	Up to	XC						
240	ℓ=3	BH	1.5414 (0.0018)	0.0701 (-0.0097)	1.6633 (-0.0014)	0.6496 (-0.0056)	1.134	0.208
240	ℓ=2	BH	1.5403 (0.0028)	0.0695 (-0.0097)	1.6057 (-0.0007)	0.6469 (-0.0060)	1.139	0.207
505	ℓ=2	BH	1.5339 (0.0038)	0.0681 (-0.0080)	1.6011 (0.0033)	0.6530 (-0.0046)	1.140	0.205
916	ℓ=2	BH	1.5346 (0.0038)	0.0684 (-0.0085)	1.6019 (0.0002)	0.6523 (-0.0048)	1.140	0.205
715	ℓ=3	HL	1.6051 (-0.0125)	0.0937 (-0.0270)	1.6791 (-0.0182)	0.5841 (-0.0238)	1.149	0.240
240	ℓ=2	BHJ	1.5394 (0.0040)	0.0699 (-0.0097)	1.6066 (-0.0009)	0.6489 (-0.0059)	1.140	0.208
240	ℓ=2	VWN	1.5547 (-0.0006)	0.0546 (0.0030)	1.6029 (-0.0001)	0.6610 (-0.0027)	1.104	0.183
240	ℓ=2	$X\alpha$ α=0.77	1.5528 (-0.0001)	0.0570 (0.0009)	1.6031 (-0.0001)	0.6590 (-0.0032)	1.108	0.187

[a] Ref. 62

TABLE 2. 2

Fermi Surface parameter in the units of 2Π/a for noble metals

Field Direction	Metal	Experimental value (a)	Our Calculation		Norman and Koelling (b)		Barbillini et al (c)	
			XC	LM	XC	LM	XC	LM
B100	Cu	0.827	0.844	0.845	0.844	0.846	0.844	0.846
	Ag	0.819	0.828	0.828				
	Au	0.878	0.885	0.885				
B110	Cu	0.743	0.742	0.740	0.742	0.741	0.737	0.735
	Ag	0.752	0.749	0.749				
	Au	0.736	0.737	0.737				
N111	Cu	0.147	0.163	0.167	0.155	0.161	0.156	0.160
	Ag	0.106	0.130	0.130				
	Au	0.139	0.144	0.144				

[a]Reference 62 [b]Reference 160 [c]Reference 27

TABLE 2. 3

ΔE_F using non local XC-potential

Field Direction	Experimental Area (a)	Calculated Area			
		XC	ΔE_F	LM	ΔE_F
B111	1.5523	1.5472	1.1	1.5431	2.0
B100	1.6026	1.6128	-2.2	1.6088	-1.4
N111	0.0581	0.0709	-9.6	0.0737	-11.5
D110	0.6707	0.6432	-7.3	0.6434	-7.2
Extreme ΔE_F (mRyd)			10.7		13.5

[a]Reference 62

TABLE 2. 4

Calculated extremal areas in a.u. for silver and ΔE_F in Ryd. (in brackets)

γ_s=3.005 a.u., k_s=0.6386 a.u.$^{-1}$

Name of the orbit			B 111	N111	B100	D110	$A=\frac{k_F[100]}{k_F[110]}$	$\frac{k_N}{k_s}$
Experimental Area[a]			1.2311	0.0238	1.2684	0.5528	1.09	0.136
pts. in BZ	Up to	XC						
240	ℓ=3	BH	1.2244 (0.0023)	0.0375 (-0.0140)	1.2664 (-0.0007)	0.5258 (-0.0043)	1.104	0.171
240	ℓ=2	BH	1.2249 (0.0022)	0.0360 (-0.0142)	1.2687 (-0.0001)	0.5252 (-0.0045)	1.106	0.168
505	ℓ=2	BH	1.2220 (0.0031)	0.0352 (-0.0122)	1.2660 (0.0008)	0.5286 (-0.0034)	1.114	0.176
715	ℓ=3	HL	1.2189 (0.0045)	0.0415 (-0.0210)	1.2645 (0.0014)	0.5248 (-0.0049)	1.106	0.166
240	ℓ=2	BHJ	1.2235 (0.0026)	0.0362 (-0.0130)	1.2678 (0.0002)	0.5266 (-0.0041)	1.107	0.168
240	ℓ=2	VWN	1.2358 (-0.0017)	0.0218 (0.0021)	1.2692 (-0.0003)	0.5373 (-0.0003)	1.080	0.130
240	ℓ=2	Xα α=0.77	1.2340 (-0.0010)	0.0243 (-0.0005)	1.2687 (-0.0001)	0.5354 (-0.0009)	1.083	0.138

[a]Ref. 62

TABLE 2.5

Calculated extremal areas in a.u. for gold and ΔE_F in Ryd. (in brackets)

r_s=3.002 a.u., k_s=0.6392 a.u.$^{-1}$

Name of the orbit			B111	N111	B100	D110	$A=\frac{k_F[100]}{k_F[110]}$	$\frac{k_N}{k_S}$
Experimental Area[a]			1.1909	0.0406	1.2837	0.5130	1.20	0.179
pts. in BZ	Up to	XC						
240	ℓ=3	BH	1.2033 (-0.0036)	0.0443 (-0.0051)	1.3010 (-0.0049)	0.5087 (-0.0015)	1.198	0.186
240	ℓ=2	BH	1.2023 (-0.0035)	0.0439 (-0.0048)	1.3014 (-0.0053)	0.5071 (-0.0021)	1.203	0.185
505	ℓ=2	BH	1.1987 (-0.0023)	0.0432 (-0.0037)	1.2988 (-0.0043)	0.5108 (-0.0008)	1.205	0.184
715	ℓ=3	HL	1.2601 (-0.0214)	0.0568 (-0.0207)	1.3570 (-0.0215)	0.4627 (-0.0187)	1.184	0.210
240	ℓ=2	BHJ	1.2015 (-0.0031)	0.0442 (-0.0051)	1.3022 (-0.0053)	0.5078 (-0.0019)	1.204	0.186
240	ℓ=2	VWN	1.2160 (-0.0080)	0.0327 (0.0115)	1.2994 (-0.0049)	0.5196 (-0.0024)	1.58	0.160
240	ℓ=2	Xα α=0.77	1.2137 (-0.0072)	0.0347 (0.0086)	1.2993 (-0.0048)	0.5180 (0.0018)	1.164	0.164
240	ℓ=2	Xα α=.693	1.2024 (-0.0033)	0.0441 (-0.0049)	1.3023 (-0.0053)	0.5078 (-0.0018)	1.161	0.185

[a] Ref. 62

TABLE 2.6

Extreme ΔE_F (in mRyd) for the noble metals—A summary

Name of the metal →→→→→→→→→→→→			Copper	Silver	Gold
pts. in BZ	Up to	XC			
240	ℓ = 3	BH	11.5	16.3	3.6
240	ℓ = 2	BH	12.5	16.4	3.2
505	ℓ = 2	BH	11.8	15.3	3.5
916	ℓ = 2	BH	12.3	-	-
715	ℓ = 3	HL	14.5	25.5	2.8
240	ℓ = 2	Xα(α=.77)	4.1	0.9	15.8
240	ℓ = 2	VWN	5.7	3.8	19.5
240	ℓ = 2	BHJ	13.7	15.6	3.4
240	ℓ = 2	Xα α=0.693	-	-	3.5

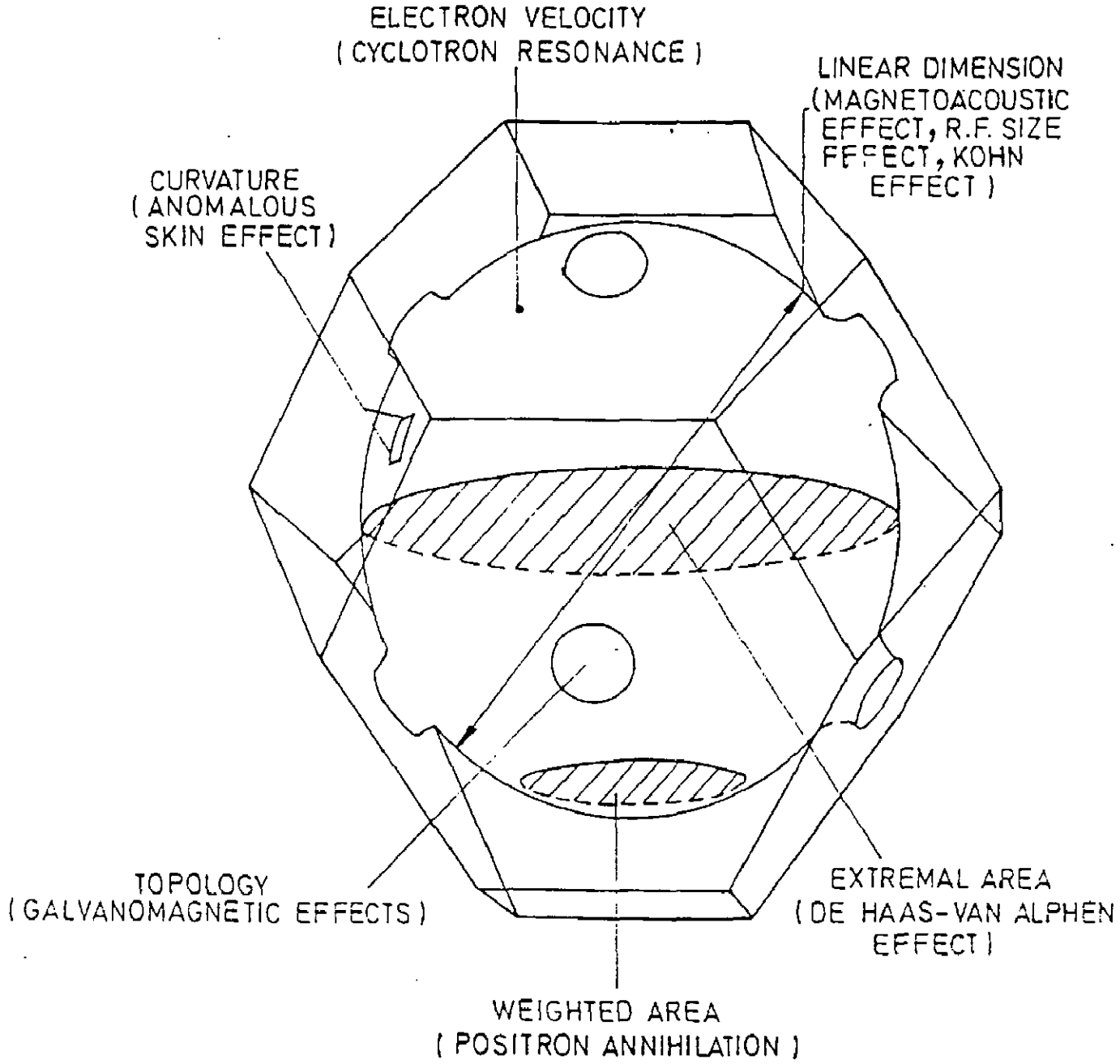

FIG. 2.1 – SUMMARY OF METHODS FOR FERMI SURFACE DETERMINATION AS APPLIED TO THE FERMI SURFACE OF COPPER.

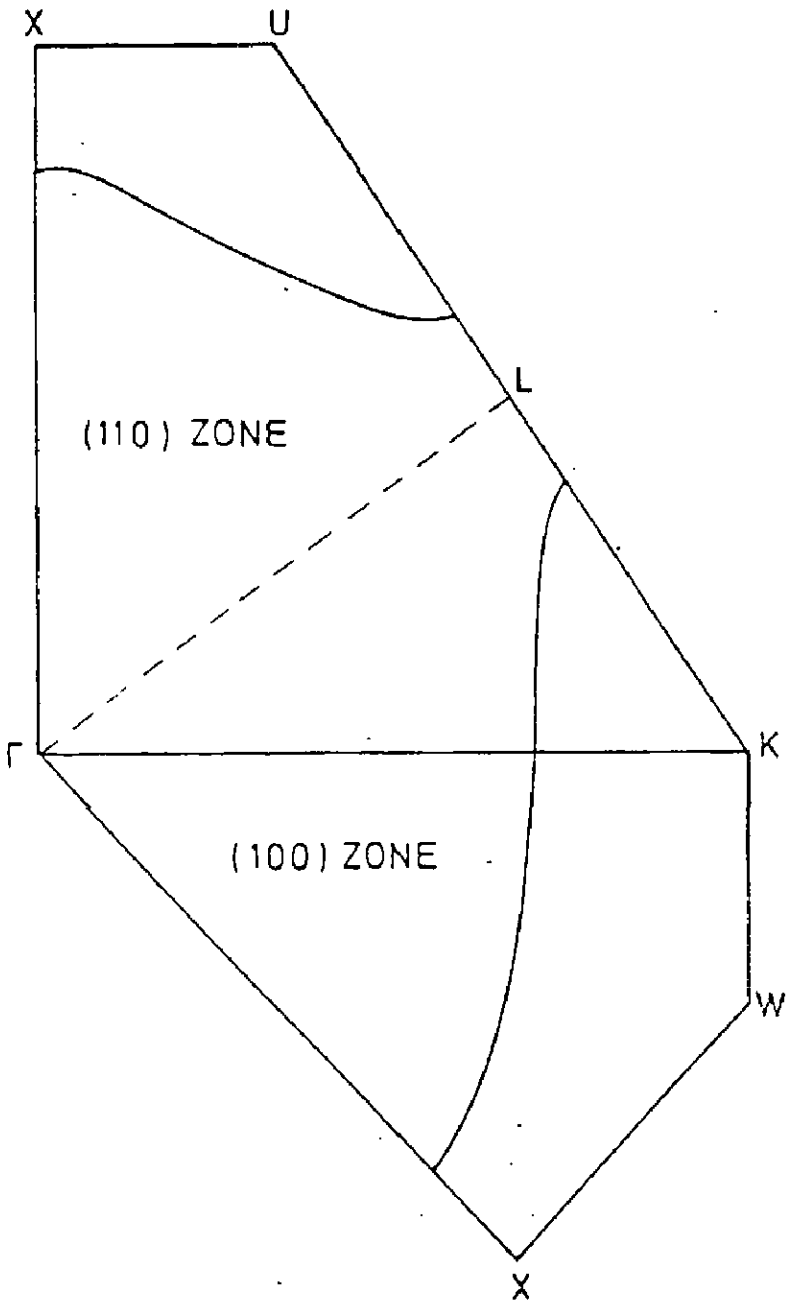

Fig. 2.2 – EXTREMAL CROSS-SECTIONS (SCHEMATIC) OF THE FERMI SURFACE OF THE NOBLE METALS NORMAL TO <100> AND <110> SYMMETRY DIRECTIONS.

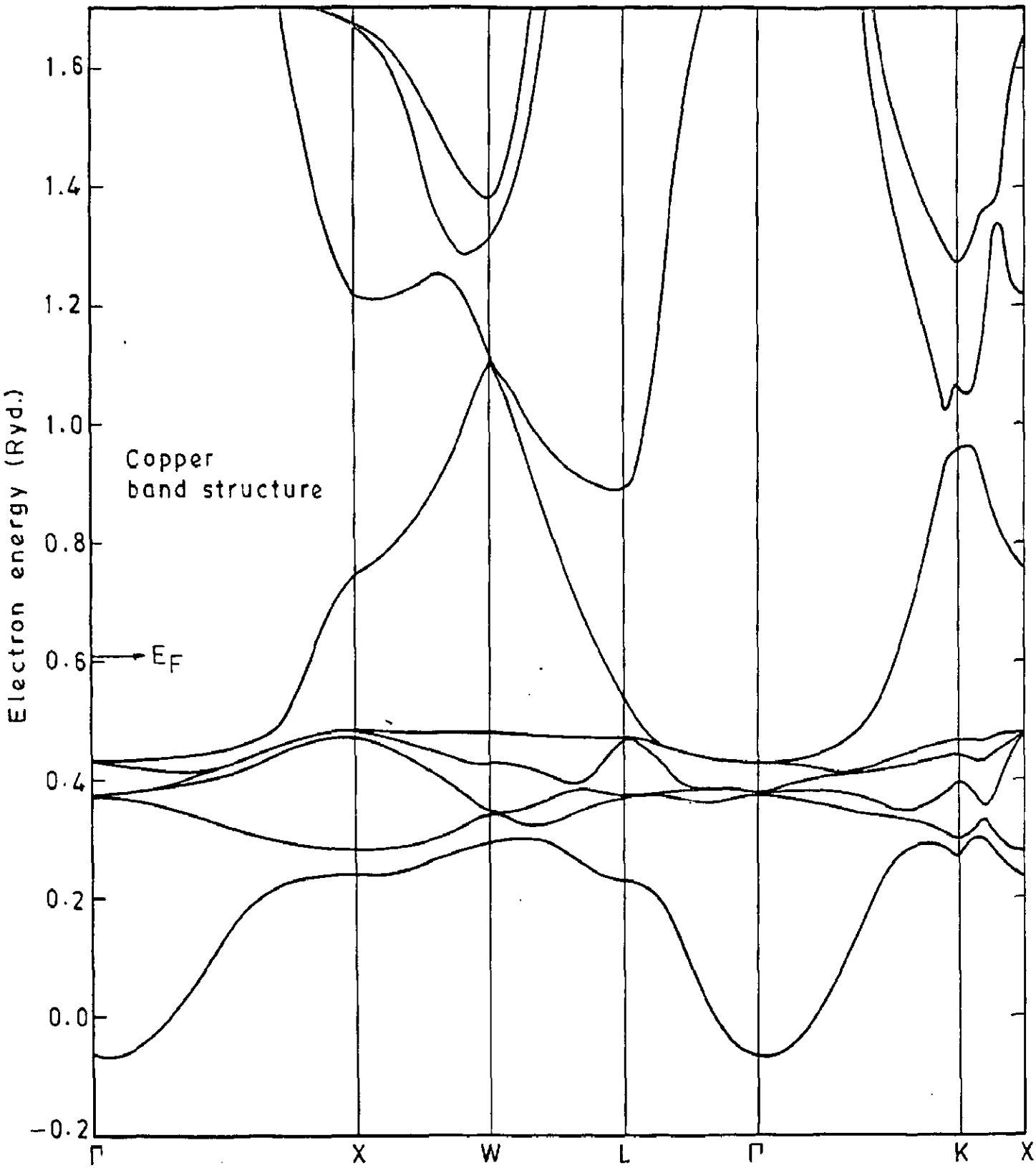
Electron energy (Ryd.)
1.6
1.4
1.2
1.0
0.8
0.6
0.4
0.2
0.0
−0.2
Copper
band structure
E_F
Γ
X
W
L
Γ
K
X

Fig. 2.3

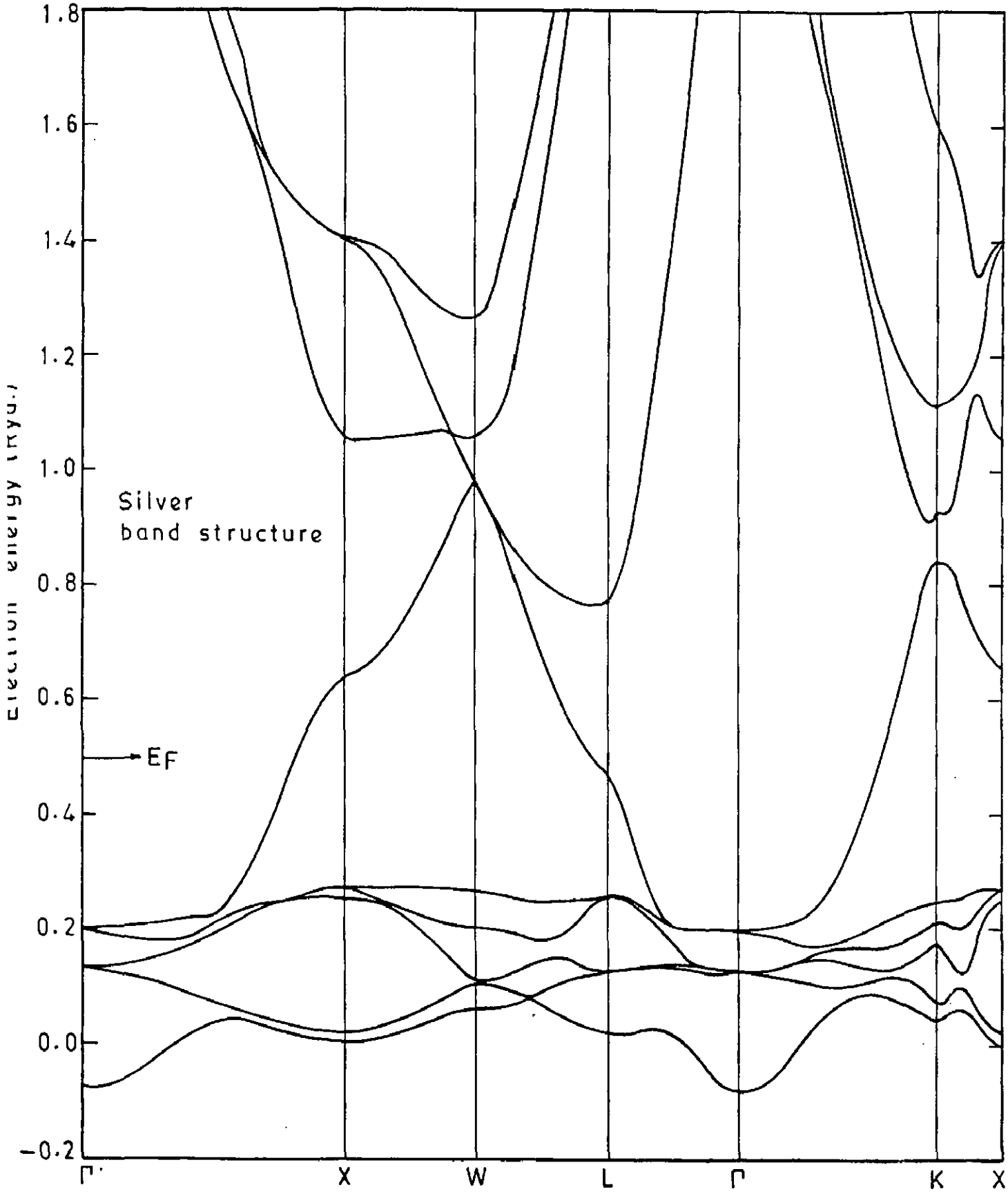
1.8
1.6
1.4
1.2
1.0
0.8
0.6
0.4
0.2
0.0
−0.2
Silver
band structure
E_F
Γ
X
W
L
Γ
K
X

Fig. 2.4

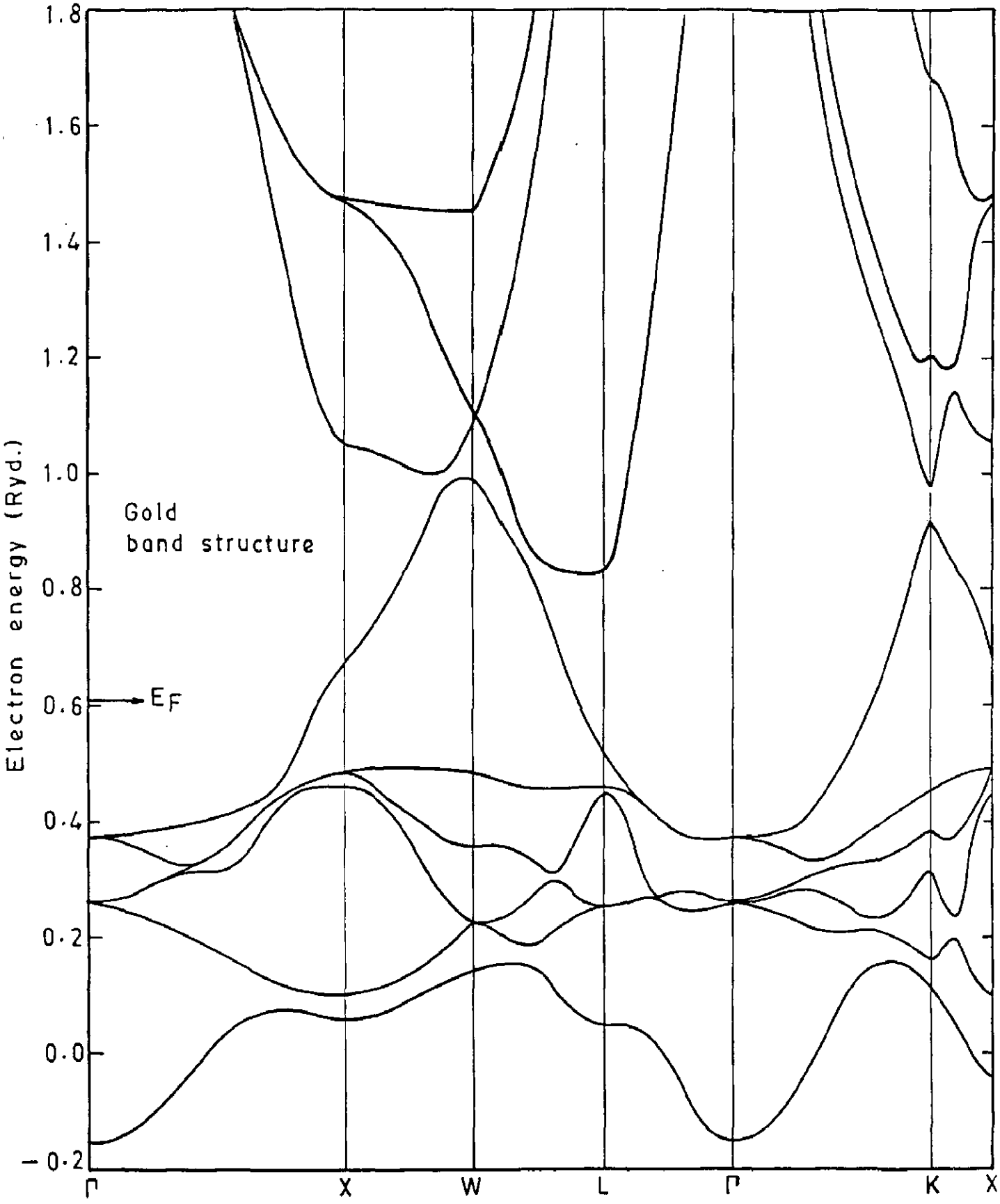
Electron energy (Ryd.)
1.8
1.6
1.4
1.2
1.0
0.8
0.6
0.4
0.2
0.0
−0.2
Gold
band structure
E_F
Γ
X
W
L
Γ
K
X

Fig. 2.5

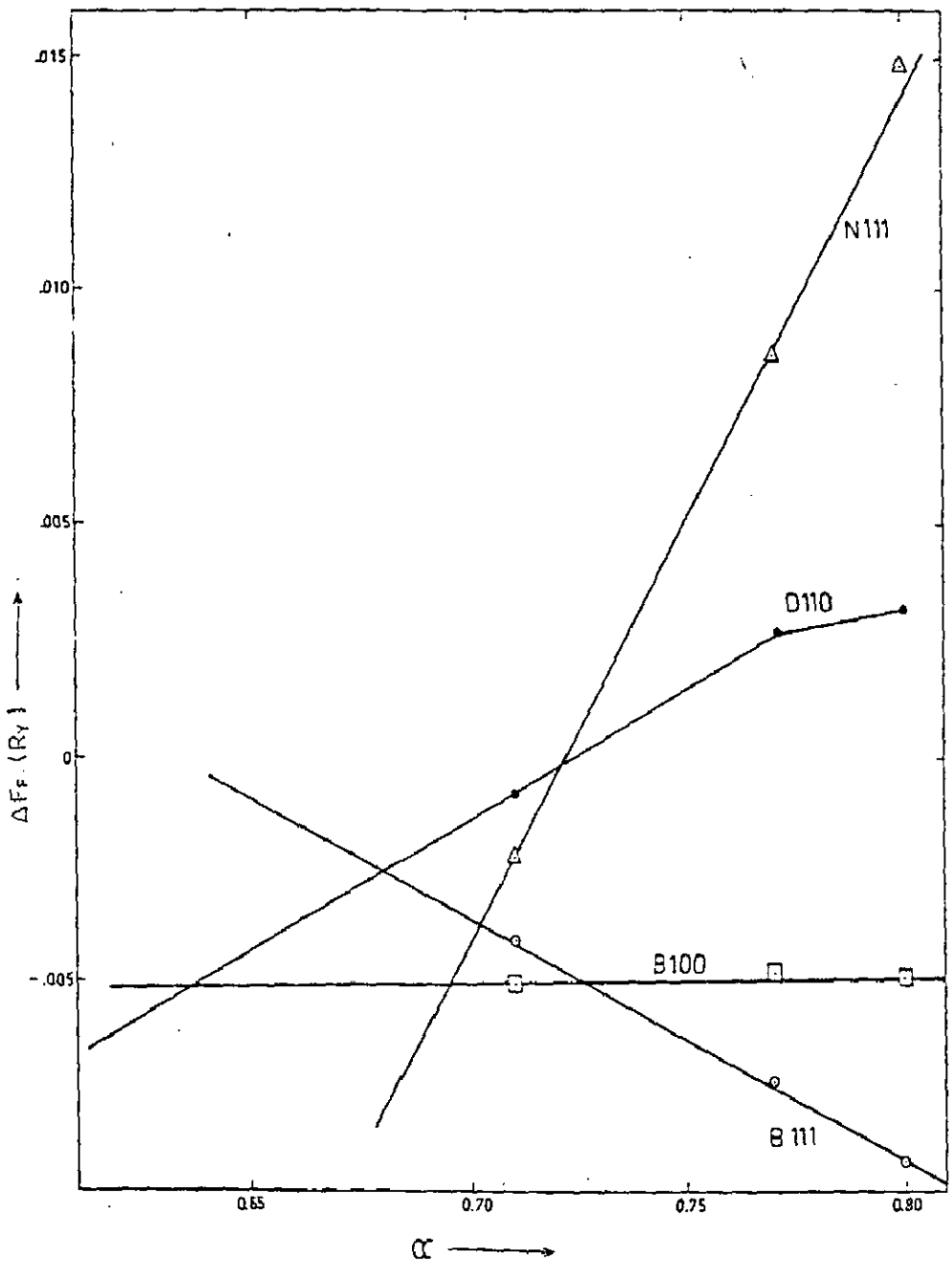

Fig. 2.6

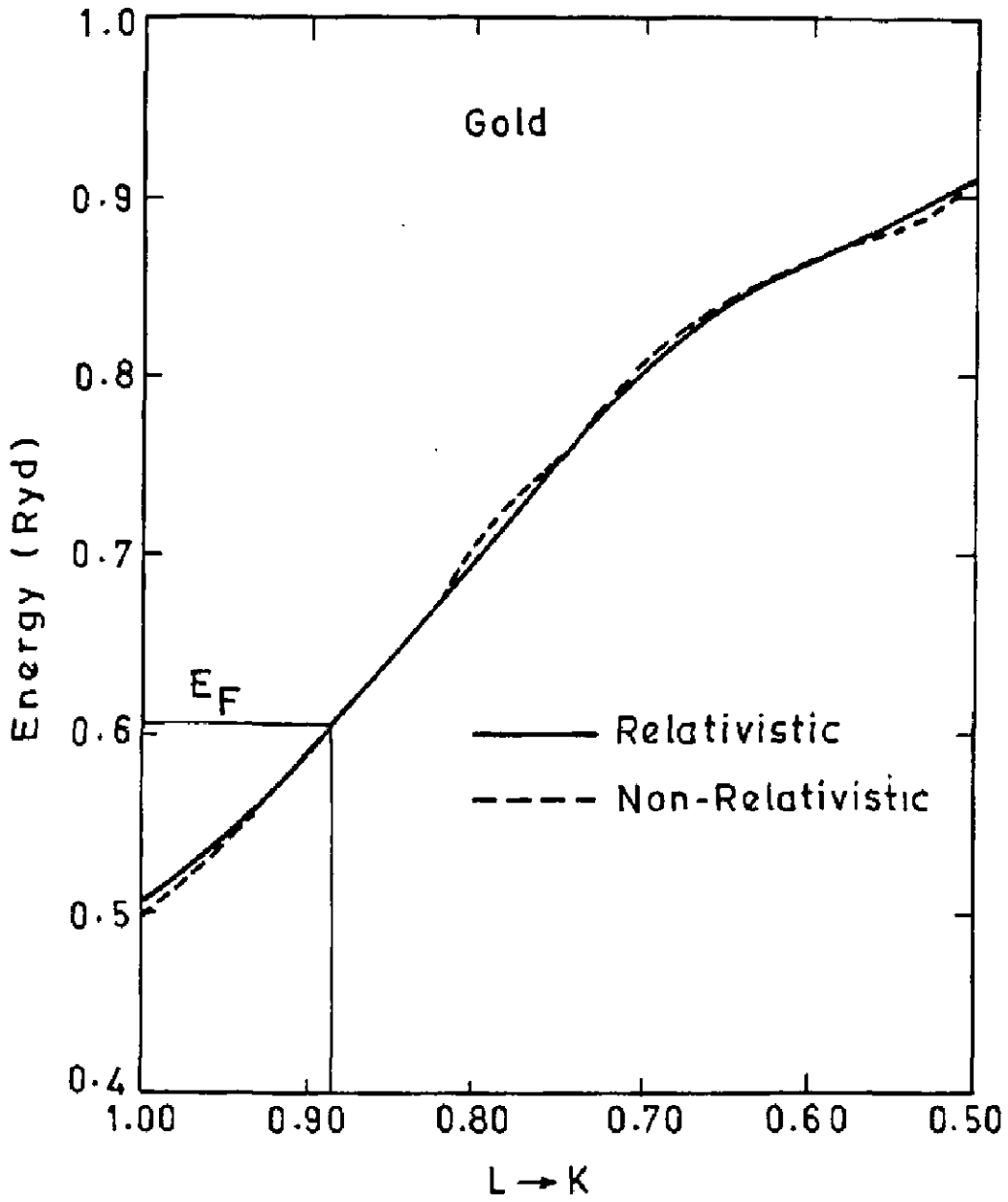
Gold
Energy (Ryd)
1.0
0.9
0.8
0.7
0.6
0.5
0.4
E_F
Relativistic
Non-Relativistic
1.00
0.90
0.80
0.70
0.60
0.50
L → K

Fig. 2.7

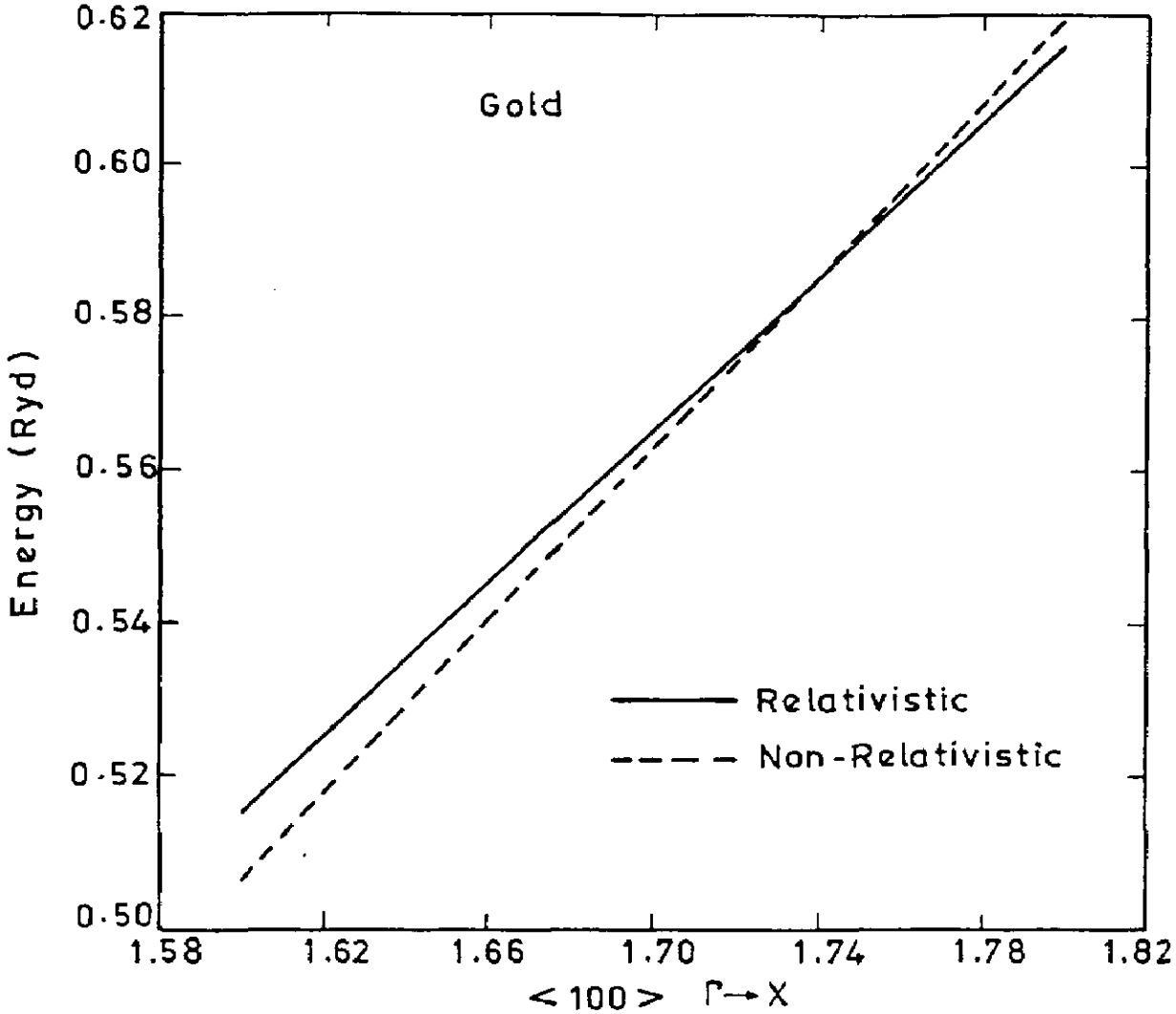
Gold
Energy (Ryd)
0·62
0.60
0.58
0.56
0.54
0·52
0·50
1.58
1.62
1.66
1.70
1.74
1.78
1.82
Relativistic
Non-Relativistic
< 100 > Γ→X

Fig. 2.8

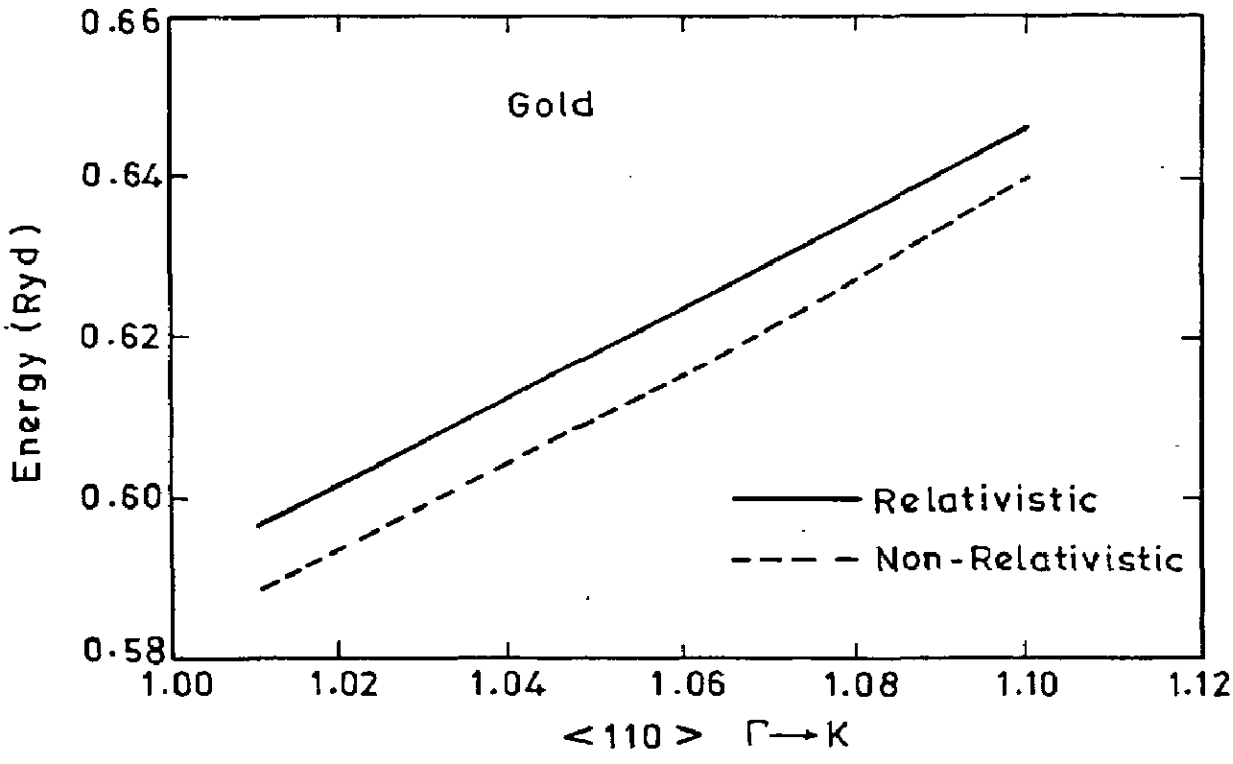
Gold
Energy (Ryd)
0.66
0.64
0.62
0.60
0·58
1.00
1.02
1.04
1.06
1.08
1.10
1.12
Relativistic
Non-Relativistic
< 110 > Γ→K

Fig. 2.9

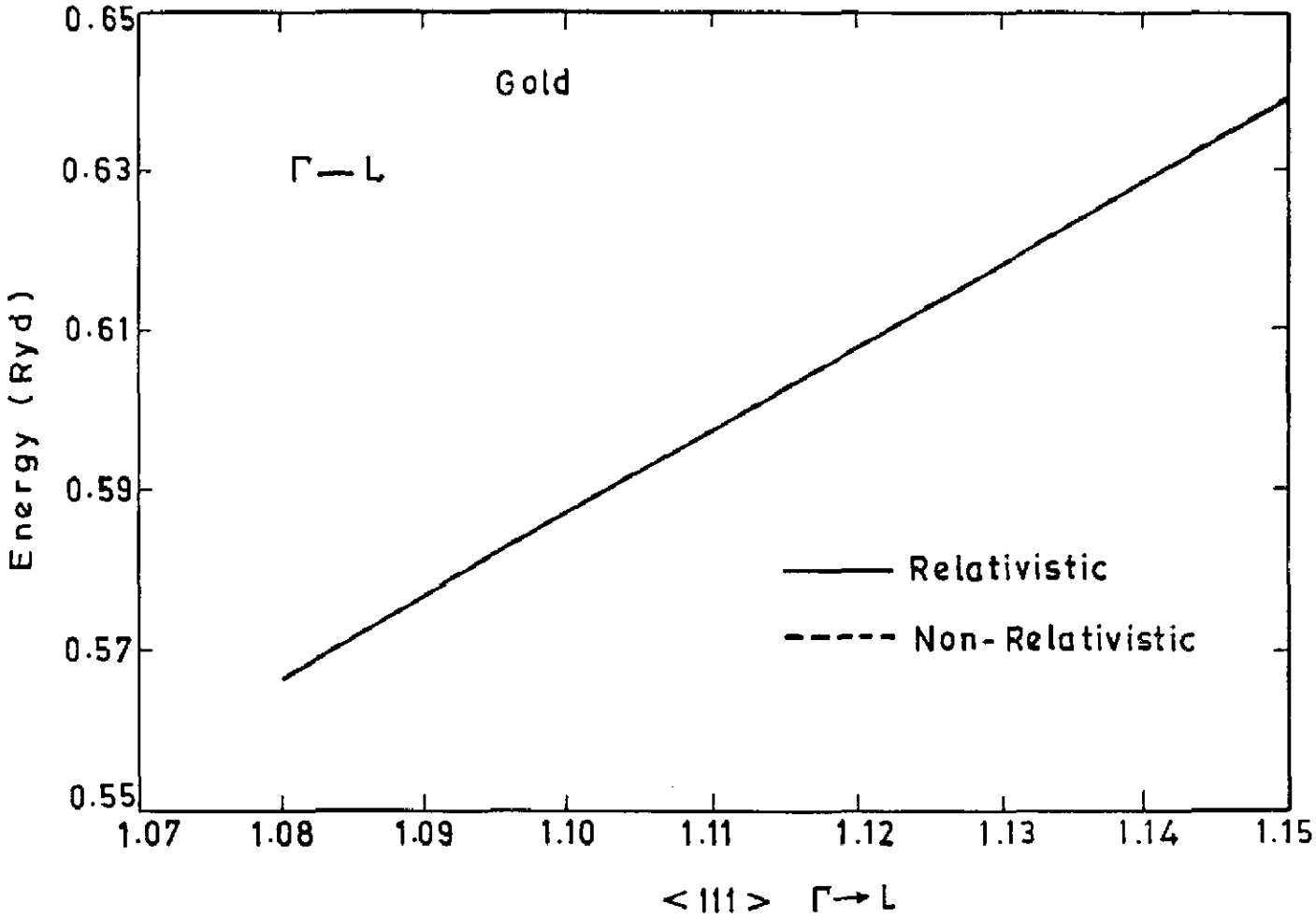
Gold
Γ — L
Relativistic
Non-Relativistic
Energy (Ryd)
0.65
0.63
0.61
0.59
0.57
0.55
1.07
1.08
1.09
1.10
1.11
1.12
1.13
1.14
1.15
< 111 > Γ → L

Fig. 2.10

CHAPTER III

FERMI SURFACE AND MASS ENHANCEMENT FACTOR FOR PALLADIUM AND PLATINUM

The existence in the periodic table of three long periods corresponding to the filling of the 3d ,4d and 5d electronic shells and ending with Ni, Pd and Pt respectively suggests that the properties of these metals correspond to a sizeable d-character in their valence states [82]. The properties of these states result from two factors. In the first place, these states are fairly localized, compared with other (sp) valence states with comparable energy. Cosequently, they are not perturbed very much by the lattice potential and do not overlap strongly with the atomic states of the other atoms. Secondly the d-wave function increases parabolically near the nucleus, which leads to a deficient screening of the nuclear charge with an atom . As a result, the d-states of an atom are filled successively in preference to the sp valence states across the transition series. Thus the transition metals possess a number of interesting properties. These are summarized below :

(1) Large electronic specific heat i.e. high density of states. This suggests a sizeable d-contribution to the density of states at the Fermi level.

(2) Complex Fermi surfaces

(3) Strong evidence of d-band contribution and for s-d scattering at Fermi level, through phonons and impurities.

(4) Regular variation of the cohesive energy through the transition periods with a large maximum for half filled d-states.

(5) Absence of permanent magnetic moment except for metals at the

end of first transition series.

For our study we have Pd and Pt because their FS is more complicated than that of the noble metals and will therefore provide more stringent test of the LMTO method. In early of 80's Dye and his group [74, 75] have given an accurate and complete dHvA measurement for Pd and Pt which leads to meaningful comparison with experiment. Pd and Pt possess outstanding in transition metals because of their unusual properties. They are of interest because of their large paramagnetic susceptibilities and associated magnetic properties, their interesting alloying properties and their importance in catalysis. In view of the wealth of the experimental data on well characterized samples of exceptional quailty, they have received much attention. There have been many theoretical calculations on these two metals and numerous hypotheses proposed concerning them. We have examined only a subset of these properties, namely those directly related to the band structure. Few other propertie of the metals are also discussed in section I for Pd and section II for Pt.

I. PALLADIUM

3.1 INTRODUCTION

In view of the success with which the LMTO method gives the Fermi surface topology of noble metals, it would be worthwhile to perform similar calculations for the transition metal palladium. As palladium possesses a complicated Fermi surface, we believe that the accuracy with which the LMTO can give Fermi surface topologies will be borne out by our results. Pd fascinates both theorists and experimentalists by its unique

electronic behaviour. It has one of the highest densities of states among transition metals, yet is neither magnetic nor superconducting [239]. The absence of ordinary s-wave superconductivity is especially striking since the trends across the transition series [44, 161] suggests that Pd should be superconducting, with a λ value between 0.2 and 0.4 and T_c perhaps as high as 0.3 °K. Direct calculation [167] using the rigid muffin tin approximation gives λ at the top of this range, while proximity effect tunneling measurements [50] suggest λ is near the lower end. In sharp contrast to the bulk, thin films of Pd which have been irradiated with He ions are found to be superconducting at 3°K [215], much higher than expected for bulk single crystals in the absence of paramagnons. Other possibilities for superconductivity and magnetism in thin film and powder geometries have been investigated theoretically by Beal-Monod [29]. The large paramagnetic susceptibility and associated magnetic properties, its affinity to elemental hydrogen and its importance in catalysis are but a few of its many interesting properties.

Alloys of Pd show equally interesting and unusual behaviour. Magnetic impurities raise the susceptibility and induce ferromagnetism at very low concentrations (about 0.1 percent for Fe) with a magnetization per impurity as much as 5 times that for the free impurity atom [66]. Alloying with Hydride and or Deuteride has the opposite effect, lowering the magnetic susceptibility and including superconductivity at concentrations above about 80 percent impurity. T_c in the alloys rises to rather high value of 9°K for the Hydride and 11°K for the Deuteride,

thus showing a strong reverse isotrope effect [151].

Apart from these many interesting properties of Pd, interest has been kept alive due to its complicated Fermi surface as well as the availability of accurate and comprehensive dHvA data on the Fermi surface geometries.The Fermi surface of Pd is one of the most extensively studied Fermi surface among the transition metals. Pd crystallizes in face-centred cubic (FCC) lattice. Its Brillouin zone (BZ) in the reciprocal space is of the form of a truncated octahedron (Fig. 3.1).

The first de Haas-van Alphen (dHvA) oscillations in Pd were observed in 1964 by Vuillemin and Priestly using pulsed field techniques. More detailed studies by field modulation [232, 233] showed a closed electron surface centred at Γ (Fig.3.2) and a set of hole ellipsoids at X (Fig.3.3). Galvanomagnetic studies and a simple rigid band argument [233] suggested a second open hole surface with very high effective mass, topologically equivalent to a set of cylinders along the <100> directions intersecting at the X-point of the BZ (Fig.3.4). The early band structure [17, 18, 157] predicted a Fermi surface consisting of the four sheets : the Γ -centred electron sheet, X-centred and open hole sheets and a very small hole pocket at L. Subsequent dHvA work at fields to 72 KG and temperature to 0.4°K [243] revealed orbits on the first three sheets but failed to show any hint of the small L pockets. The first experimental observation of these pockets (Fig.3.3) came through the ultrasonic attenuation experiments [42]. Dye et al [74] through dHvA experiments using a much higher field and lower temperature than earlier work were able to obtain accurate information on all the

four Fermi sheets of Pd.

3.2 BRIEF SURVEY OF EARLIER WORK

Quantitative studies on palladium, either theoretical or experimental, had a slow start in comparison to studies on other transition metals. Comparatively little was known about either the band structure or the Fermi surface of palladium until the mid sixties, when the first galvanomagnetic and de Haas-van Alphen results [232, 233] giving precise information about a number of features of the Fermi surface began to appear. One of the early band structure calculations on Pd was the APW calculations of Freeman, Dimmock and Furdyna [81]. It was a non relativistic application dealing with the gross features of the energy bands, density of states and Fermi surface topoloty. Mueller et al [157] reported a detailed investigation of the electronic structure of Pd using the APW method. They have also performed calculation including relativistic effects in the context of the interpolation scheme [155] and find that these incluence the eigenvalues at X and L. Their APW calculations gave the main features of the Fermi surface in agreement with the experimental data available at that time. The relativistic calculation predicted sheets centred at L. This was not taken seriously as there was no dHvA evidence for the L-centred pocket. Anderson [18] around the same time performed relativistic APW calculations of the band structure of Pd. He obtained a Fermi surface in agreement with the experimental data. The calculations also predicted hole ellipsods at L for which no dHvA data were available and a small L hole pocket of "dubious" existence. None of these calculations were self-consistent and none of these gave

any reasonable idea of the accuracy of calculated Fermi surface. This was perhaps due to the lack of experimental data.

Skriver et al [197] reported the first self consistent calculation of the band structure using the LMTO method. Calculations were done without and with correction terms. They calculated some extremal orbits on the Pd Fermi surface and obtained good agreement with the experimental data. Dye et al [74] have completed a detailed study of the Fermi surface using the dHvA effect and reported accurate extremal areas on all the four sheets of the Fermi surface including data for the L-centered holes. Using a KKR parametrization Dye et al [74] have been able to deduce extremal areas which they do not measure. They have also measured the effective mass of various Fermi surface orbits and from their KKR fit obtained the electron velocity on the various Fermi surface sheets. Moruzzi et al [153] have also performed self consistent band structure calcuation using KKR method.

Anderson and Mackintosh [17] used the RAPW method to calculate the Fermi surface (effective masses) in fcc transition metals, while Christensen [59] has also used the RAPW method with a muffin-tin potential to calculate the density of states, joint density of states, the imaginary part of the dielectric function and photoemission spectra. However this work did not include the calculation of matrix elements.

MacDonald et al [147] have studied the influence of relativistic contributions to the effective potential on the electronic structure of Pd ,and Pt. They have compared three separate self consistent density functional calculations with (i)

exchange only (ii) exchange and correlation and (iii) exchange and correlation plus relativistic interaction corrections using a relativistic generalisation of the linear APW method. The calculated Fermi surface is compared with the experiment. It was found that correlations had a dramatic effect on the Fermi surface but the relativistic interactions did not have any significant influence on the Fermi surface. MacDonald et al did not obtain good agreement with the open hole surface. It would therefore be interesting to perform self-consistent calculations of the Fermi surface under various approximations of exchange correlation potentials to see if this is indeed the case.

At the same time Smith [200, 202 - 204, 222] reported photoemission spectra and band structure of d-band metals. They have constructed model band structures using a combined interpolation scheme including the spin orbit coupling and other relativistic corrections. Schmidt and Mrosan [183] have calculated the band structure by means of the linear H-NFE-TB method on a grid of 240 $\vec{k}$ points in the irreducible part of the Brillouin zone and treated exchange and correlation in terms of Hedin and Lundquist approach.

Bordoloi and Auluck [35] have used the combined interpolation scheme to parametrize the Fermi surface and optical gaps. This parametrization is valid over a large energy regime and has been used to calculate the dielectric function. Although easy to use and fast on the computer, there are too many parameters needed to obtain a good fit to the Fermi surface. In view of this we have decided to see if the LMTO method could be used to predict the Pd Fermi surface and hence discard any

parametrization scheme.

Recently Chen et al [53] have reported self-consistent, all electron, local density-functional study of the electronic structure of paramagnetic fcc palladium using a linear combination of Gaussian orbitals. Associated with the band structure, they also presented the results obtained for the density of states, Fermi surface, X-ray form factors, compton profiles and optical conductivity.

The harvest on the experimental side in the meanwhile has not altogether been poor. There have been a number of experimental work [42, 222, 232, 233] on the Fermi surface of Pd which have been discussed earlier. Traum and Smith [222] used an angle-integrated photoemission technique to study the electronic structure of polycrystalline Pd films. Dahlbach et al [67] have used angle-resolved photoemission measurements on single crystals of Pd to obtain more detailed information about its band structure. X-ray photoemission spectra (XPS) of Pd have been the subject of study of a number of workers [30, 102, 108, 109, 113, 170, 203, 225]. High resolution photoelectron studies have also been made by Poole et al [171] and quite recently by Anosen and co-workers [21]. XPS studies on Pd have also been done by Podloucky et al [169] who in addition have studied the soft X-ray emission spectra and compton scattering characteristics of the metal.

3.3 CALCULATIONS AND RESULTS

In this section we report calculations of the Fermi surface of Pd using various XC potentials. We have used same

method of calculation as discussed in chapter I. Figure 3.5 shows the intersection of the symmetery planes of the BZ with the Fermi surface of Pd and the band structure obtained by us using Xα-XC potential along symmetry directions is shown in Fig. 3.6. We have calculated ΔE_F for the four FS sheets of Pd i.e. a closed electron surface centred at Γ, a sheet of hole ellipsoidals centred at X and at L and an open hole surface. The open hole surface is of prime importance because it is formed by very flat d-bands and hence supports orbits with high band masses. The hole ellipsoids centred at L are very small and a shift in Fermi energy of around a few mRyd is sufficient to bring them into existence. We have also studied the effect of increasing number of $\vec{k}$ points, including angular momentum expansion up to ℓ=3 and inclusion of relativistic effects. As in the case of the noble metals we find that increase in number of $\vec{k}$ points and use of angular momentum expansion up to ℓ=3 have no significant effect on the results. Here relativistic effects play very important role.

3.3.1 Non-relativistic calculations

We have calculated the FS of Pd using the self-consistent parameters with three XC potentials (i) BH, (ii) BHJ and (iii) VWN. We found that none of these were able to give the existence of the L-centred hole surface. This is in accordance with the results of Mueller [157] and Anderson [18]. The calculated extremal orbits on the other three sheets are in agreement with the experiment. Again we characterize the goodness of the agreement by calculating the shift in the Fermi energy ΔE_F needed to bring the calculated extremal area in agreement with the

experimental area. We obtain the extreme ΔE_F to be 15.3 mRyd (BH), 15.2 mRyd (BHJ) and 17.9 mRyd (VWN) for the three XC potentials. These values of extreme ΔE_F are of the same order of magnitude as obtained for the noble metals [2]. Considering that the Pd FS is rather complex these extreme ΔE_F are to be regarded as indicating fairly good agreement with the experiment.

3.3.2 Relativistic calculations

The major drawback of the nonrelativistic results is non existence of the L-centred hole surfaces. We therefore decided to include relativistic effects as described in chapter I in the LMTO calculations. These relativistic corrections are added in last self-consistent loop in LMTO method. As expected from previous calculations of Mueller et al [157] and Anderson [18], now the L-centred hole surface comes into existence. Table 3.1 gives the extremal areas calculated with four different XC potentials (i) BH, (ii) BHJ, (iii) VWN and (iv) Slater Xα. The extreme ΔE_F for these are 5.7 mRyd (VWN), 9.1 mRyd (BH) and 9.5 mRyd (BHJ) indicating a definite improvement in the agreement with data. The extreme ΔE_F for KKR parametrization [74] is 0.5 mRyd and for interpolation scheme parameterization of Bordoloi [35] is 1.5 mRyd. Hence the extreme ΔE_F of 6 mRyd is to be regarded as good considering that there are no adjustable parameters.

MacDonald et al [147] have calculated FS areas using the RAPW method with exchange and correlation potential. We have calculated ΔE_F for MacDonald et al using their areas. The value of extreme ΔE_F is around 5.4 mRyd which is consistent with our results. Skriver et al [197] have also calculated the FS area of

some orbits and the extreme ΔE_F for these orbits is around 6.8 mRyd. Our results are consistent with Skriver's et al results because of the fact that we are using the same method and the same XC potential. It is indeed very pleasing to note that *ab initio* calulations give accurately the complicated FS such as in Pd. With a view to see if we can do any better, we have varied α in the Xα-XC potential from 0.65 to 0.80. We have plotted ΔE_F versus α in Fig. 3.7. The graph illustrates that α=0.75 gives the best agreement with experimental data. In fact this ΔE_F (4.0 mRyd) is small and comparable to the ΔE_F obtained by Bordoloi and Auluck [35] with the interpolation scheme.

We have also performed calculations to check the effect of increasing $\vec{k}$ points from 240 to 505 in the BZ summation. We have calculated ΔE_F using the VWN-XC potential. The value of the extreme ΔE_F with 505 points is around 6.1 mRyd which is more or less the same as with 240 points. These results are given in Table 3.1. We have also calculated ΔE_F using the angular momentum expansion up to ℓ=3. These calculations are done using the Slater Xα-XC potential with α=0.75. The extreme ΔE_F is around 4.9 mRyd as compared to 4.0 mRyd with ℓ=2 expansion. These results are shown in Table 3.1. We think that this change in ΔE_F is due to the value of α. The value of α may be different for ℓ=3 as compared to ℓ=2. So increasing the $\vec{k}$ points and expansion in angular momentum upto ℓ=3 do not give any significant changes in the extreme ΔE_F.

Thus the RLMTO (with relativistic effects) can give the Pd FS as accurately as the combined interpolation scheme. The KKR parametrization is still far superior. The extreme ΔE_F of 4 mRyd

is about the lowest ΔE_F we obtained for the noble metals [2] (1 mRyd for Ag, 4 mRyd for Cu and 3 mRyd for Au). Considering that the Pd FS is much more complicated, we can say that the agreement for Pd s as good as for the noble metals.

3.4 DYNAMICAL PROPERTIES OF QUASIPARTICLES

3.4.1 Renormalization factor and Fermi velocity

The quasiparticle excitation spectrum $E(\vec{k})$ for an interacting system may be expressed as [145]

$$E(\vec{k}) = E^b(\vec{k}) + \Sigma(\vec{k},E) \qquad (3.1)$$

where $E^b(\vec{k})$ is the bare electron energy as computed from a one electron potential and $\Sigma(\vec{k},E)$ is the proper self-energy which has contributions arising due to electron-electron interaction and electron-phonon interaction. The electron- phonon interaction contributes signifiantly to the self energies of only those quasiparticles whose energies lie within about $\pm\hbar\omega_{max}$ of the Fermi energy, where ω_{max} is the maximum phonon requency [145]. On the other hand, the electron-electron interaction contributes to a comparable extent to the self energies of all electronic states. Within the energy range $\pm\hbar\omega_{max}$ of the Fermi energy, the quasiparticle excitation spectrum as modified by electron-phonon interaction is given by [145]

$$E(\vec{k}) - E_F = (E^b(\vec{k}) - E_F)/ (1 + \lambda_{\vec{k}}) \qquad (3.2)$$

where $\lambda_{\vec{k}}$ is the renormalization constant. It is evident from (3.2) that the electron-phonon interaction does not affect the shape of the Fermi surface but the quantities, such as Fermi velocity and cyclotron mass which involve derivatives of $E(\vec{k})$ at Fermi surface, will be strongly influenced by the electron-phonon

interaction.

The Fermi velocity is given by

$$\vec{v}(\vec{k}) = \frac{1}{\hbar} \vec{\nabla}_{\vec{k}} E(\vec{k}) \qquad (3.3)$$

where $\vec{k}$ lies on the Fermi surface. Using eq. (3.2) and neglecting the $\vec{k}$-dependence of $\lambda_{\vec{k}}$ we get

$$\vec{v}(\vec{k}) = \vec{v}^{o}(\vec{k})/(1 + \lambda_{\vec{k}}) \qquad (3.4)$$

Experimentally one measures the properties of quasiparticles and thus measures $\vec{v}(\vec{k})$. Theoretically one calculates $v^{o}(\vec{k})$

$$v^{o}(\vec{k}) = \frac{1}{\hbar} \vec{\nabla}_{\vec{k}} E^{b}(\vec{k}) \qquad (3.5)$$

Thus eq. (3.4) gives a method of calculation of $\lambda_{\vec{k}}$.

We have calculated Fermi velocities using Xα-XC potential with α= 0.75 (which gives best fit to the experimental data) $v^{o}(\vec{k}) = |v^{o}(\vec{k})|$ for $\vec{k}$ lying on the FS for all the four Fermi sheets of Pd. The results are shown in Figures 3.8 - 3.11. The band Fermi velocity obtained by MacDonald et al [147] obtained using LAPW method and enhanced Fermi velocity by Dye et al [74] obtained by inverting the mass data using the KKR parametrization are also plotted in Figures 3.8 to 3.11 for comparison. The figures reveal a striking similarity of the general trends. For the Γ - centred sheet (Fig.3.8), our $v^{o}(\vec{k})$'s reveal a trend more in conformity to the results of MacDonald et al than those of Dye et al. Our calculated $v^{o}(\vec{k})$'s are in general smaller than those obtained by MacDonald et al but are largr than the ones obtained by Dye et al. Thus we expect our $(1 + \lambda_{\vec{k}})$ to have value intermediate between the values obtained by these workers. The values of $v(\vec{k})$ and $(1 + \lambda_{\vec{k}})$ obtained by us and other workers are

given in Table 3.2. We find that $\lambda_{\vec{k}}$ is highly anisotropic and varies from sheet to sheet. Our values of $(1 + \lambda_{\vec{k}})$ are greater than that obtained by Bordoloi and Auluck [37] and smaller than that obtained by the MacDonald et al.

3.4.2 Cyclotron masses

In the cyclotron resonance experiment one measures the frequency of resonance for the quasiparticles orbiting the FS. From this one can obtain the cyclotron mass m_c of the FS orbits. Using the value of m_c given by

$$m_c = \frac{\hbar}{2\pi} \oint_{orb.} \frac{d\vec{k}}{v_\perp(\vec{k})} \tag{3.6}$$

and eq.(3.4) one can write

$$m_c = \int_{orb.} \frac{1 + \lambda_{\vec{k}}}{v^o_\perp(\vec{k})} d\vec{k} \tag{3.7}$$

where $v^o_\perp(\vec{k})$ is the component of $v^o(\vec{k})$ normal to the orbit and in a plane of the orbit. Since one does not know $\lambda_{\vec{k}}$ one calculates band mass m_b

$$m_b = \int_{orb.} \frac{1}{v^o_\perp(\vec{k})} d\vec{k} \tag{3.8}$$

Because of the renormalization due to electron-phonon interaction m_c will be larger than m_b . A comparison of the two yields orbital mass enhancement factor $1 + \lambda_c$

$$1 + \lambda_c = \frac{m_c}{m_b} \tag{3.9}$$

We have calculated the band masses of different FS extremal orbits listed in Table 3.3. The band masses are calculated using $X\alpha$ - XC potential with α= 0.75. The values of experimental masses calculated by Dye et al along with $(1 + \lambda_c)$ for different orbits

are also given. We have compared our results with those of Bordoloi and Auluck [37] and Schmidt and Mrosan [183] where former has calculated the masses using the interpolation scheme while later have calculated cyclotron masses using the band structure obtained from the H-NFE-TB method. Our values of $(1 + \lambda_c)$ more closer to the values of Schmidt and Mrosan than in comparison to Bordoloi and Auluck.

3.4.3 Thermal Mass and Mass Renormalization

Since $\lambda_{\vec{k}}$ as well as λ_c are anisotropic over the entire Fermi surface, it is therefore useful to have a value λ_γ which is a value of $\lambda_{\vec{k}}$ averaged over the entire Fermi surface. Information on λ_γ can be obtained from the low temperature specific heat data. Thermal effective mass is a measure of low temperature specific heat of the conduction electrons in a metal and can be calculated from a knowledge of the density of states at the Fermi energy. The thermal mass is defined as [65]

$$\frac{m_{th}}{m_o} = \frac{N(E_F)}{N_o} \qquad (3.10)$$

where $N(E_F)$ is the density of states at the Fermi energy given by

$$N(E_F) = \frac{1}{(2\pi)^3} \int \frac{dS}{|\nabla_{\vec{k}} E(\vec{k})|_{E(\vec{k})=E_F}}$$

$$= \frac{1}{(2\pi)^3} \frac{1}{\hbar} \int_a \frac{dS}{|V(\vec{k})|} \qquad (3.11)$$

where we have used Eq. (3.3). Here 'a' signifies that the surface integration extends over the available Fermi surface areas.

$N(E_F)$ can further be written as

$$N(E_F) = \frac{S_F}{(2\pi)^3} \cdot \frac{1}{\hbar} \left\langle \frac{1}{|\, v(\vec{k}) \,|} \right\rangle \qquad (3.12)$$

where

$$\langle \text{------} \rangle = \frac{\int_a dS \text{-----}}{\int_a dS}$$

and $S_F = \int_a dS$ is the available Fermi surface area. N_o in Eq. (3.10) is the density of states at the Fermi energy corresponding to free electron model.

$$N_o = \frac{m_o k_F^o}{2\pi^2 \hbar^2} \qquad (3.13)$$

where

$$k_F^o = (3\pi^2 n_v)^{1/3}$$

Here n_v is the number of conduction electrons per unit volume. Now if we write

$$v_F^o = \hbar k_F^o / m_o$$

and

$$S_F^o = 4 \pi (k_F^o)^2$$

we get

$$N_o = \frac{S_F^o}{(2\pi)^3 \hbar v_F^o} \qquad (3.14)$$

Using eqs. (3.4), (3,10), (3.12) and (3.14), we can now write

$$\frac{m_{th}}{m_o} = \frac{S_F v_F^o}{S_F^o} \left\langle \frac{1 + \lambda_{\vec{k}}}{v^o(\vec{k})} \right\rangle \qquad (3.15)$$

Theoretically one ignores $\lambda_{\vec{k}}$ in the calculation of thermal mass and thus gets a lower value than obtained from experiment. On comparison, one then obtains

$$1 + \lambda_\gamma = \frac{(m_{th})_{expt.}}{(m_{th})_{calc.}} \qquad (3.16)$$

from equations (3.7), (3.9), (3.15) and (3.16) we see that $\lambda_{\vec{k}}$, λ_c and λ_γ are related to each other provided we assume that the same interactions manifest in all these experiments.

One need not calculate the thermal mass from a band model as such, but can follow an alternative way to calculate $(1 + \lambda_\gamma)$. We see from Eqs. (3.10) and (3.16) that $(1 + \lambda_\gamma)$ can be expressed as

$$1 + \lambda_\gamma = \frac{[\, N(E_F) \,]_{expt.}}{[\, N(E_F) \,]_{calc.}} \qquad (3.17)$$

$$= \frac{(m_{th})_{expt.}}{(m_{th})_{calc.}}$$

Here $N(E_F)$ is the density of states (DOS) at the Fermi energy calculated from the low temperature specific heat constant γ. If one also determines the DOS at E_F from a band model, then Eq. (3.17) provides a way of calculating $1 + \lambda_\gamma$.

The electronic heat capacity (at constant volume), $C_{e\ell}$ is given by

$$C_{e\ell} = \gamma T$$

$$= \frac{\pi^2}{3} k_B^2 N(E_F) T \qquad (3.18)$$

where k_B is the Boltzmann's constant and T is the Kelvin temperature. The experimental value of $N(E_F)$ then easily follows from this relation.

The linear specific heat coefficient γ has been measured by numerous workers. Table 3.4 summarizes the data of γ and also gives the value of $N(E_F)_{expt.}$ which have been calculated using Eq. (3.18). We have also calculated the density of states $N(E_F)$ from our RLMTO calculation with Xα-XC (α= 0.75) potential and find $N(E_F)_{calc.}$ = 1.20 states/eV-atom-spin. The variation in the reported values of γ appears to be largely due to the purity of the sample of Pd under study. We have therefore used a representative value 9.42 mJ $mole^{-1}deg^{-2}$ for γ to calculate the experimental value of $N(E_F)$. If we take an average γ corresponding to the more recent specific heat data, we get $1 + \lambda_\gamma = 1.68$, which agree well with the values of $(1 + \lambda_c)$ and $(1 + \lambda_{\vec{k}})$. The value of $(1 + \lambda_\gamma)$ obtained by different workers are also given in Table 3.5. Our values are nearly the same as most of other workers because all have used *ab-initio* methods. Except for the work of Anderson [18] and Knapp et al [129], no calculation of $(1 + \lambda_\gamma)$ has been explicitly reported by others workers.

3.5 CONCLUSIONS

In conclusion, the FS obtained using LMTO/RLMTO is in agreement with the available experimental data. The FS velocity for all the four sheets are in agreement with the band velocities of MacDonald et al [147] and the enhanced velocities of Dye et al. [74]. The enhancement factors calculated by three different ways are consistent with each other. It is also in agreement with results of most of the other workers. Bordoloi and Auluck obtained [37] a lower enhancement factor because in trying to fit the FS data they have absorbed a part of the enhancement factor.

II. PLATINUM

3.6 INTRODUCTION

A glance at periodic table of elements shows that Platinum (Pt) which has atomic number 78, is a metal of the fcc group belonging to the heavier 5d transition metal series. The interest in the Fermi Surface (FS) of Platinum has been kept alive because of its increasing tendency towards ferromagnetism and simultaneous disapperance of superconductivity through the sequence of the 4d and 5d transition metals Ir, Rh, Pt and Pd [116]. Several years ago it was suggested that a new type of excitation was important in nearly ferromagnetic systems; these are the so called paramagnon or short-lived spin fluctuations arising out of strong exchange interactions among the d-electrons and thought to be playing a significant role in producing mass enhancement [31, 73, 184]. In Pt the paramagnon enhancement may be the dominant contribution. The success with which the Linear Muffin Tin Orbital (LMTO) method gives the Fermi surface (FS) topology of noble metals [2] prompted us to perform calculations for transition metals Pd [3] and Pt. These metals possess a complicated FS and we believe that the accuracy with which the LMTO method can give FS topologies will be borne out by our results. For the above reasons Pt is worthy of an especially intense effort to understand its electronic properties. The intersections of the symmetry planes of the BZ with the FS of Pt are shown in Fig. 3.12. Pt is characterized by three Fermi sheets : the Γ-centred electron surface, the X-centred hole ellipsoids and the open hole surface. The small L-centred hole pockets are not observed in Pt. One of the earliest de Haas-van Alphen (dHvA)

measurement in Pt was by Stafleu and de Vroomen [211] who in 1965 recorded the existence of the small ellipsoids indentified with regions of holes at X. Ketterson et al [125] subsequently found two further sets of dHvA oscillations corresponding to the Γ-centred and open hole sheets, respectively. dHvA measurements on the extremal areas of the FS of Pt were carried further by Ketterson and Windmiller [126]. Dye et al [75] in 1978 reported more extremal orbits on the open hole surface with heavier mass, centred at Γ and X for the magnetic field along the [100] and [110] directions.

Theoretical studies, ab initio or otherwise, on the band structure and FS properties of Pt have not in the meanwhile been lagging behind. The relativistic augmented plane wave (RAPW) calculations of Mackintosh, and Anderson [17, 18], the relativistic Korringa-Kohn-Rostoker (RKKR) approaches of John et al [118] and Ketterson et al [124] and phase-shift parametrization work of Shaw et al [188] are a few examples of such studies. The work of Friedel et al [83], Mueller et al [155, 158] and of Smith and his coworkers [200, 202 - 204, 222] have also contributed greatly towards this theoretical understanding. Smith and his coworkers have been following the techinique of using the interpolation scheme to obtain the band structure adjusted to their own photoemission data. Bordoloi and Auluck [36] have used the combined interpolation scheme to parametrize the Fermi surface and optical gaps. Although this scheme is easy to use and fast on the computer, it needs many parameters and hence one can not extract any useful information from such calculations.

Using a relativistic non-muffin-tin, Korringa-Kohn-Rostoker formalism, Dye et al [75] have been able to calculated the extremal areas for the various orbits by the parmetrization techinque. They have used nine extermal areas and masses with different field directions. While fitting the measured masses, Dye et al have absorbed the many-body enhancement into the phase shift derivatives. By combining the parameters obtained from the extremal area fits and the phase shift derivatives, the Fermi velocity is computed and compared with the experimental velocity. They have also calculated the enhancement factor obtained from these velocities. MacDonald et al [147] have studied the influence of relativistic contributions to the effective potential on the electronic structure of Pd and Pt. They have compared three separate self-consistent density functional calculations with (i) exchange only (ii) exchange and correlation and (iii) exchange and correlations plus relativistic interaction correction using RAPW method. The comparison of these three show that relativistic corrections are significant in the case of Pt but the non-muffin terms included with much effort are less important.

3.7 CALCULATIONS AND RESULTS

As we discussed above, the FS of Pt consists of three sheets (Fig.3.12) i.e. a closed electronic surface centred at Γ, a sheet of hole centred at X and an open hole surface. The band struture obtained by us along symmetry directions of the BZ using Slater Xα-XC potential is shown in Fig. 3.13. We have calculated extremal areas for the three FS sheets and studied the effect of (i) various exchange correlation (XC) potentials such as von

Barth-Hedin (BH), Slater Xα, Barth-Hedin modified by Janak (BHJ) and Vosko Wilk and Nussair (VWN) approximated by different workers (ii) including angular momentum expansion up to ℓ=3 (iii) increasing the number of $\vec{k}$ points in the irreducible Brillouin zone (BZ) summations and (iv) inclusion of relativistic effects. From our calculations we observe that increasing the number of $\vec{k}$ points and inclusion of angular momentum expansion up to ℓ=3 does not affect FS areas for Pt. Keeping this in mind, we have done all calculations with 240 $\vec{k}$ points and angular momentum expansion up to ℓ=2.

3.7.1 Non-relativistic calculations

We have calculated FS areas using BH, BHJ, VWN XC potentials. We find that non-relativistic calculations with none of the above said exchanges give the existance of open hole orbit β<110>. We have adopted a different criteria to determine how good the agreement with experiment is by calculating ΔE_F. We obtained an extreme ΔE_F of 40.7 mRyd (BH), 42.0 mRyd (BHJ) and 39.6 mRyd (VWN) XC potentials. Thus the extreme ΔE_F is very large compared to the noble metals. As is clear from the work on Pd, it is necessary to include relativistic corrections.

3.7.2 Relativistic calculations

Since the non-relativistic calculations give large ΔE_F ,non existance of the orbit β<110> and also because the relativistic effects play important role in elements with large Z, we included relativistic corrections in our calculations. We observe that this results in favourable changes and in drastic improvement when comparison is made with the experimental data.

Now we obtained an extreme ΔE_F of 9.0 mRyd (BH), 9.0 mRyd (BHJ) and 8.0 mRyd (VWN) XC potentials. These results are shown in Table 3.6. For Slater Xα XC we have varied the values of α from 0.65 to 0.85. The variation of ΔE_F with α is shown in Fig. 3.14. From the figure we find that α=0.815 gives the best agreement with the experimental data. We find that ΔE_F in this case is around 2.7 mRyd which is comparable to ΔE_F of Dye et al [75] (0.6 mRyd), Bordoloi and Auluck [36] (1.6) and MacDonald et al [147] (4.1 mRyd).

To see the effect of increasing the number of $\vec{k}$ points from 240 to 505 in the BZ summation, we find that the extreme ΔE_F using Xα XC potential is now around the same as with 240 $\vec{k}$ points. Hence an increase in number of $\vec{k}$ points i.e. use of a finer mesh in the BZ does not affect the FS areas. We studied the effect of using angular momentum expansion up to ℓ=3, the ΔE_F now comes around 3 mRyd (Xα-XC) as compared to 2.7 mRyd (Xα-XC) with ℓ=2. So we find that increasing the number of $\vec{k}$ points and angular momentum expansion up to ℓ=3 do not have any significant effect on the extreme ΔE_F . Hence the relativistic LMTO method can give as accurate a prediction of the FS as obtained by the combined interpolation scheme. The KKR parametrization is still in better agreement with experiment, however we must bear in mind that ours is a first principles method which is certainly superior to parametrization techniques.

3.8 DYNAMICAL PROPERTIES OF QUASIPARTICLESB

The linear specific heat coefficient γ has been measured by number of workers (for a survey see Bordoloi) [34]. Some of the values are listed in Table 3.7. We have used the Slater Xα-XC

with the value of α=0.815, as discussed in preceding section to calculate $N(E_F)$. By calculating $N_\gamma(E_F)$ from specific heat data, we have compared this $N(E_F)$ from our calculations. The value of $(1+\lambda_\gamma)$ obtained by different workers are given in Table 3.7 along with our values. We find that our value of $(1+\lambda_\gamma)$ is 1.19 which is lowest among the given results (1.22 to 1.63).

We have calculated the enhancement factor$(1+\lambda_c)$using cylotron data for different FS orbits. We have calculated the band masses for these orbits using Slater Xα-XC and experimential cyclotron mass from Dye et al [75] are used.We have listed $(1+\lambda_c)$ in the Table 3.8 and find that our results are consistent with the results of Bordoloi and Auluck [37] and Smith [202].

Mass enhancement factor from electron velocites are reported in Table 3.9. The Fermi velocities obtained for the three Fermi sheets are plotted in Figs. 3.15-3.17. The Fermi velocites obtained by Watson-Yang et al [238] and Dye et al [75] are also shown for comparison. The calulations of the former have been on the basis of first principle RAPW warped muffin-tin method, while those of latter are results of RKKR fitting scheme. The Figures 3.13, 3.14and 3.15 reveal a general trend in our calculated Fermi velocities similar to either of above mentioned calculations. The values of $(1+\lambda_{\vec{k}})$ obtained by us and other workers listed in Table 3.9. Our results are consistent with those from Bordoloi and Auluck [37], Watson-Yang et al [238] and of Dye et al [75].

3.9 CONCLUSIONS

The results of the calculated FS of Pt using LMTO method are

given in the section II of this chapter. We studied the effect of (i) various XC potentials (ii) inclusion of relativistic effects (iii) increasing the number of $\vec{k}$ points in BZ summations and (iv) including angular momentum expansion up to ℓ=3 on our results. We observe that first two effects play an important role in topology of the FS of Pt. Inclusion of relativisitic effects reduces the extreme ΔE_F by a factor of five. The choice of XC-potential is also important. The extreme ΔE_F with 240 $\vec{k}$ points and angular momentum expansion up to ℓ=2 is around 9.0 mRyd using BH, BHJ and VWN-XC potential but the Slater $X\alpha$ with α=0.815 gives extreme ΔE_F of 2.7 mRyd which is one third in comparison to other exchanges. This is because we are using an adjustable parameter α. We also find that the effect of increasing no. of $\vec{k}$ points from 240 to 505 and including angular momentum expansion up to ℓ=3 do *not affect the extreme* ΔE_F. *Hence we conclude that all these* effects are not important for studying the FS topology of Pt. We have calculated the Fermi velocites and enhancement factor λ using the Slater $X\alpha$ (α=0.815) potential. The enhancement factor calculated using band masses, specific heat data and electron velocities are consistent with other results as well as with each other.

TABLE 3. 1

ΔE_F using different XC potentials (ΔE_F in mRyd.)

Field Direction	Experimental Area(at.units) (a)	using VWN XC	using BH XC	using BHJ XC	using Xα-XC α=0.75	using VWN-XC 505 pts.	using Xα-XC F-band
L-Center							
<111>LKW	0.005090	0.1	-0.3	-0.4	-0.1	0.4	1.4
<111>	0.007804	-0.1	-0.6	-0.6	-0.2	-1.5	-0.03
<110>LKΓ	0.008782	1.4	-2.3	-2.3	-1.6	-1.8	-0.8
<100>	0.006137	0.5	-1.1	-1.2	-0.6	-0.8	0.1
<110>	0.005806	0.1	-0.1	-0.1	0.1	-0.1	0.7
X-Center							
<100>XWU	0.01529	2.1	2.0	2.0	2.0	1.8	2.1
<010>XWΓ	0.02376	2.0	3.0	3.1	2.4	1.7	2.6
<110>XUΓ	0.02387	2.0	3.1	3.1	2.4	1.8	2.6
<110>	0.01839	2.1	2.3	2.3	2.2	1.8	2.4
<111>	0.02005	-0.5	-1.1	-1.1	-0.7	-0.8	-0.7
Γ-Center							
<100>	0.7312	5.0	-3.5	-3.7	1.6	4.8	-0.3
<111>	0.6480	3.4	-2.2	-2.3	1.1	3.1	-0.1
<110>	0.8265	5.2	-6.1	-6.4	0.7	5.3	-2.3
Open hole							
<100>α	0.07190	0.1	1.0	1.0	0.5	-0.1	0.1
<100>ε	1.969[b]	0.4	0.9	0.9	0.7	0.2	0.2
<110>β	0.308[b]	0.2	1.2	1.2	0.5	-0.2	1.7
<110>γ	0.2018	-0.2	0.2	0.7	0.4	-0.1	0.9
<111>β	0.2326	1.1	1.9	1.9	1.4	0.8	1.3
Extreme ΔE_F		5.7	9.1	9.5	4.0	6.1	4.9

[a] Reference 74

[b] Reference 74 [KKR fit]

TABLE 3. 2

Mass enhancement factor $1 + \lambda_k$ for Pd (Fermi velocities are in Ryd)

Surface	Direction	Exp. $\lvert v_k \rvert$ (a)	Enhancement		
			Present calculation	MacDonald et al (b)	Bordoloi & Auluck (c)
Electron	Γ - X	0.602	1.868	2.13	1.58
	Γ - L	0.603	1.666	1.81	1.62
	Γ - K	0.555	1.225	1.46	1.05
X-Pockets	X - Γ	0.139	1.708	1.91	1.14
	X - K	0.239	1.610	1.66	1.22
	X - W	0.255	1.578	1.59	1.20
L-Pockets	L - Γ	0.096	0.937	1.54	0.80
	L - K	0.105	1.152	1.35	1.08
	L - W	0.104	1.115	1.34	1.08
Open hole	Γ - X	0.233	1.190	1.33	1.08
	Γ - K	0.126	1.388	1.71	1.25
	X - K	0.127	1.358	1.70	1.18

[a] Reference 74

[b] Reference 147

[c] Reference 37

TABLE 3.3

Mass enhancement factor $(1+\lambda_c)$ for Pd

Field Direction	Expt. m_c (a)	Enhancement $(1+\lambda_c)$		
		Present Calculation	Bordoloi & Auluck (c)	Schmidt & Mrosan (d)
Γ-Center				
<100>	2.02	1.44	1.28	1.58
<110>	2.30	1.59	1.45	1.62
<111>	1.96	1.36	1.26	1.63
X-Center				
<100>XWU	-0.63	1.57	1.41	1.58
<110>XUΓ	-1.03	1.63	1.25	1.38
<110>	-0.78	1.63	1.38	
<111>	-0.87	1.93	1.42	1.23
L-Center				
<110>LKΓ	-1.21	1.92	1.41	
Open hole				
<100>ε	10.96[b]	1.65	1.36	1.63
<110>β	-12.77[b]	1.22	1.14	1.32
<111>β	-5.7	1.26	1.09	
<110>α	-2.4	1.66	1.49	1.42

[a]Reference 74

[b]Reference 74 [KKR fit]

[c]Reference 37

[d]Reference 183

TABLE 3. 4

The electronic specific heat constant γ and density of states (calculated from γ) for Pd

Reference	Temperature range (K)	Purity (% Pd)	γ (mJ mole^{-1}K^{-2})	N (E_F) States/atom eV-spin
Rayne [179]	1.5 - 4.1	99.999 99.98	9.87 ± 0.11 9.64 ± 0.08	2.117 ± 0.02 2.068 ± 0.02
Hoare et al [106]	1.8 - 4.2	99.99	9.31 ± 0.05	1.997 ± 0.01
Mackliet et al [148]	1.5 - 4.2	99.95	9.385 ± 0.035	2.012
Veal et al [226]	1.4 - 100	99.99	9.42 ± 0.02	2.021
Chouteau et al [54]	0.3 - 3	?	9.40 ± 0.05	2.016 ± 0.01
Smith et al [205]	1 - 4.2	?	9.43 ± 0.02	2.023
Boerstoel et al [33]	1.2 - 30	99.999	9.45 ± 0.03	2.027
Knapp et al [129]	-	-	9.2	1.974
Mizutani et al [152]	Liquid He	99.991	9.48 ± 0.01	2.034

TABLE 3. 5

Many-body mass enhancement factor $(1 + \lambda_\gamma)$ for Pd calculated from low temperature specific heat data (γ in mJ/mol/K and DOS in states/eV atom spin)

References	Theoretical method	Expt. value used	Calculated value	DOS exp.	DOS calculated	$1+\lambda_\gamma$
Andersen[a]	RAPW	9.42	5.67			1.66
Andersen & Mackintosh[b]	RAPW	9.42		2.02	1.18	1.71
Christensen[c]	RAPW	9.42		2.02	1.18	1.71
Knapp & Jones[d]	sp. heat	9.2	5.5			1.7
MacDonald et al[e]	LAPW	9.42		2.02	1.28	1.58
Muller et al[f]	RAPW	9.42		2.02	1.14	1.77
Bordoloi & Auluck[g]	interpolation	9.42		2.02	1.48	1.36
Present calculation	RLMTO	9.42		2.02	1.20	1.68

[a]Reference 18 [b]Reference 17 [c]Reference 59 [d]Reference 129

[e]Reference 147 [f]Reference 157 [g]Reference 37

TABLE 3. 6

ΔE_F for Pt using different XC potentials (in mRyd)

Field Direction	Expt.[a] Area (a.u.)	using BH-XC	using BHJ-XC	using Xα-XC α=0.815	using VWN-XC
Γ-Centered					
<100>	0.770	-2.0	-2.0	1.7	2.0
<110>	0.857	-3.0	-3.0	1.3	0.0
<111>	0.687	-2.0	-2.0	2.4	3.0
X-Centered					
<100>XWU	.00298	6.0	6.0	0.8	8.0
<110>	.00467	4.0	4.0	-0.3	4.0
Open Hole					
<100>ε	1.890	1.0	1.0	2.3	6.0
<110>β	0.341	2.0	2.0	0.6	3.0
<100>α	0.074	2.0	2.0	0.9	4.0
Extreme ΔE_F		9.0	9.0	2.7	8.0

[a]Reference 75

TABLE 3. 7

Many body enhancement factor ($1+\lambda_\gamma$) for Pt caculated from low temperature specific heat data. γ is in mJ/mole/ k and DOS is in states/eV-atom-spin

References	Theortical Method	Expt. value used	Calc. value	DOS Expt.	DOS Calc.	$1+\lambda_\gamma$
Anderson (a)	RAPW	6.56	4.02			1.63
Knapp & Jones (b)	Sp.Heat	6.70	4.10			1.60
MacDonald et al (c)	LAPW	6.54		1.403	0.92	1.53
Bordoloi & Auluck (d)	Interpolat -ion	6.54		1.403	1.15	1.22
Present Calculation	RLMTO	6.54		1.403	1.18	1.19

[a]Reference 18

[b]Reference 129

[c]Reference 147

[d]Reference 37

TABLE 3. 8

Mass Enhancement Factor $1+\lambda_c$ For Pt

Field Direction	Expt. m_c (a)	Enhancement Factor $1+\lambda_c$		
		Our Calculation	Bordoloi &Auluck (b)	Smith (c)
Γ- Centered Electron				
<100>	2.44	1.37	1.30	1.50
<110>	3.16	1.36	1.32	1.52
<111>	2.06	1.30	1.26	1.42
X-Centered Hole				
<100>XWU	-0.272	1.01	1.18	0.85
<110>	-0.426	1.33	1.47	1.09
Open Hole				
<100>α	-1.53	1.42	1.30	1.29

[a]Reference 75

[b]Reference 37

[c]Reference 202

TABLE 3. 9

Mass Enhancement Factor $(1+\lambda_{\vec{k}})$ for Pt

(Fermi velocities are in Ryd)

Surface	Direction	Expt. $\lvert V_k \rvert$ (a)	Enhancement factor $1+\lambda_{\vec{k}}$			
			Our Calculation	Watson-Yang et al [b]	Bordoloi Auluck [c]	Dye et al [d]
Electron	Γ -X	0.266	1.39	1.50	1.35	1.50
	Γ -L	0.217	1.22	1.43	1.09	1.43
	Γ -K	0.485	1.46	1.53	1.31	1.53
X Pocket	X -Γ	0.150	1.20	1.38	1.12	1.38
	X -K	0.219	1.14	1.36	1.26	1.36
	X -W	0.218	1.15	1.38	1.26	1.38
Open Hole	Γ -X	0.555	1.72	1.54	1.99	1.54
	Γ -K	0.178	1.53	1.69	1.38	1.69

[a] Reference 75

[b] Reference 238

[c] Reference 37

[d] Reference 75

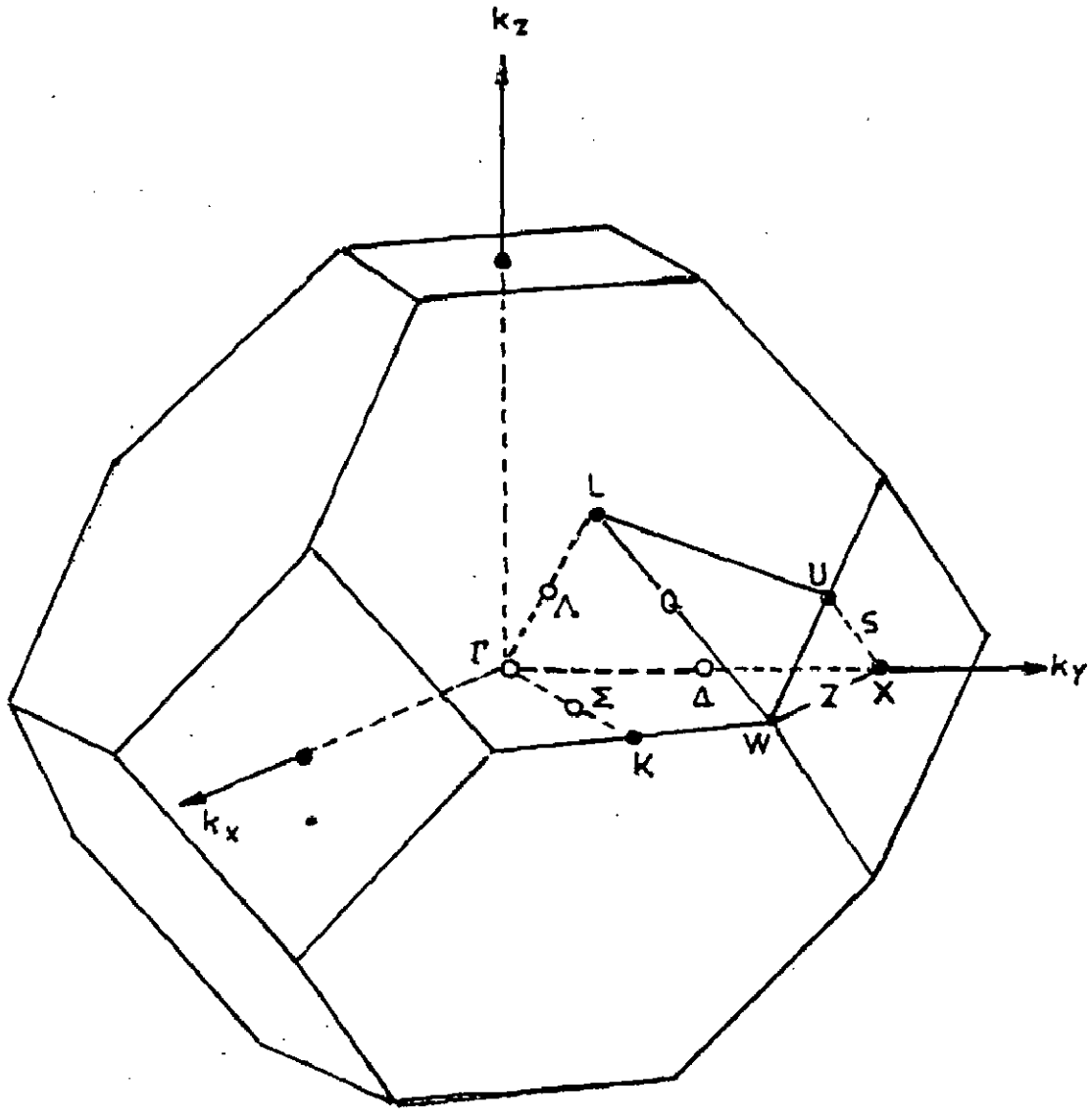

FIG. 3·1

The Brillouin zone of the fcc lattice, showing the symmetry point designations

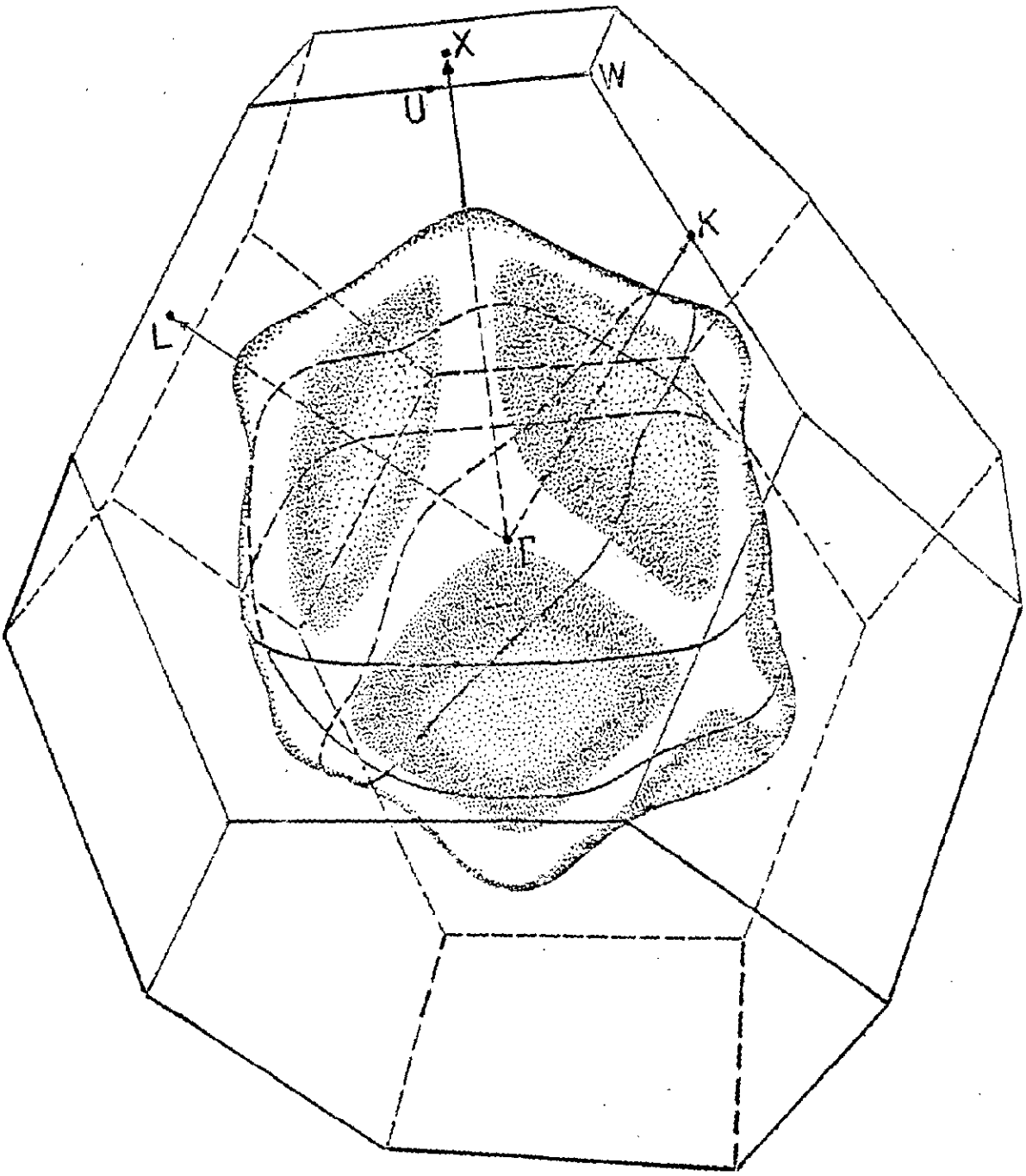

Fig. 3.2

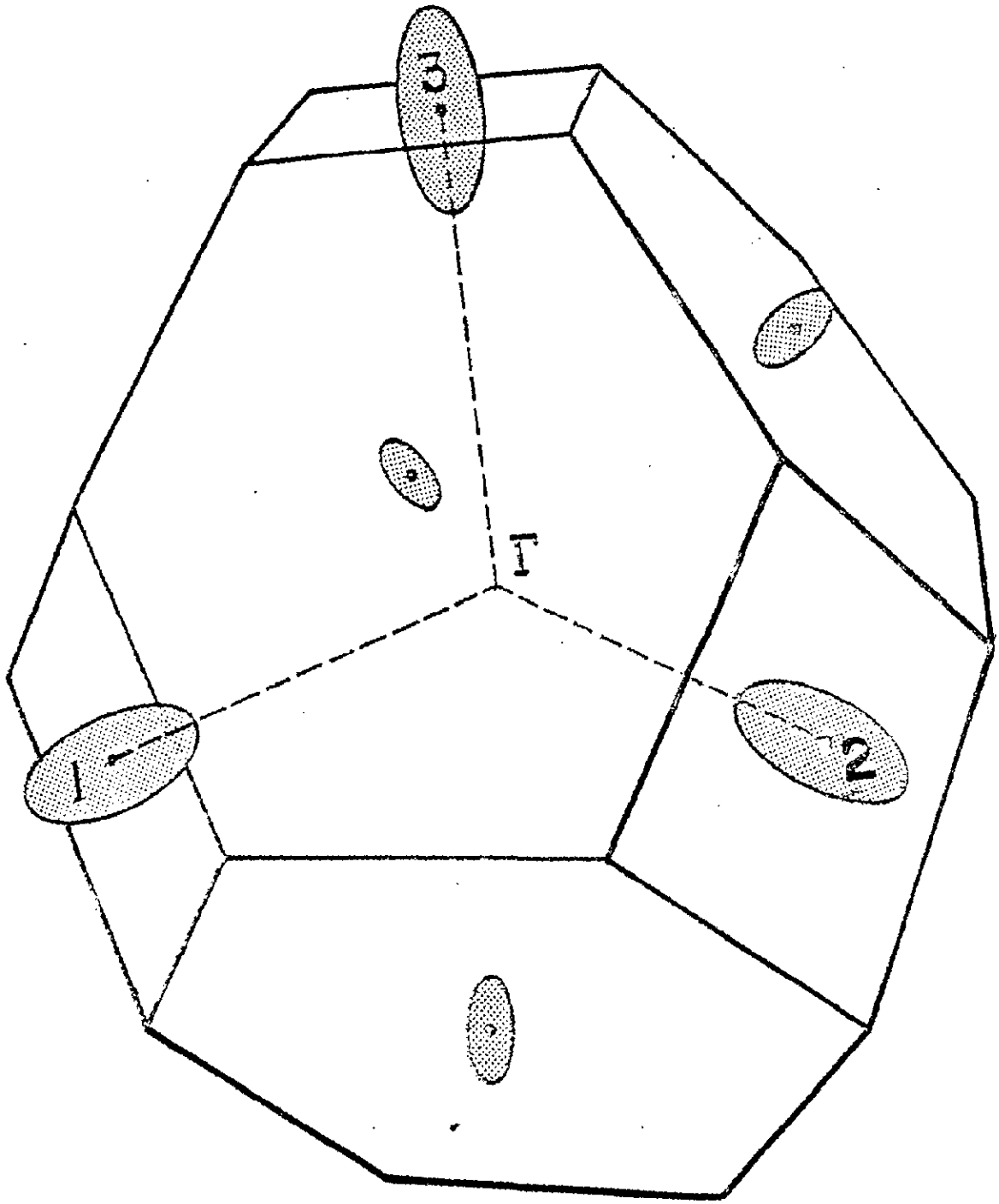

FIG. 3·3

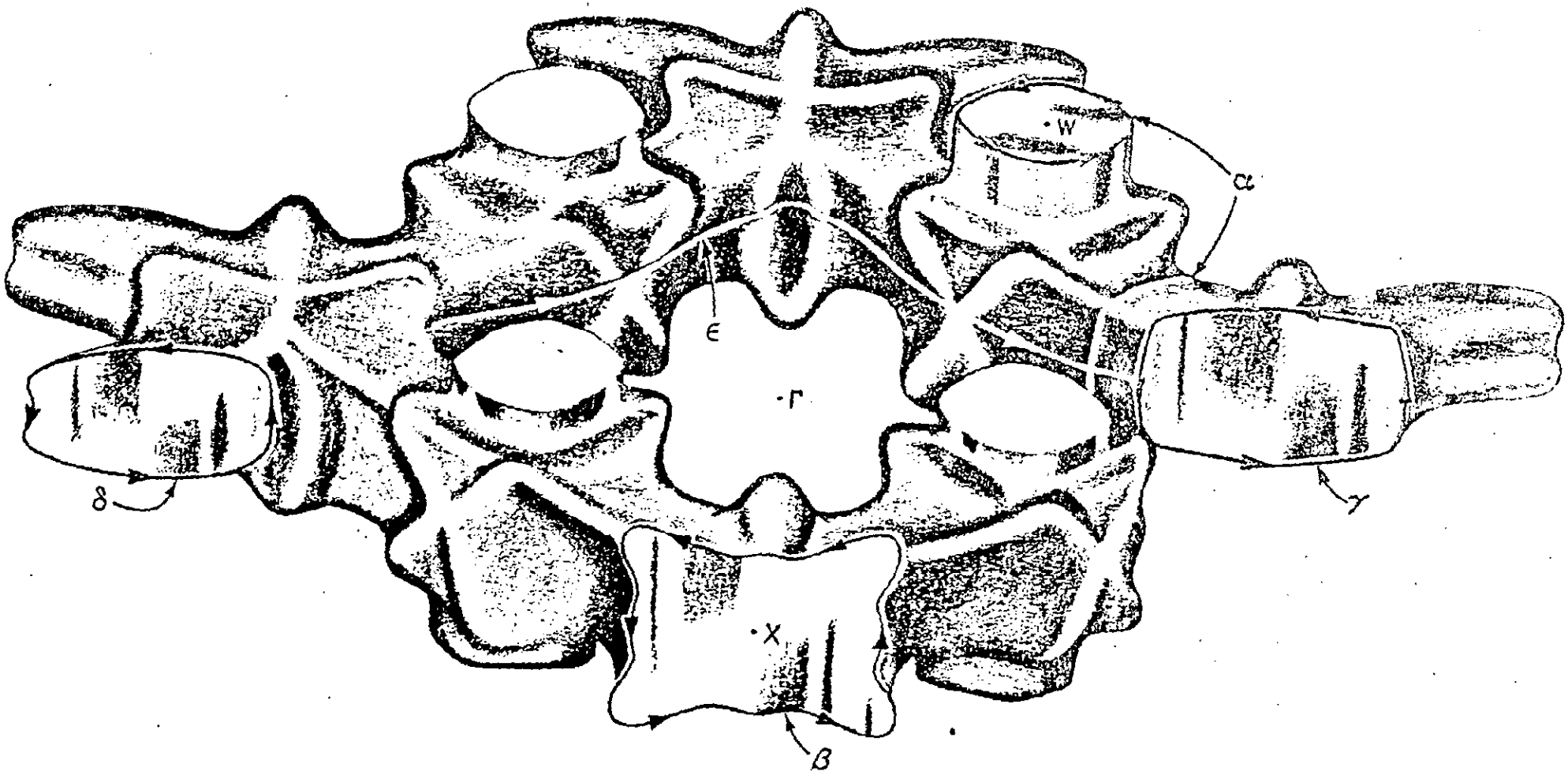

FIG. 3-4

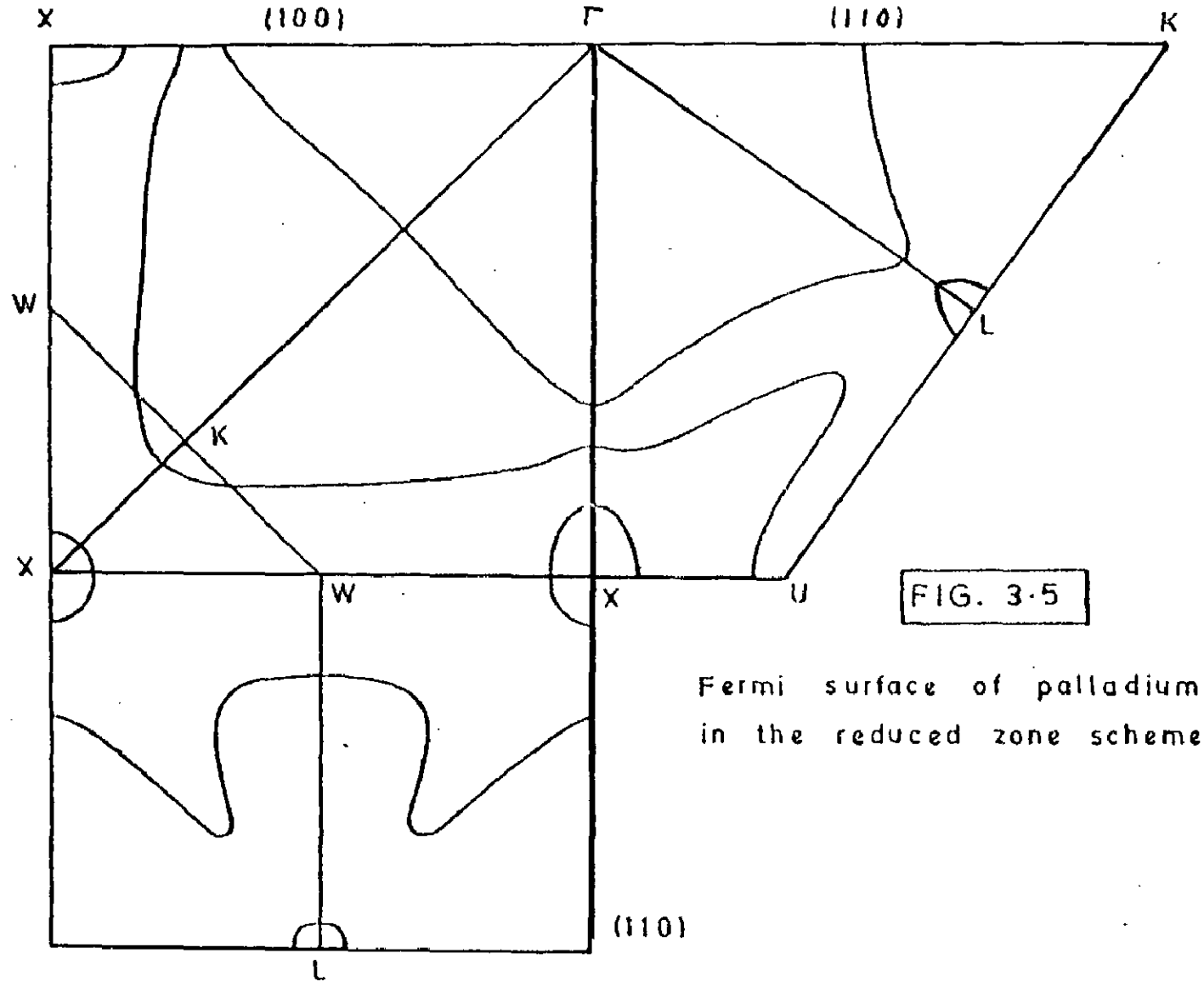

FIG. 3·5

Fermi surface of palladium in the reduced zone scheme

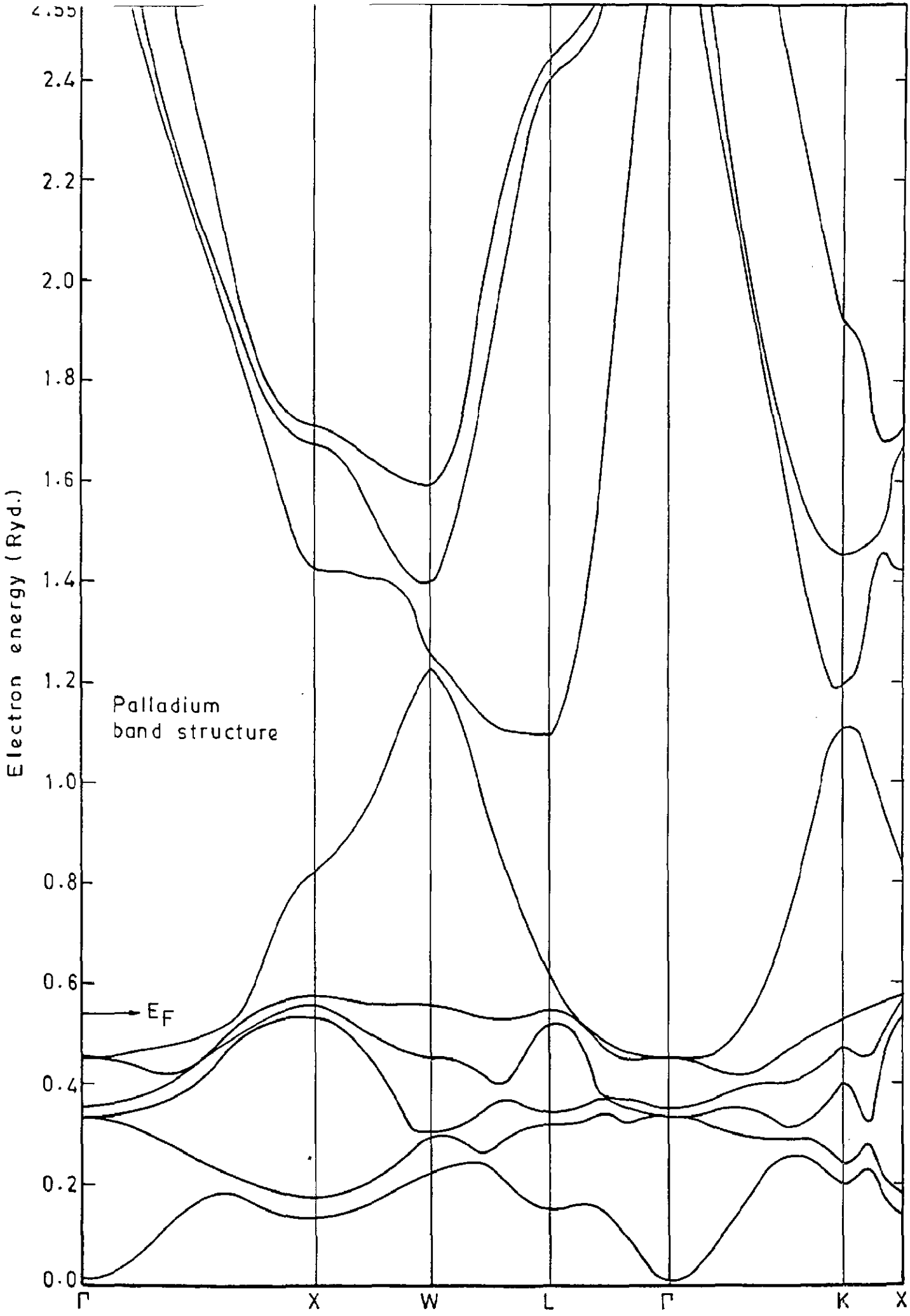
Electron energy (Ryd.)
2.4
2.2
2.0
1.8
1.6
1.4
1.2
1.0
0.8
0.6
0.4
0.2
0.0
Palladium
band structure
E_F
Γ
X
W
L
Γ
K
X

Fig. 3.6

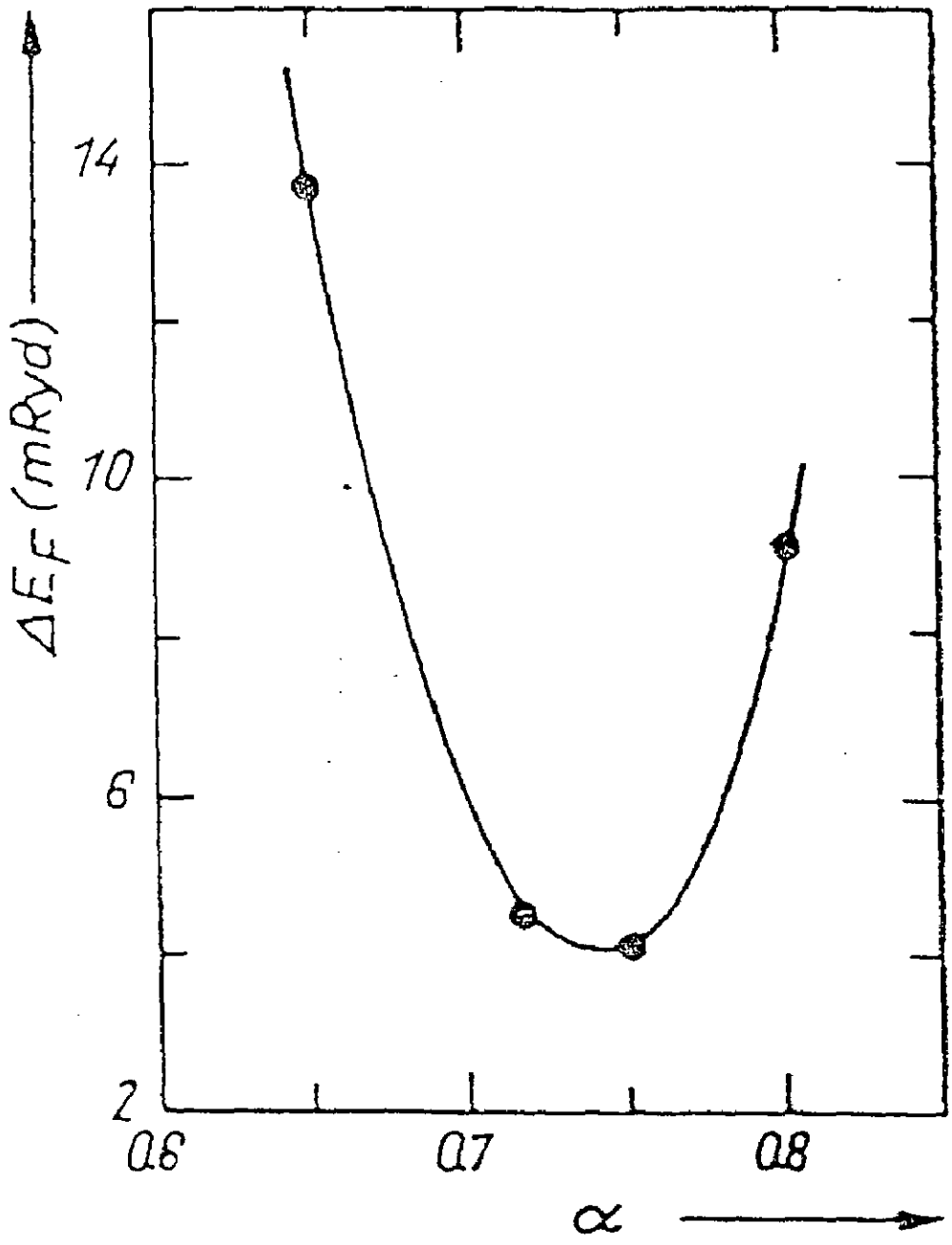

Fig. 3.7

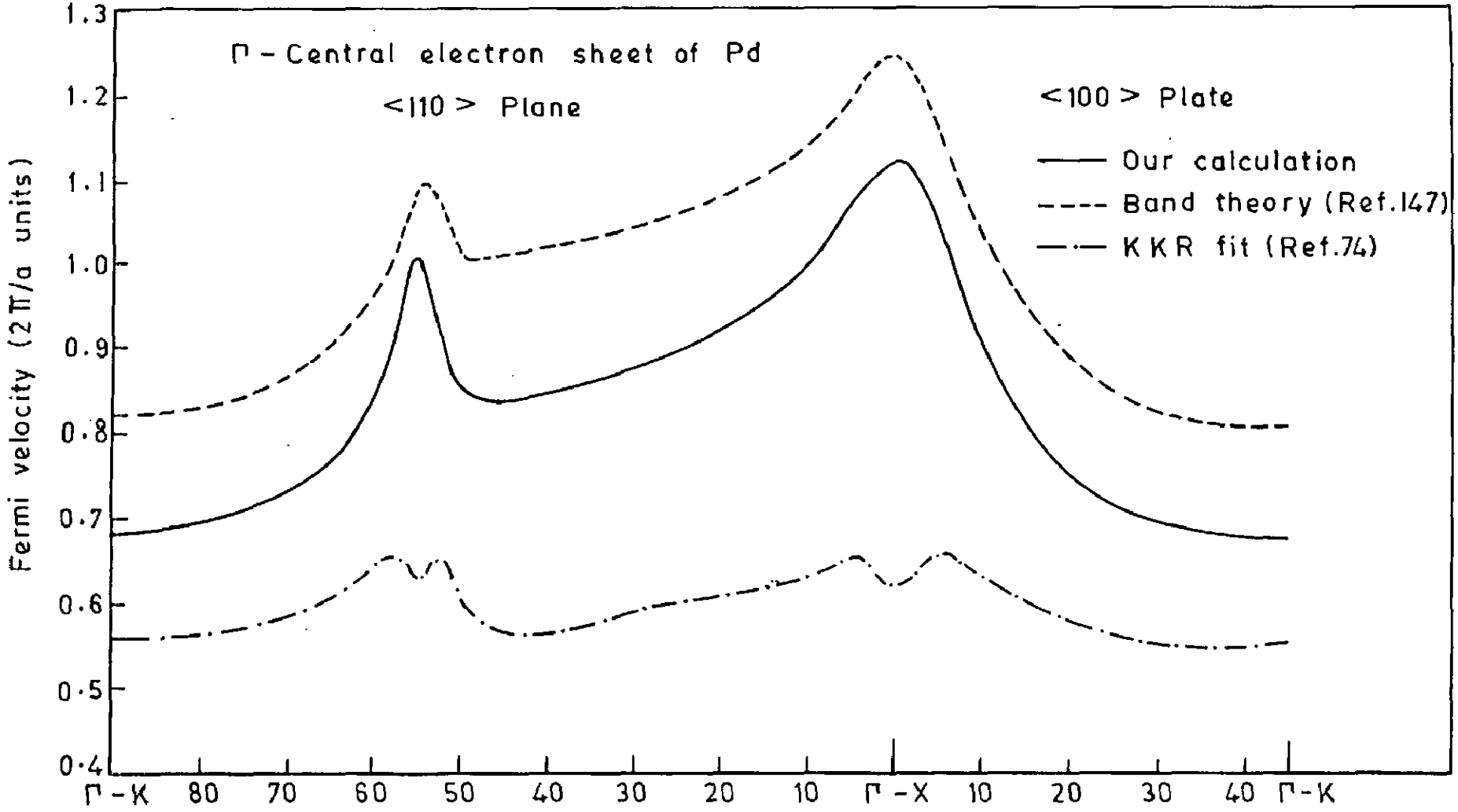
Γ - Central electron sheet of Pd
<110> Plane
<100> Plate
Our calculation
Band theory (Ref.147)
KKR fit (Ref.74)
Fermi velocity (2π/a units)
1.3
1.2
1.1
1.0
0.9
0.8
0.7
0.6
0.5
0.4
Γ - K
80
70
60
50
40
30
20
10
Γ - X
10
20
30
40
Γ - K

Fig. 3.8

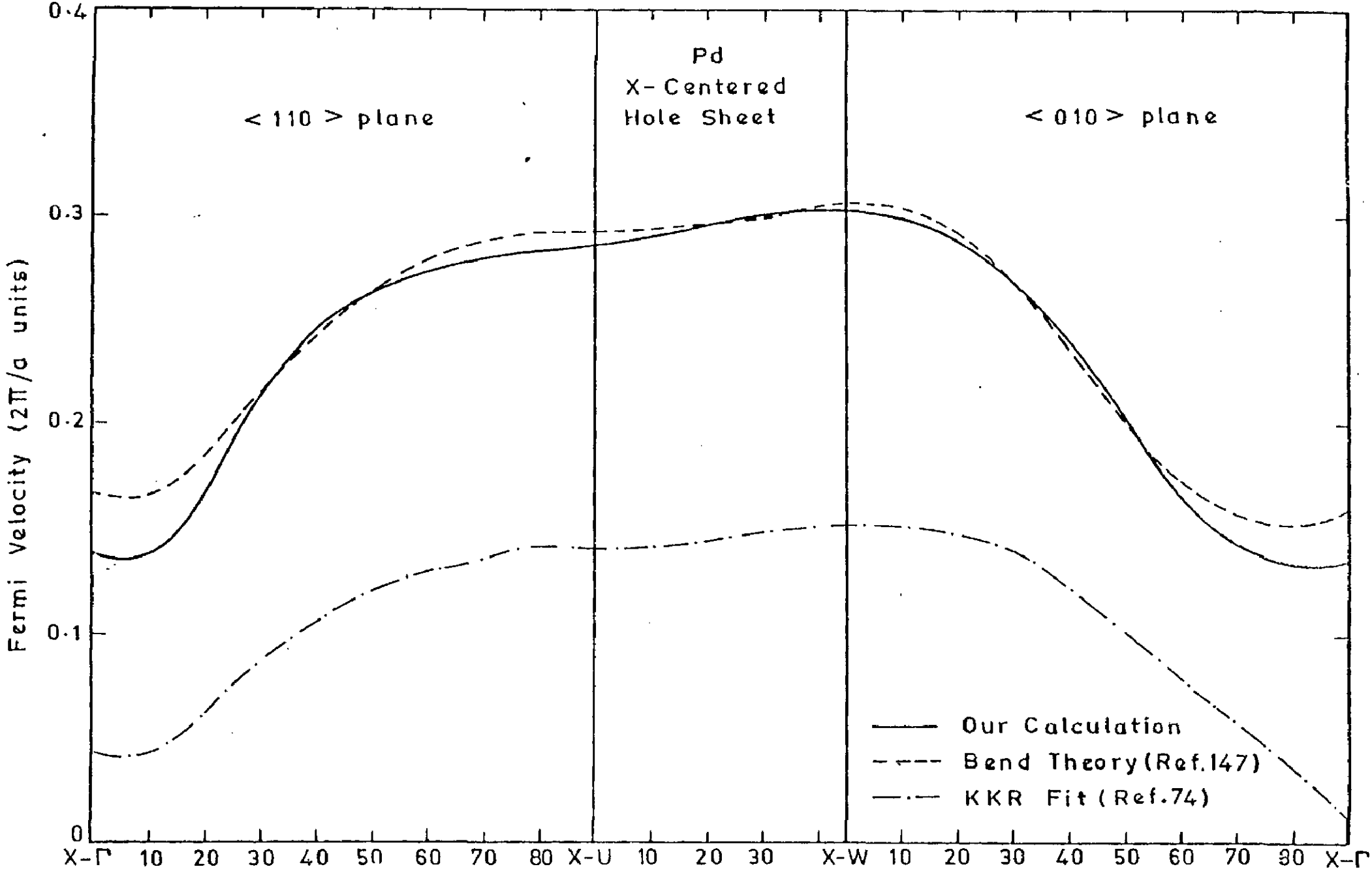
Pd
X-Centered
Hole Sheet
< 110 > plane
< 010 > plane
Fermi Velocity (2π/a units)
0·4
0·3
0·2
0·1
0
X-Γ 10 20 30 40 50 60 70 80 X-U 10 20 30 X-W 10 20 30 40 50 60 70 80 X-Γ
Our Calculation
Bend Theory (Ref.147)
KKR Fit (Ref.74)

Fig. 3.9

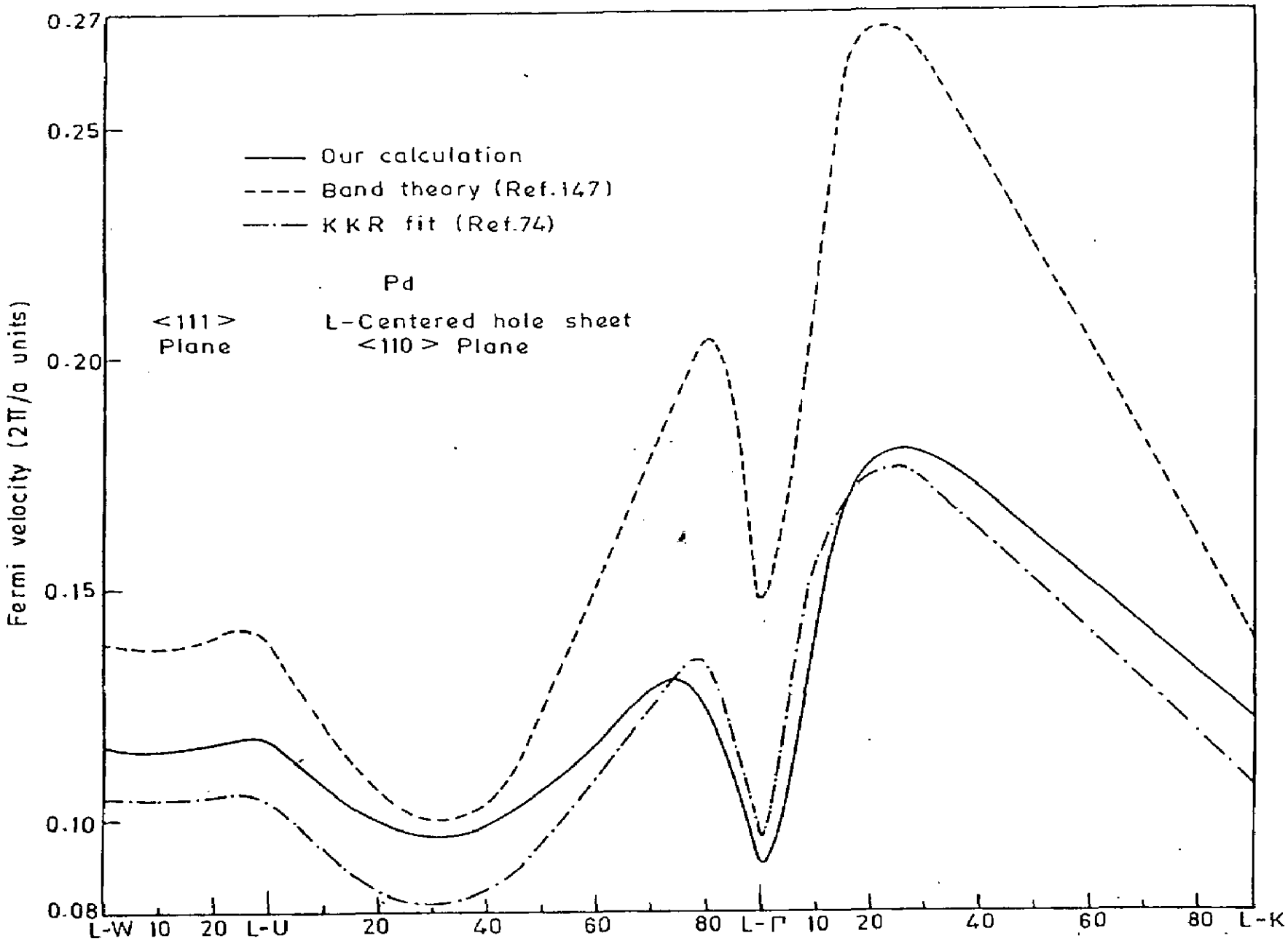
0.27
0.25
0.20
0.15
0.10
0.08
Fermi velocity (2π/a units)
Our calculation
Band theory (Ref.147)
KKR fit (Ref.74)
Pd
<111> Plane
L-Centered hole sheet
<110> Plane
L-W 10 20 L-U 20 40 60 80 L-Γ 10 20 40 60 80 L-K

Fig. 3.10

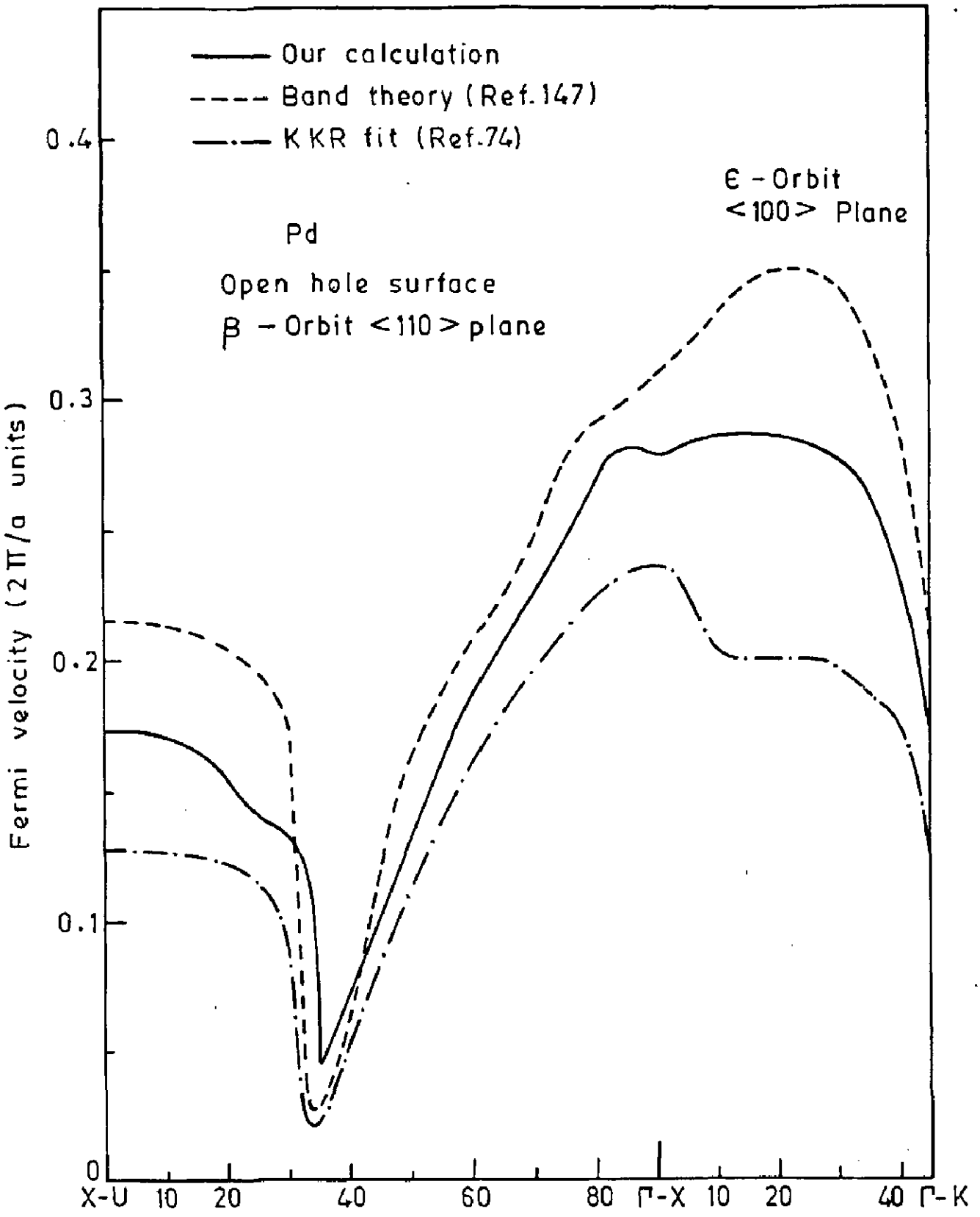
Our calculation
Band theory (Ref.147)
KKR fit (Ref.74)
Pd
Open hole surface
β - Orbit <110> plane
ϵ - Orbit
<100> Plane
Fermi velocity (2π/a units)
0.4
0.3
0.2
0.1
0
X-U
10
20
40
60
80
Γ-X
10
20
40
Γ-K

Fig. 3.11

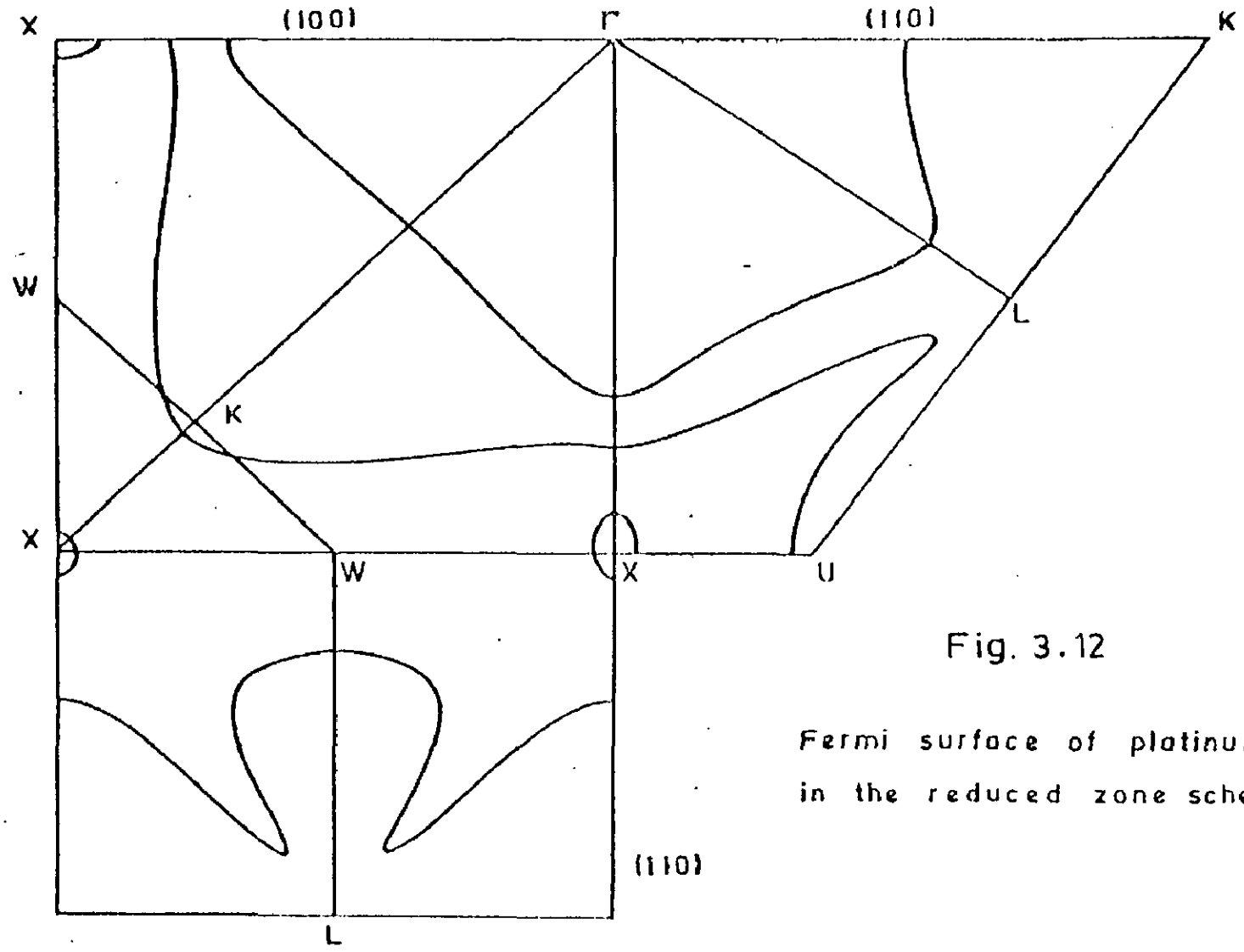

Fig. 3.12

Fermi surface of platinum in the reduced zone scheme

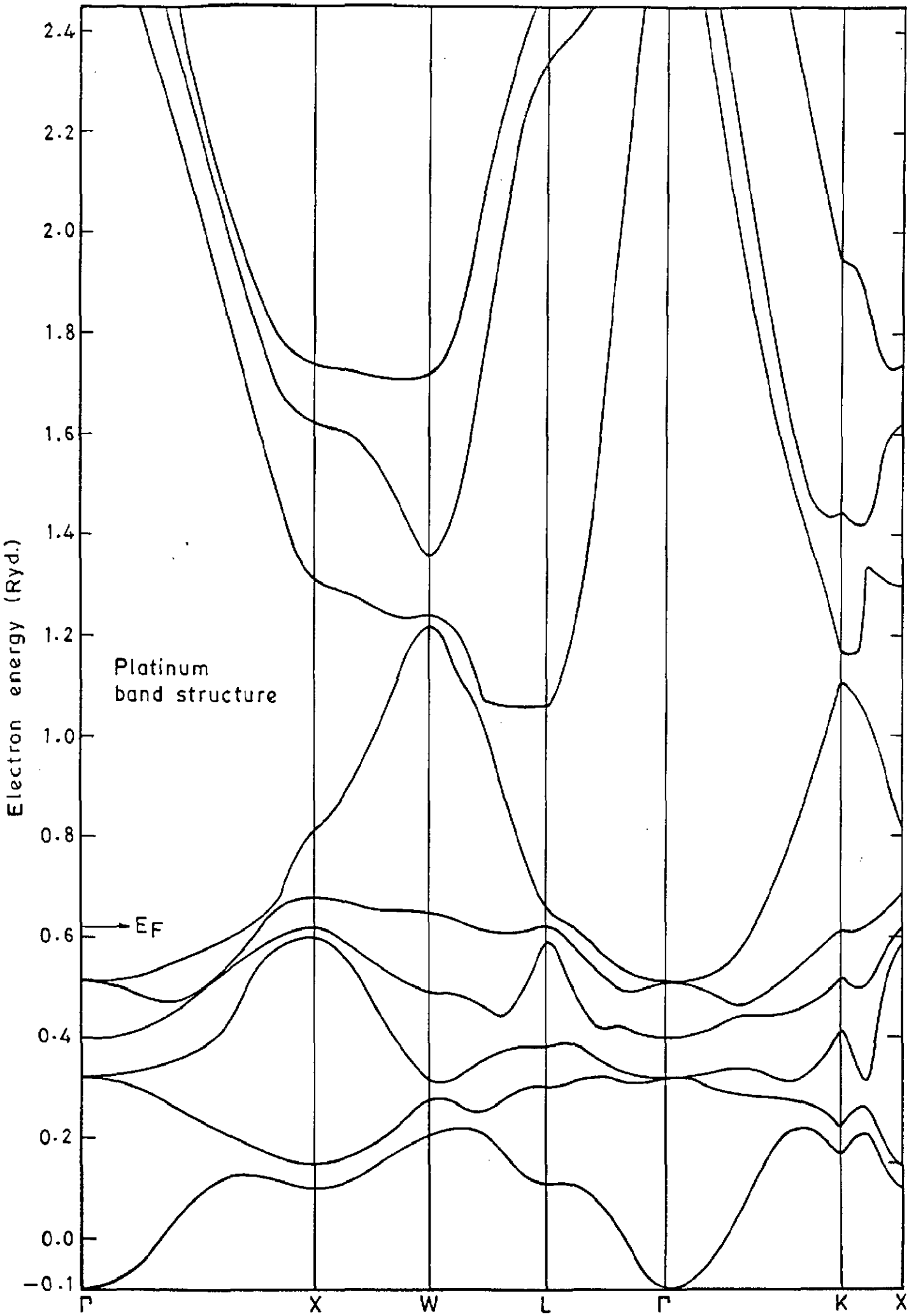
Platinum
band structure
Electron energy (Ryd.)
2.4
2.2
2.0
1.8
1.6
1.4
1.2
1.0
0.8
0.6
0.4
0.2
0.0
−0.1
E_F
Γ
X
W
L
Γ
K
X

Fig. 3.13

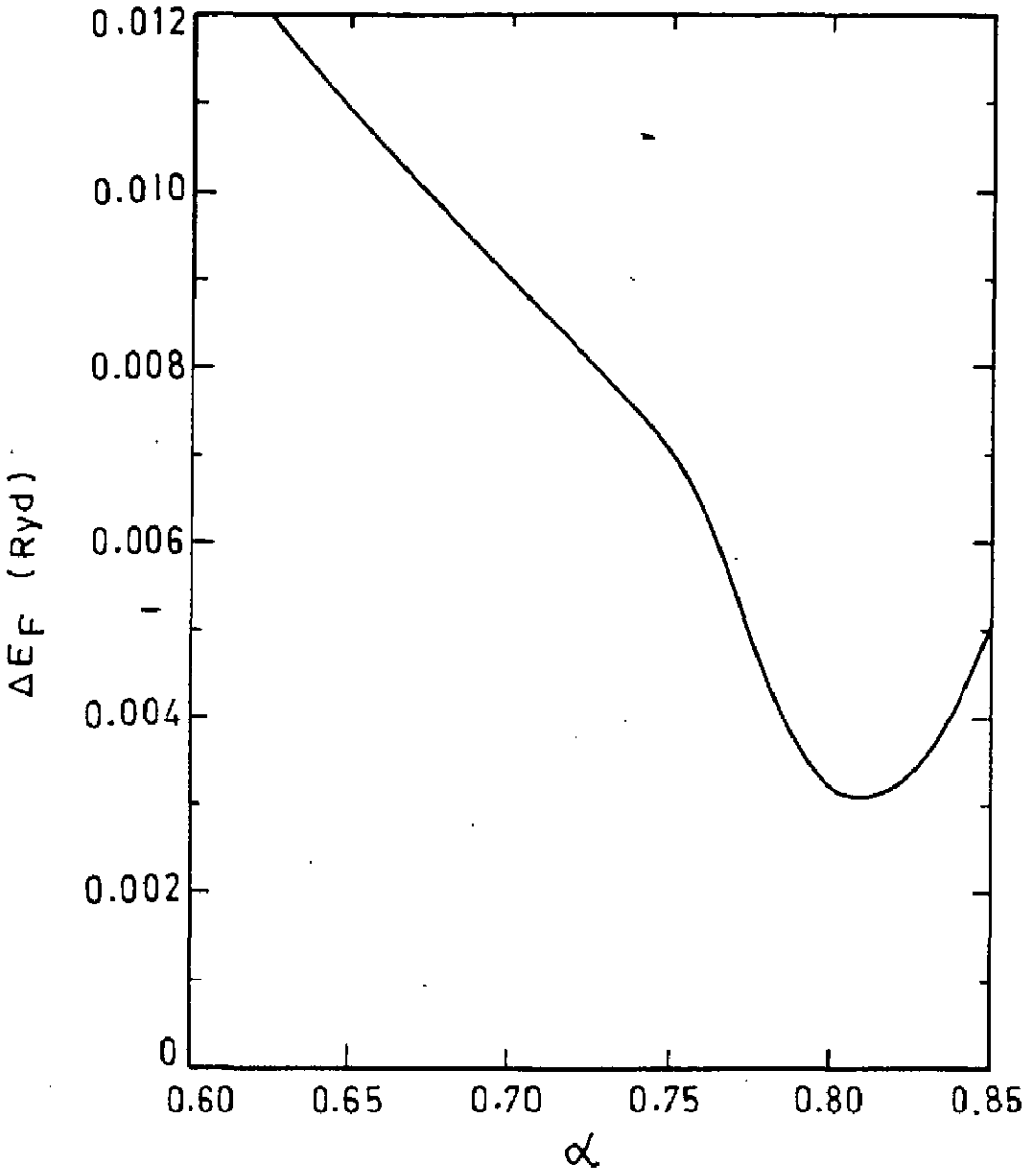
0.012
0.010
0.008
0.006
0.004
0.002
0
ΔE_F (Ryd)
0.60
0.65
0.70
0.75
0.80
0.85
α

Fig. 3.14

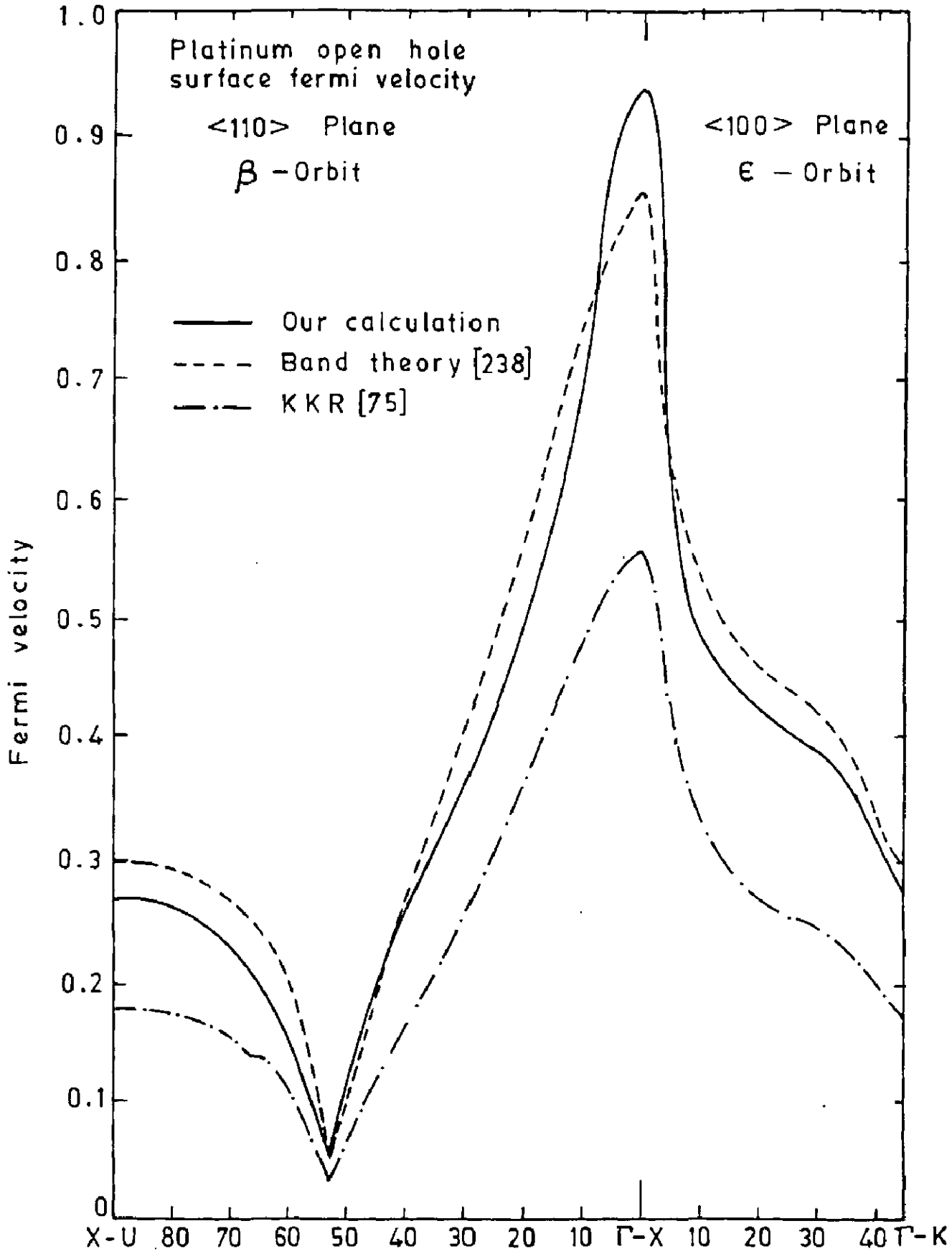
Platinum open hole
surface fermi velocity
<110> Plane
β -Orbit
<100> Plane
ϵ -Orbit
Our calculation
Band theory [238]
K K R [75]
Fermi velocity
1.0
0.9
0.8
0.7
0.6
0.5
0.4
0.3
0.2
0.1
0
X-U 80 70 60 50 40 30 20 10 Γ-X 10 20 30 40 Γ-K

Fig. 3.15

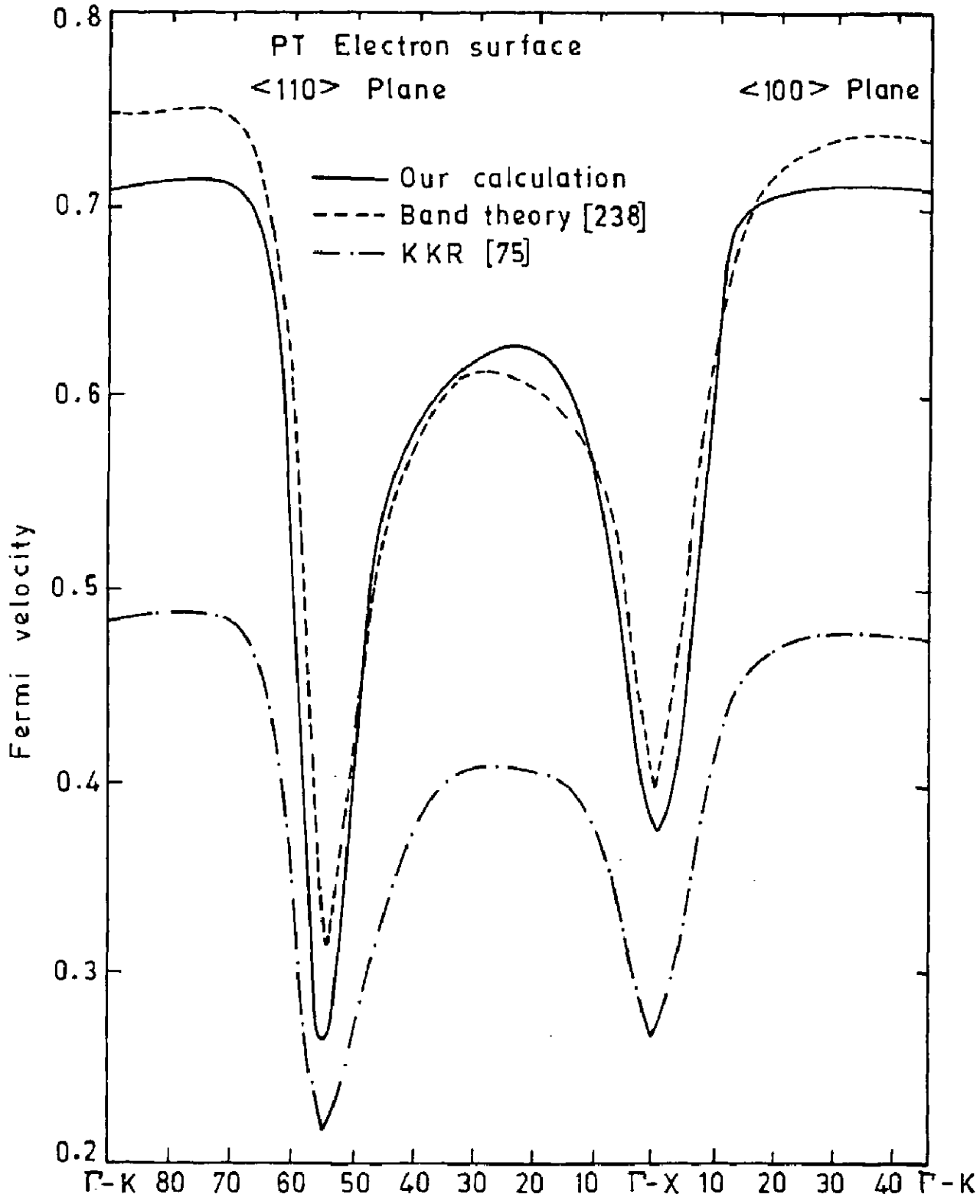
PT Electron surface
<110> Plane
<100> Plane
Our calculation
Band theory [238]
KKR [75]
Fermi velocity
0.8
0.7
0.6
0.5
0.4
0.3
0.2
Γ-K 80 70 60 50 40 30 20 10 Γ-X 10 20 30 40 Γ-K

Fig. 3.16

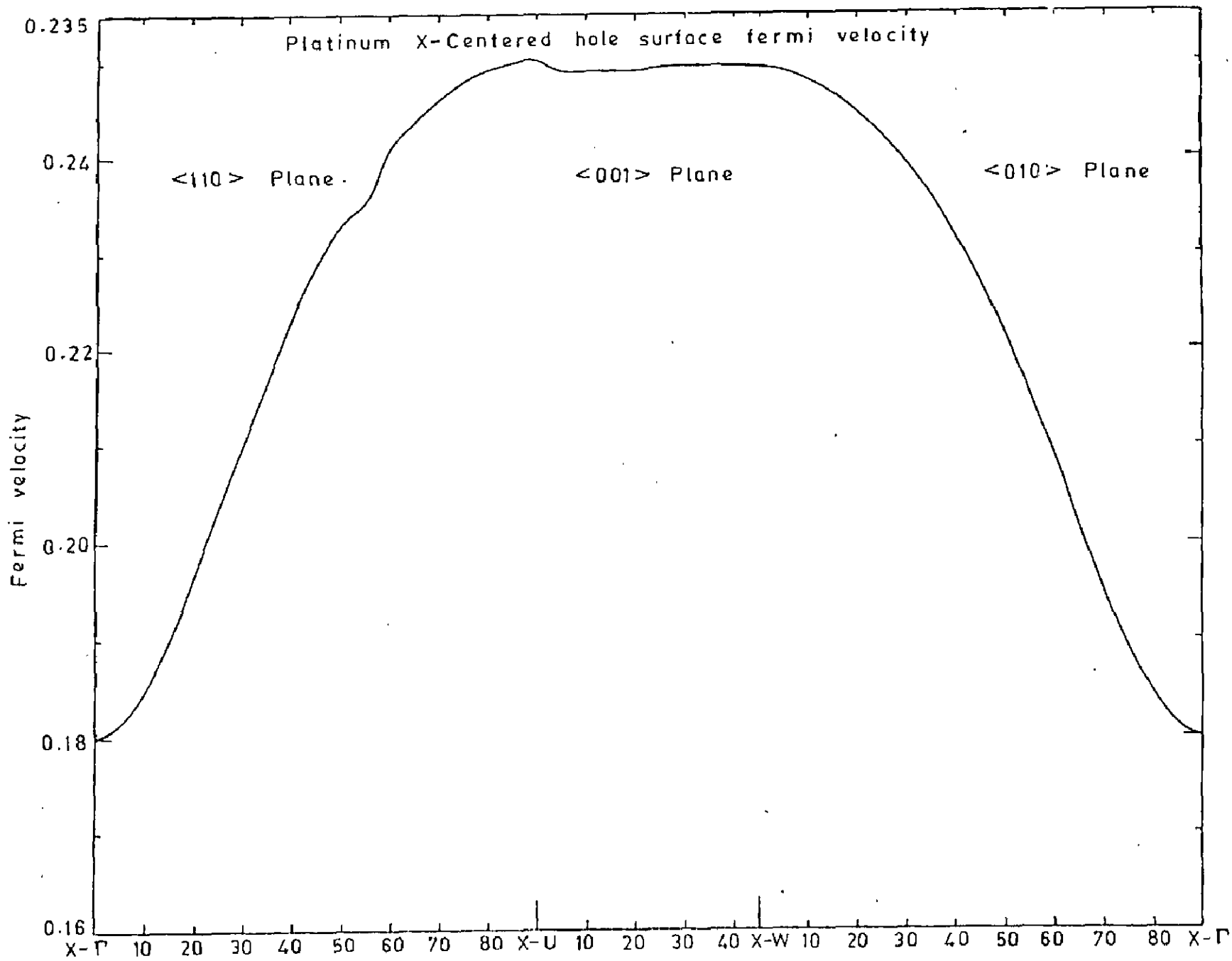
Platinum X-Centered hole surface fermi velocity
<110> Plane
<001> Plane
<010> Plane
Fermi velocity
0.235
0.24
0.22
0.20
0.18
0.16
X-Γ 10 20 30 40 50 60 70 80 X-U 10 20 30 40 X-W 10 20 30 40 50 60 70 80 X-Γ

Fig. 3.17

CHAPTER IV

4.1 INTRODUCTION

In our earlier chapters we have discussed the FS of the noble metals and the transition metals Pd and Pt. As far as the FS of noble metals is concerned, it is very simple consisting of a single Γ-centred sheet. The agreement with the experiment and with some other theoretical calculations seems to suggest the correctness of our methodology and of the LMTO method. Then we took up a study of the transition metals Pd and Pt as they have partly filled d-bands and the Fermi level crosses the d-bands resulting in a complicated FS. The LMTO method gave a FS in agreement with the experimental data. All metals discussed so far are paramagnetic. In order to check the capability of our method we have decided to look at nickel- a fcc ferromagnetic metal. The FS of the nickel is simple in comparision to other ferromagnetic metals and has been the subject of intensive experimental and theoretical investigations for many years. Using the LMTO method, many workers have calculated the total energy, electronic structure, bulk modulus, magneton numbers for Nickel but none has calculated the FS of the nickel which is of course of our interest. The exchange spilitting and spin-orbit coupling play a very important role in the ferromagnetic metals.

4.1.1 Role of Exchange Splitting :

The ferromagnetism of nickel, cobalt and iron has been attributed to the exchange iteraction between the d-electrons. That the d electrons are mobile and contribute to the conduction was not established until the advent of detailed experimental

studies of their Fermi surface. The exchange interaction is responsible for the lower potential energy of conduction electrons with spin-up compared to the potential energy of the spin down states by an amount Δ_x the exchange splitting. When Fermi surfaces are created by filling the electron states in a band, the up and down spin sub-bands fill to the levels for which electrons at the Fermi level have the same total energy. As a consequence of the exchange splitting the spin-up bands will fill to a higher kinetic energy than the spin-down bands and will therefore contain more carriers, hence the terms majority and minority carriers for the spin-up and spin-down electrons, respectively. To a first approximation the exchange splitting does not alter the shape of either the spin-up or the spin-down bands. Since the separation Δ_x of the bands is quite large, the topological features of the Fermi surface for spin-up electrons are completely different from those of spin-down electrons.

4.1.2 Role of Spin Orbit Coupling :

In a ferromagnetic metal there is a basic incompatibility between the axes of quantization of the spins (parallel to direction of Magnetization $\vec{M}$) and of orbital momentum and this leads to the complicated dependence of spin-orbit energy gaps on $\vec{k}$ and $\vec{M}$. The spin orbit coupling is weak, of the order of a few percent of exchange splitting, but has considerable influence through the resolution of degeneracies on the topological features of Fermi surface orbits. In transition metals the situation is particularly complicated. There are often instances where majority and minority-Fermi surface intersect. The presence of spin orbit coupling hybridizes the spin-up and spin-down

surfaces so that an actual electron orbit changes character at the point of intersection. Also the size of spin-orbit energy gaps in ferromagnetic metals depends on the relation of $\vec{k}$ to $\vec{M}$ and may be quenched in some parts of the BZ. Gold [90] gave a simple rule that the spin-orbit energy gap at a point $\vec{R}$ in the zone is largest if $\Gamma\vec{R}$ is parallel (or antiparallel) to $\vec{M}$, and smallest, or even zero, if $\Gamma\vec{R}$ is perpendicular to $\vec{M}$.

4.2. Band structure and Fermi surface :

The band structure of ferromagnetic metals has been calculated by a number of workers. Hanus [99] performed the first APW calculation for the paramagnetic nickel. Connolly [64] obtained energy bands in ferromagnetic nickel within the framework of the unrestricted Hartree-Fock scheme, in which the exchange terms were approximated by a local potential. He used a self-consistent APW method and comparison with the experimental data showed that the unrestricted Hartree-Fock scheme may be an acceptable model for the ground state of ferromagnetic solids. Yamashita et al [244], Wakoh and Yamashita [234] and Wakoh [235] have obtained the electronic structure of nickel using the Green's function method. Callaway and Zhang [45] and Langlinais and Callaway [136] have used the tight binding method tc calculate energy bands in feromagnetic nickel. They have constructed a basis set using a linear combination of Gaussian orbitals and used the Slater $X\alpha$ method to costruct an exchange potential. Wang and Callaway [237, 46] have reported a self-consistent calculation of the energy bands in ferromagnetic nickel using the tight binding method including the effects of inclusion of spin-orbit coupling. Comparison of their results

with the experiments indicates that a simple energy-band theory employing a local exchange potential can sucessfully predict the essential features of the Fermi surface and of the optical properties of nickel. Hodges et al [103] has studied the field induced changes in the band structure and Fermi surface of nickel. They have used the interpolation scheme and made use of several parameters obtained from a first principle APW band calculations; use was also made of the experimental magneton number as well as other experimental information such as size of <111> 'neck' in the copper like sheet of the Fermi surface. Using Mueller's interpolation scheme Zornberg [246] calculated the band structure which is good agreement with the available experimental data. Stark [213] has measured the large Γ- centred $s^{\uparrow}$ and $s_{\downarrow}$ sheets of the Fermi surface with which band structures obtained by Hodges et al [103] and Zornberg [246] did not give good agreement. Prasad et al [172] used a modified form of the Hodges-Ehrenreich-Lang interpolation scheme [104, 200] and they got good agreement with the experimental results on the large Γ-centered sheets as well as on smaller Fermi-surface sheets. They have also reported calculations for extremal areas and band masses of various orbits, magneton number and density of states. Smith and Chiang [201] has calculated the photoelectron spin polarization for ferromagnetic Ni using a combined interpolation scheme of Smith and Mattheiss [200]. Intially they used the APW method to calculate the band structure which was adjusted to reproduce the experimental magneton number. The most detailed Fermi surface and band structure calculation of spin polarized nicked was presented by Anderson et al [19]. They have reported

the band structure and Fermi surface using the APW method. They have also studied the electronic structure of nickel as a function of the lattice constant. These results confirm previous findings by Wang and Callawy regarding the diffrent forms of the local exchange approximation.

Recently Eckardt and Fritsche [77] has obtained self-consttent band structure of nickel with an exchange splitting gap of 0.39 eV which is considerably closer to the experiment value than those which have so far been obtained by using the familiar potential of Von Barth and Hedin. They have also done calculations at finite temperatures which leads to a lowering of the magnetic moment. Fritsche et al [84] have used relativistically exteded version of the one-particle formalisim. They have calculated self-consitently the electronic structure of nickel, iron and palladium metal. In addition, their calculation provides magnetic anisotropy energies. Recenty Ebert et al [76] have presented fully relativistic calculations of the magnetic moments and hyperfine fields of the ferromagnetic metals Fe, Co and Ni. Their approach is based on the multiple scattering version of the Green function method and they also coded that for the first time, orbital contributions to the hyperfine fields of these metals were accessible to a calculation. Spin polarised relativistic augmented spherical wave (SPRASW) method has been used by Krutzen and Springelkamp [133] to report the self-consistent calculations for the ferromagnetic Ni and Gd. Their results for the Occuption numbers and magnetic moments of nickel compare favourably with the experiment as well as other calculations.

Barbiellini et al [27] have studied the effect of gradient corrections to the XC potentials on the electronic structure in metals. Gradient correction proposed by Perdew and Wang and to some extent by Langreth, Mehl and Hu (LMH) have been used in self-consistent LMTO band calculations in order to determine groundstate and band properties in some transition and alkali metals. They have made a comparison of the equilibrium properties (such as lattice constant and bulk moduli) calculated using the LD and PW approximations experimental data. The result show that the PW potential increases the calculated values of the lattice constants and compressibilities which often improves the agreement with experiment. As far as magnetic properties are concerned they found that PW does not give better result than the local density potential. In case of the FS properties, they have calculated some FS dimensions in different directions. For nickel, they have calculated the Fermi surface radii for the majority sixth band and find that both LD and PW radii are similar and close to the dHvA data. Barbiellini et al conclude that the gradient-corrected potentials are not yet sufficiently good to replace the LD potential.

The band structure of nickel is similar to that of the copper except that the Fermi level now lies within the d-bands. The Fermi surface of ferromagnetic nickel is shown in Fig. 4.1. We consider first the Fermi surface sheets related to the part of band structure which is derived essentially from the atomic 4s level. Because the ferromagnetic splitting in nickel is quite small, one can easily identify the two large exchange-split 's' sheets which are similar in shape and size to the Fermi surface

of copper. The majority $s^{\uparrow}$ sheet has copper like necks which contact the {111} zone faces near the points L, while the minority $s_{\downarrow}$ sheet has pronounced bulges in the <111> directions but does not make contact with zone boundry. According to our current understanding, the five $d^{\uparrow}$ bands are completly filled so that there are no $d^{\uparrow}$ sheets of the Fermi surface. On the other hand, the higest two $d_{\downarrow}$ bands are not fully occupied and give rise to one large central $d_{\downarrow}$ sheet which intersects both s sheets, together with a set of much smaller $d_{\downarrow}$ hole pockets centered on the point X. Thus the FS of ferromagnetic nickel consists of a spin-up copper like Γ-centered surface with neck at L, two sets of spin down hole pockets centered at X, and two large spin down pieces centered at Γ.

Despite of recent advances, certain aspects of itinerant ferromagnetism are still relatively poorly understood and require further study. The Fermi surface of feromagnetic nickel and iron are reviewed to some extent by Gold [90] and Lonzarich [143]. Here we begin with a brief discussion of the information which may be obtained by what is thought to be perhaps the most powerful technique for investigating magnetic phenomena. The Fermi surface of nickel has been measured using de Haas-Van Alphen (dHvA) effect by Tusi [223] and Stark and Tusi [214]. Tusi [223] observed two distinct sets of dHVA-frequency branches. The lower set extends the spin $^{\uparrow}$ s-band neck data previously measured by Joseph and Thorsen [122]. No experimental evidence had been found till then for any second and smaller (111) neck which could be associated with the $s_{\downarrow}$ sheet. The higher frequency set of dHVA branches show details of the $d_{\downarrow}$ hole pockets which is

measured by Tusi and Stark [214, 223, 224] and Hodges et al [103]. These hole pockets have been associated with the level X_5. They did not observe any dHvA oscillations which could be assigned to either the X_2 pockets of the Fermi surface from which it is concluded that the X_2 eigenvalue must lie below the Fermi energy. Stark [213] has succeeded in detecting dHvA oscillations arising from large Γ- centred $s^{\uparrow}$ and $s_{\downarrow}$ sheets of the Fermi surface. Using a cubic harmonic expansion method of Mueller and Priestly [154, 156] Stark was able to invert this extremal area data to yield radius vectors.

The band structure along the symmtery direction in BZ for BH-XC obtained by us shown in Fig. 4.2, The figure shows the energy bands in the vicinity of the Fermi level. These are the bands which give rise to the Fermi surface and hence can be compared with experiment. From our band structure, the spin down bands based on $X_{5\downarrow}$ state produce the hole pockets which give dHvA oscillations that are easily observable and another set of hole pocket resulting from $X_{2\downarrow}$ level is predicated by our calculation. Although these aditional pockets have been found in all first-principles band calculations as far we know, they have not been directly observed by experimental techniques (measurements of dHvA effect) because these orbits have a small area and a large value of the cyclotron mass ratio. Gersdrof [88] has suggested that measurements of magneto crystaline anisotropy provide evidence for the existence of these $X_{2\downarrow}$ hole pockets and estimate a much large mass ratio of about 197. The ordering of levels at L near the Fermi level for the spin-up bands from highest to lowest is L_2'-L_3-L_3 which is in agreement with the

calculations by Connolly [64] and Wang and Callaway [237] (necks are formed from L_2' branch).

4.3 RESULTS AND DISCUSSIONS

We have calculated the ΔE_F for the spin up and spin down sheets for different XC-potentials i.e. BH, VWN and $X\alpha$. All the calculations are done with 240 $\vec{k}$ points and angular momentum expansion up to ℓ=2 because we have not found any effect of increasing the number of $\vec{k}$ ponts as well as angular momentum expansion on the Fermi surface of the noble metals and Pd and Pt.

We have calculated the extremal areas of the FS orbits for the magnetic field along (001), (110) and (111) directions. These results are presented in Table 4.1 together with the experimental results of Tusi [223] and Stark [213]. Also given are the results of Anderson et al [19], Prasad et al [172] and Wang and Callaway [237]. The first principles calculation of Wang and Callaveey does give qualitative agreement with the Fermi surface data with an extreme error of 17 mRyd. Moreover it predicts two sets of X-centred hole pockets, one arising from level $X_5$and other from level X_2 , whereas experimentally only one set of hole pockets associated with level X_5 has been observed. The HSG model [103] also gives qualitative agreement with the data of Stark and Tusi. Since Hodges et al have not reported the band mases of the FS orbit, we have calculated ΔE_F using experimental masses. As the band masses have lower value than the eperimental masses, the HSG model should give a higher value of the extreme error than the value of 16 mRyd calculated by us. Similarly we have calclculated ΔE_F for the results of Zornberg

[246]. In this case we get the smaller ΔE_F in comparsion to that of Wang and Callaways [237]. Prasad et al [172] have reported the energy band structure calculated using a modified interpolation scheme and get good agreement with the experimental results on the large Γ- centered sheets as well as on the smaller FS sheets. They have reported an extreme ΔE_F of around 0.5 mRyd which is very low in comparision of the other's. Prasad et al have missed a factor of 2 while calculating the extreme ΔE_F so it should be 1.0 mRyd instead of the 0.5 mRyd. All earlier calculations discussed above does not give a complete calculation for all the FS areas. The first such detailed calculation was presented by Anderson et al [19] who has used the self-consistent spin-polarized augmented- plane-wave method to calculate the FS areas using the BH-XC potentials. We have calculated ΔE_F for these FS areas using their band masses. We found the large ΔE_F for the necks of the majority band and an overall extreme ΔE_F around 42 mRyd.

Keeping the overall view of the all the above calculations discussed so far, our attempts in this direction using the self-consistent *ab-initio* LMTO method give a successful attempt to calculate FS areas. Looking at the results of our calculation, we note that we have obtained good agreement with the experimental data with an esxtreme ΔE_F of 9.0 mRyd (BH), 9.9 mRyd (VWN-XC) and 24.3 mRyd ($X\alpha$) with α = 0.715 . Here we have varied the value of α in $X\alpha$ XC-potential from 0.65 to 0.80. The α=0.715 gave the best agreement with experimental data i.e. a minimum extreme ΔE_F . So our calculations give a smaller ΔE_F in comparsion with the calculation of Wang and Callaway [237] and

the self-consistent calculation of Anderson et al [19]. The extreme ΔE_F is large in comparision to the calculation of the Prasad et al [172] who have used the interpolation scheme. Here we are not using any adjustable parameter and we are not fitting the FS, resulting in a larger ΔE_F.

We have calculated the FS radii and FS area for the nickel using the non-local Lagrenth and Mehl correction which was added to the local XC fuction of Barth-Hedin. The calculations are done with 240 $\vec{k}$ points and taking angular momentum expansion up to ℓ=2. The calculations are compared with our local XC results of BH-XC in order to compare the nonlocal correction effect and with the work of Barbiellini et al [27]. The Fermi Surface radii calculated using the LM XC given in Table-4.2 are *almost same as calculated with the BH-XC. The difference is very* small cosistent with the conclusions of Barbiellini et al [27].

To see the better picture of effect of nolocal corrections we have calculated the FS areas of majority and *miniorty spin orbits (given Table* 4.3). *The extreme* ΔE_F *in case* of BH exchange is 9.0 mRyd which comes from the majority 6th band centred at Γ. The ΔE_F for the same orbit using LM-XC is around 11.6 mRyd and extreme ΔE_F is 12.0 mRyd. A look at Table-4.3 shows that the ΔE_F for the majority spin FS neck orbits doubled using the LM corrections but for the miniority spin down X-centred and Γ centred orbits the ΔE_F is almost unchanged. Thus the inclusion of the nonlocal corrections increased the extreme ΔE_F from 9.0 mRyd (incase of local potential) to 12.0 mRyd (incase of LM-XC). Hence inclusion of nonlocal correction degraded the agreement with the experimental data .

4.3.1. Magneton number

The magneton number, $n^{\uparrow} - n_{\downarrow}$ i.e. the difference between the number of occupied states of the majority and miniority spins, was calculated by neglecting spin-orbit coupling and then solving the secular determinant for each spin seperatly. According to Zornborg [246] this approximationcan introduce an error of less than 0.01 electrons/atom in the calculation of magneton number. We have calculated the magneton number using different exchange correlation potentials. The values of magneton number with different XC-potential along with experimental value and from other calculations are given in the Table 4.4. The value of magneton number are 0.566 *electros/atom for* BH-XC, 0.574 electrons/atom for VWN-XC and 0.619 for the Xα-XC potential. The calculated value using BH-XC and VWN-XC are very close to experimental value [68] of 0.56 electrons/atom in comparision with the value of 0.63 electrons/atoms calculated by Anderson et al using APW method with the BH-XC potential and 0.62 electrons/atoms calculated by Barbiellini et al using self-consistent LMTO method with the local density potential and the nonlocal exchange of Perdew and Wang.

4.4. CONCLUSIONS

We have compared several different treatments of the exchange and correlation potentials in our spin-polarized LMTO calculations for nickel. We find that the BH-XC gives somewhat better results for the Fermi surface in comparison to the other XC-potentials. This is in contrast to our work on the noble metals and transition metals Pd and Pt which shows that the Xα-XC gives the best agreement with the experimental data. Xα- XC (α=

0.715) gives an extreme ΔE_F which is about two and half times the other XC-potentials, a fact also noted by Wang and Callaway [237]. The nonlocal XC potential does not improve the results but it goes in negative side.

TABLE 4.1

Cross-sectional areas of the Fermi-surface (ΔE_F in mRyd.)

ORBIT	Orientation	Center	Band	Expt. value	calc. (c)	Calc. (d)	Calc. (e)	Our calculation		
								BH-XC	VWN-XC	Xα-XC
Neck	[111]	L	$6\uparrow$	.0071[a]	.0071 0.0	0.0236 -30.9		0.0095 (-4.7)	0.0099 (-5.3)	0.0119 (-9.1)
Neck	[110]	L	$6\uparrow$	.0102[a]		0.0402 -32.9		0.0118 -2.6	0.0124 -3.5	0.0156 -7.3
Neck	[112]	L	$6\uparrow$			0.0313		0.0104	0.0109	0.0134
Large Square	[001]	Γ	$6\uparrow$	1.15[b]	1.154 -0.1	1.23 -13.1	1.24 -6.4	1.2079 -9.0	1.2115 -9.6	1.2818 -23.2
Pockets	[001]	X	$3_\downarrow$	0.0267	.0258 -0.4	0.023 -1.3	0.018 -2.1	0.0246 -1.4	0.0250 -1.3	0.0262 -0.4
Pockets	[100]	X	$3_\downarrow$	0.0665	.0671 0.1	0.049 -3.9	0.038 -6.9	0.0536 -1.6	0.0559 -1.4	0.0610 -0.8
Pockets	[110]	X	$3_\downarrow$	0.0585		0.034 -4.6		0.0445 -2.1	0.0463 -1.9	0.0506 -1.5
Pockets	[101]	X	$3_\downarrow$			0.028		0.0274	0.0281	0.0299
Pockets	[111]	X	$3_\downarrow$	0.0442		0.028		0.0347 -1.8	0.0359 -1.6	0.0388 -1.5
Pockets	[001]	X	$4_\downarrow$			0.050		0.0408	0.0309	0.0356
Pockets	[100]	X	$4_\downarrow$			0.086		0.1044	0.1074	0.1165
Pockets	[110]	X	$4_\downarrow$			0.070		0.0529	0.0542	0.0582
	[001]	Γ	$5_\downarrow$			2.04		2.1124	2.1037	2.0824
	[110]	Γ	$5_\downarrow$			1.59		1.5969	1.5865	1.5621
	[111]	Γ	$5_\downarrow$			2.08		2.1371	2.1224	2.0895
Small Square	[001]	Γ	$6_\downarrow$	0.9[b]	0.903 0.1	0.80 9.2	0.84 2.2	0.8997 0.0	0.8968 0.3	0.8871 1.1
	[110]	Γ	$6_\downarrow$			0.96		0.8977	0.8948	0.8853
	[111]	Γ	$6_\downarrow$			0.71		0.7725	0.7698	0.7671
Extreme ΔE_F (mRyd)					0.5	42.1	9.1	9.0	9.9	24.3

[a]Reference 223 [b]Reference 213

[c]Reference 172 [d]Reference 19 [e]Reference 237

TABLE 4.2

Fermi surface parameters in unit of $2\pi/a$

	Expt. [a]	Barbiellini et al[b]		Our calculation	
		XC	PW	XC	LM
$K_{\Gamma X}$	0.77	0.77	0.77	0.775	0.778
$K_{\Gamma K}$	0.58	0.59	0.60	0.589	0.594
K_{LW}	0.05	0.05	0.04	0.055	0.047

[a] Reference 103, 224

[b] Reference 27

TABLE 4.3

Cross-sectional areas of the Fermi-surface (ΔE_F in mRyd.)

ORBIT	Orien-tation	Cent-er	Band	Expt. value	calc. (c)	Calc. (d)	Calc. (e)	Our calculation	
								BH-XC	LM-XC
Neck	[111]	L	$6_\uparrow$	.0071[a]	.0071 0.0	0.0236 -30.9		0.0095 (-4.7)	0.0118 -8.9
Neck	[110]	L	$6_\uparrow$	.0102[a]		0.0402 -32.9		0.0118 -2.6	0.0148 -6.5
Neck	[112]	L	$6_\uparrow$			0.0313		0.0104	0.0131
Large Square	[001]	Γ	$6_\uparrow$	1.15[b]	1.154 -0.1	1.23 -13.1	1.24 -6.4	1.2079 -9.0	1.2245 -11.6
Pockets	[001]	X	$3_\downarrow$	0.0267	.0258 -0.4	0.023 -1.3	0.018 -2.1	0.0246 -1.4	0.0244 -1.8
Pockets	[100]	X	$3_\downarrow$	0.0665	.0671 0.1	0.049 -3.9	0.038 -6.9	0.0536 -1.6	0.0571 -1.3
Pockets	[110]	X	$3_\downarrow$	0.0585		0.034 -4.6		0.0445 -2.1	0.0470 -2.1
Pockets	[101]	X	$3_\downarrow$			0.028		0.0274	0.0279
Pockets	[111]	X	$3_\downarrow$	0.0442		0.028		0.0347 -1.8	0.0363 -2.1
Pockets	[001]	X	$4_\downarrow$			0.050		0.0408	0.0322
Pockets	[100]	X	$4_\downarrow$			0.086		0.1044	0.1082
Pockets	[110]	X	$4_\downarrow$			0.070		0.0529	0.0546
	[001]	Γ	$5_\downarrow$			2.04		2.1124	2.0988
	[110]	Γ	$5_\downarrow$			1.59		1.5969	1.5795
	[111]	Γ	$5_\downarrow$			2.08		2.1371	2.1154
Small Square	[001]	Γ	$6_\downarrow$	0.9[b]	0.903 0.1	0.80 9.2	0.84 2.2	0.8997 0.0	0.8958 0.4
	[110]	Γ	$6_\downarrow$			0.96		0.8977	0.8942
	[111]	Γ	$6_\downarrow$			0.71		0.7725	0.7686
Extreme ΔE_F (mRyd)					0.5	42.1	9.1	9.0	12.0

[a]Reference 223 [b]Reference 213 [c]Reference 179

[d]Reference 19 [e]Reference 237

TABLE 4.4

Magneton number for Nickel

	Experiment	Calculation (b)	Ours Calculation		
			BH-XC	VWN-XC	Xα-XC
$n^{\uparrow} - n_{\downarrow}$	0.56[a]	0.63	0.566	0.574	0.619

[a]Reference 68

[b]Reference 19

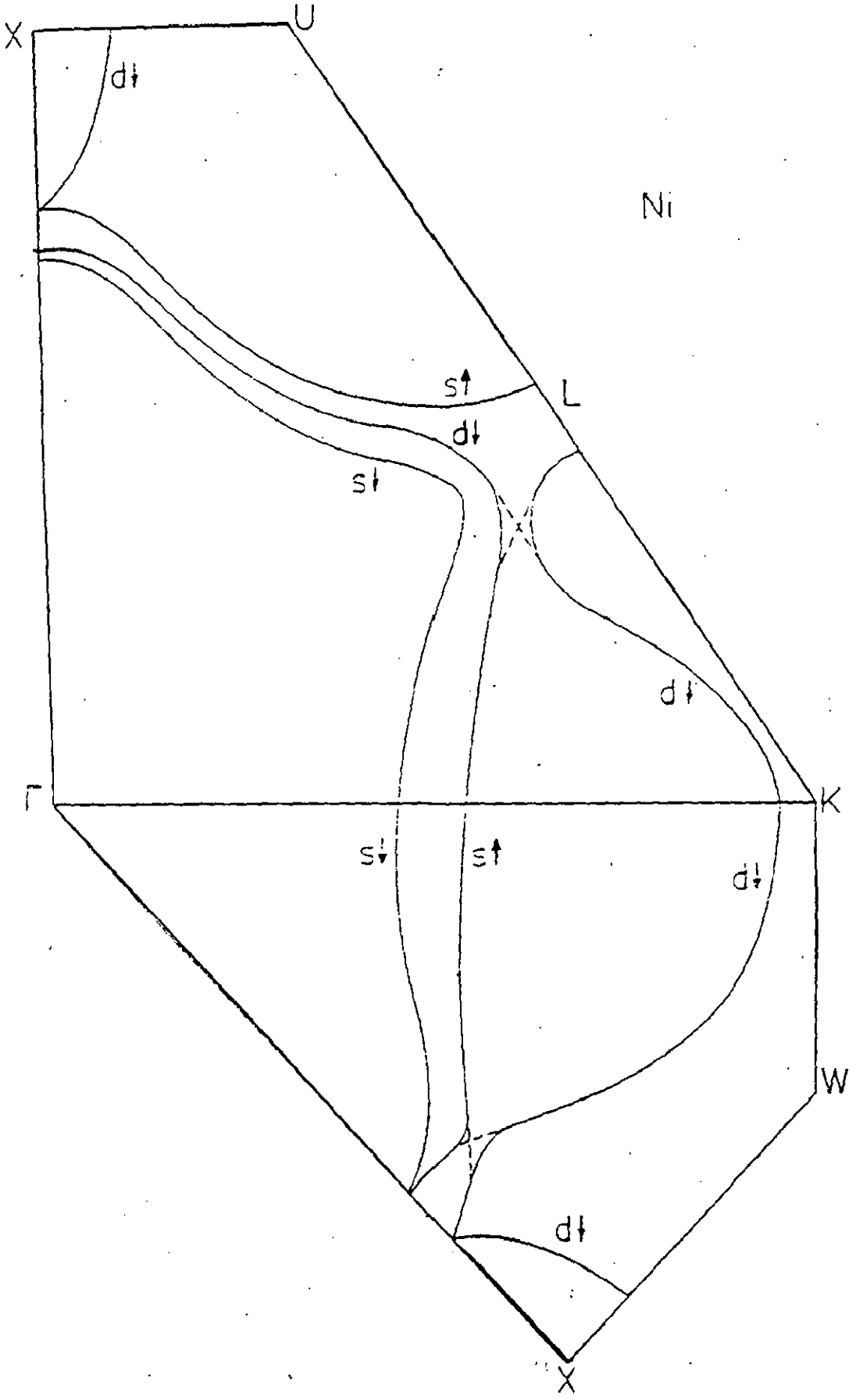

Fig. 4.1

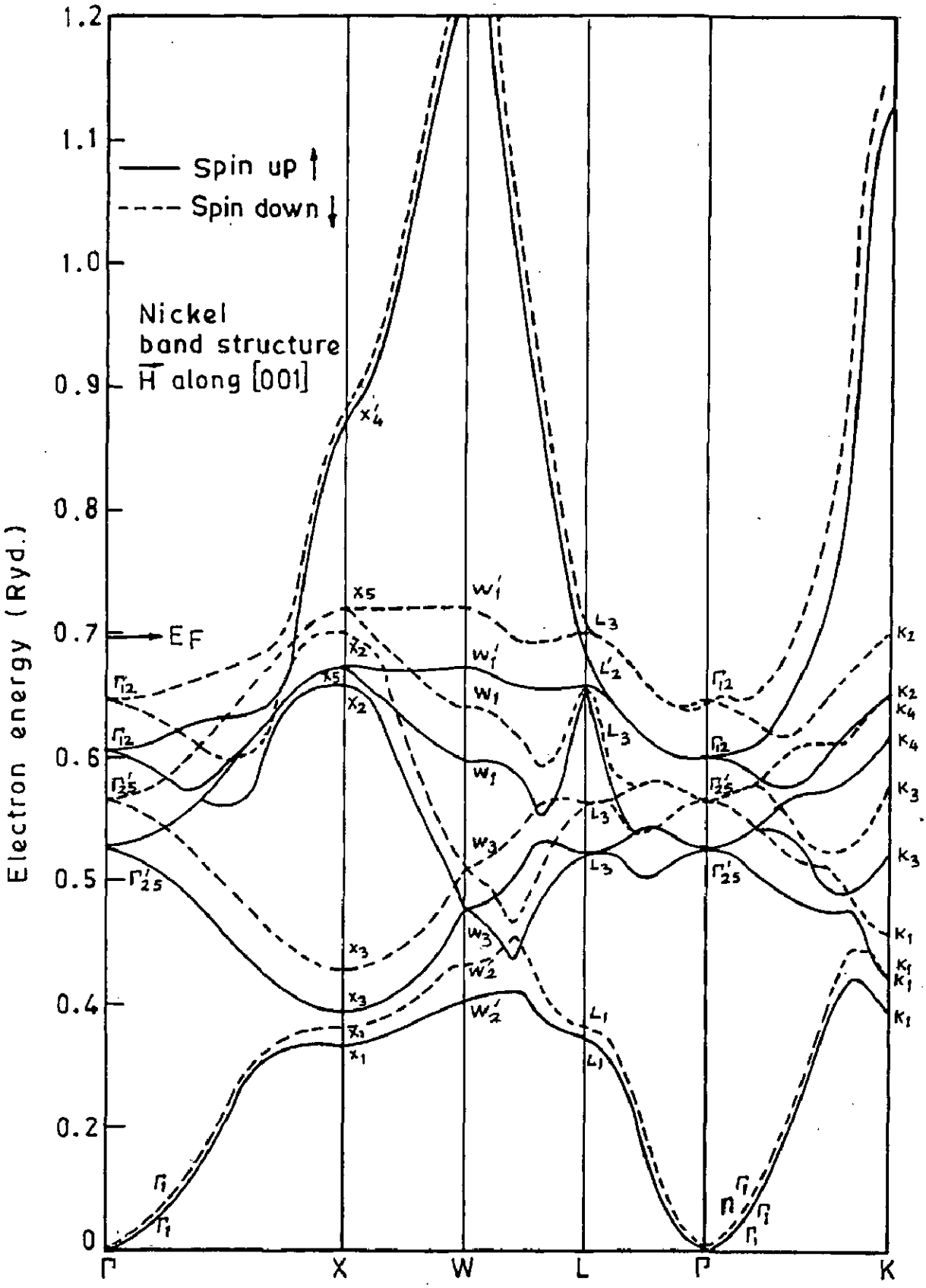
Spin up
Spin down
Nickel
band structure
H along [001]
Electron energy (Ryd.)
EF
1.2
1.1
1.0
0.9
0.8
0.7
0.6
0.5
0.4
0.2
0
Γ
X
W
L
Γ
K

Fig. 4.2

CHAPTER V

EFFECT OF PRESSURE ON THE FERMI SURFACE OF THE NOBLE METALS, TRANSITION METALS PALLADIUM, PLATINUM AND FERROMAGNETIC NICKEL

The interpretation of pressure effects on both, electron transport and crystallographic properties of metals, usually requires some knowledge of the way in which the FS is affected by pressure and also provide a valuable check on the reliability of band structure calculations. Although studies of the pressure dependence of the FS of few metals have appeared in the literature, only recently have any comprehensive studies become available. Such measurements have been shown to provide rather critical tests of the physical significance of the theoretical models proposed to describe the FS of these metals. Therefore interest from both experimental and computational standpoints has increased in the past several years. This growth can be attributed to at least three factor : (i) Development of experimental tools of sufficient resolution to measure accurately the changes in the dimensions of the FS with pressure. These changes are often of the magnitude of the compressibility so that highly accurate measurements are required. (ii) Improvement in techniques for the generation of hydrostatic pressures at too low temperatures which are suitable for use on fragile single crystal specimens. (iii) Concurrent development of sufficiently detailed theoretical models for the FS which permit direct comparison of the experimental results with model predictions.

Simultaneous operation of these factors was probably necessary in order to overcome the rather negative impressions created by some early work. This work suffered from lack of

reproducibility of experimental results and disagreement with even qualitative predictions of the theory. It has been now fairly well established that most of these difficulties stem from the nonhydrostatic pressure techniques employed on the highly anisotropic materials which were the subject of early study.

There exist abundant experimental data on the effect of pressure on the FS of the noble metals, palladium, platinum and nickel. As we have calculated the FS of metals at ambient pressure, it will be a useful extension to study the effect of pressure on the FS of these metals. Since relative accuracy is always better than absolute accuracy we expect to obtain reliable values for the pressure derivatives of the various extremal areas in these metals. At present we are not aware of any self-consistent calculations of pressure effects. Our calculations will hopefully fill this gap. We have calculated the pressure derivatives self-consistently i.e.self-consistent band structure calculations are performed at two different radii. This will give a value for the pressure derivatives of the various FS orbits. Further, there also exist some band structure calculations (although not self-consistent) for comparison with the present calculations. We hope our calculations will generate more interest in this area. In section I of this chapter we discussed the effect of pressure on FS of the noble metals while section II and III are devoted to palladium, platinum and nickel respectively.

I. NOBLE METALS

5.1 INTRODUCTION

The utility of pressure studies of the FS of metals as an

important complement to normal volume measurements has been demonstrated recently. The purpose of this section is to represent results of studies utilizing pressure derivatives of FS in conjunction with precise normal volume cross sectional areas to critically assess the physical significance of band theoretical description of the noble metals. We chose to investigate noble metals for a number of reasons. Both 'first principle' and parametrized band calculations have been published for noble metals and also excellent data with which comparison can be made exists. The FS of noble metals are well known and are topologically simple. Moreover, since we have already calculated the zero pressure FS, it is natural to calculate their pressure derivatives. As there exist only few *ab-initio* calculations, unlike to that ours is self-consistent, i.e., pressure derivatives of extremal areas (1/A dA/dP) are obtained performing self-consistent band-structure calculations at two different radii. We see that in such type of calculations self-consistency plays vital role. From our conclusion, we borrow that the choice of the XC potential is also crucial which is not studied to this extent earlier. Here we present detailed calculations of the effect of pressure on the FS of the noble metals.

Attempts to study the pressure dependence of the noble metals experimentally have been made by various workers. There are a good many experimental tools for investigation of the FS of the metals, but only a few have been employed effectively as far as pressure studies are concerened. This stems from the fact that for most metals the magnitude of the effects of FS dimensions is of order of compressibility which means fractional changes of a

few parts in 10^{3} or 10^{-4} kbar^{-1} are typical. Measurements must either be made to this sort of precision or differential techniques employed which give the change directly. The work on the hydrostatic pressure dependence of the Fermi surfaces of metals has been reviewed by Brandt, Itskevich and Minina [41], by Svechkarev and Panfilov [219], and most recently and comprehensively by Schirber and his group [47, 181, 182, 216] and later Templeton [220, 221] have measured the pressure derivatives of cross-sectional areas of the FS of noble metals using the fluid-He de Hass-van Alphen phase-shift method. So we have accurate data as needed for comparison with our calculation.

The existing calculations of the effect of pressure on the FS of noble metals fall into two broad categories. (i) *ab initio* calculations such as those of Davis et al [70] for copper and Ramchandani's for gold [175]. (ii) Empirical methods such as those of Shaw et al [189], Bosacchi et al [39] and Gavenda et al [87] for copper. Consider first the *ab initio* calculation of the Davis et al [70] who have reported the change in the electronic band-structure of copper with change in lattice spacing. The calculations were performed using constant energy search techniques based on the KKR method with 26066 points for different lattice constants and using the measured value of volume compressibility they were able to calculate the change in FS with pressure. The calculations were consistent with the dHvA data available at that time. while Ramchandani [175] has reported RAPW calculations for the gold for different lattice spacing. He has calculated the pressure coefficient of the neck area which was within a factor of 3 of the measured value. As far as the

empirical methods are concerned Bosacchi et al [39] have used the Fourier series expansion technique for inverting the pressure dependence of the dHvA areas into corresponding change in the Fermi radii. They adjusted the Fourier coefficients to fit the FS data while Shaw et al [189] have utilized the KKR method for parametrizing the experimental FS data using the techniques which are based on the standard least-squares methods. They fitted the pressure derivatives using as lattice constant derivatives of phase shifts as adjustable parameter. In early of 80's Gavenda et al [87] and his group have used a straightforward method for finding expansion functions with the symmetry of strained lattice. They have applied this method to copper under hydrostatic and uniaxial strains. Changes in FS cross-sectional areas are computed, based on a fit to energy shifts calculated by Gray and Gray [91, 92] who have used this technique in conjunction with modified plane-wave method. Their results compare favorably with experimental values.

Since we have already calculated FS orbital areas and masses for four orbits, belly B111, belly B100, dog bone D110 and neck N111 where the numbers denote the direction of magnetic field at equilibrium lattice constant [2]. We have performed similar calculations with the lattice expanded by about 0.1%. This is small enough to exclude nonlinear effects and sufficiently large to accurately calculate FS changes. Again, the self-consistent parameters are determined and the FS area is calculated. From these two calculations, we obtain dA/A corresponding to a 0.1% change in the lattice constant. Using the values of compressibility [128] 7.39×10^{-4} kbar^{-1} for copper,

10.06×10^{-4}kbar^{-1}for silver and 5.84×10^{-4}kbar^{-1}for gold, we obtain 1/A dA/dP. These calculations are done with Xα, BH, BHJ and VWN-XC potentials. In Xα-XC, α was taken to be 0.77 for copper and silver and 0.693 for gold because these gave a good fit to the zero-pressure FS.

5.2 RESULTS AND DISCUSSIONS

The 1/A dA/dP obtained for the four FS orbits using various XC potentials are given in Tables 5.1-5.3 along with experimental values and other theoretical calculations. Consider first the case of copper given in Table 5.1. The pressure derivatives for the B111, B100 and D110 orbits are almost identical for all the XC's used. The N111 is the most sensitive to the choice of the XC potential used. On comparison with the experimental data of Templeton [221] and of Schirber and Sullivan [181] we observe that the VWN and Xα-XC potentials give good agreement with the data. Also given are the pressure derivatives obtained by Shaw et al [189] and Bossachi et al [39] using phase shifts and Fourier coefficients. These are definitely in better agreement with the data compared to ours because the parameters were adjusted to fit the data. It is indeed heartening to note that the results of Davis et al [70] using KKR also agree with the data except that the N111 derivative is slightly lower than the experimental value. Gavenda et al, using the method of interpolation functions, have obtained the pressure derivatives which are consistent with the experimental data and with our calculations. Thus our values for the pressure derivatives for the four FS orbits (using Xα and VWN) are in good agreement with the experimental data.

Table 5.2 gives our results for silver along with the experimental values of Schirber and Sullivan [181] and Templeton [221] along with the empirically adjusted values. Unfortunately, we are not aware of any *ab initio* calculations. Once again we observe that the B111, B100 and D110 are not sensitive to the choice of the XC potentials, whereas N111 is. For silver only the Xα (α=0.77) gives agreement with the experimental data. Our previous work [2] on silver indicates that Xα (α=0.77) gives the best fit to the zero pressure FS data.

Values of 1/A dA/dP for gold are given in Table 5.3. We are aware of only one *ab initio* calculation by Ramchandani [175] who used the RAPW method to obtain 1/A dA/dP for N111 which was 1/3 of the experimental value. As in the case copper and silver we find that the B111, B100 and D110 are not influenced much by the XC potentials; only the N111 is. Our calculations indicate that the Xα (α=0.693) and BH-XC's give good agreement with the experimental data. Our previous work [2] for gold indicates that these XC'S give the best fit to the zero-pressure FS data.

As mentioned above, the pressure derivatives were obtained by performing self-consistent band calculations at the equilbrium lattice constant and at a lattice constant increased by 0.1%. This is small enough to exclude non-linear effects and sufficiently large to accurately calculate the FS changes. We have also calculated the band structure at lattice constant 0.4% larger than the equilibrium value. This yields 1/A dA/dP within 10% of the values given in the Tables 5.1 - 5.3. This could be well due to the non-linear variation of FS area with pressure.

5.3 CONCLUSIONS

In conclusions we can say that our calculations of 1/A dA/dP for the noble metals suggest that the LMTO method gives values that are in good agreement with experiment. Our results show that B111, B100 and D110 orbits are insensitive to the choice of XC used, while the N111 orbit is greatly influenced by the XC. Hence the pressure data can be used to determine the most appropriate XC potential. Our calculations indicate that the $X\alpha$ (α variable) gives correct values of 1/A dA/dP for all the noble metals as does VWN for copper and BH for gold. It would seem interesting to compare this with our zero-pressure results [2], which show that no single XC potential gives a good representation for the FS of noble metals. The $X\alpha$-XC with a variable α gives the best agreement with the expermential data and with previous *ab initio* methods for all the noble metals. Perhaps this reflects the need and importance of self-consistency in band structure calculations. Also, our values of 1/A dA/dP are in no way inferior to the values obtained by the empirical methods. In fact, these are equally good and obtained with no adjustable parameter.

II. PALLADIUM AND PLATINUM

5.4 INTRODUCTION

In this section , the calculation of the effect of pressure on the FS of the transition metals palladium and platinum has been reported. The FS of these metals at zero-pressure is discussed in detail in our chapter III. Our calculations indicate that the LMTO does give a good description

of the FS for both Pd and Pt. As these metals possess the fascinating electronic properties, it will be very interesting to study the effect of pressure on the FS of these metals. This will obviously be a natural extension to the work reported in chapter III. There exists very few papers concerning the effect of pressure on the FS of Pd and Pt both theoretical as well as experiment. The first experimental study of the effect of pressure on the FS of these metals was reported by Vuillemin and Bryant [234]. They have measured the pressure derivative of the Fermi surface cross-section at <100> and <111> for the electrons in Pd and Pt in the range 0-25 atm. The dHvA measurements of the change in cross sectional area of the electron sheets of these two similar FS as a function of hydrostatic pressure has been presented and the change was measured by the fluid-helium phase-shift method at temperatures as low as 0.95°K. Their results suggest that the electron pressure derivatives in Pd and Pt are nearly isotropic. After a gap of a decade Skriver et al [197] and Venema et al [227] reported the pressure derivatives of extremal cross sections of the FS of Pd by means of dHvA measurements under pressures up to 3.7 kbar. In this paper Skriver has reported the pressure dervatives for hole pockets centred at X and L in addition to the electron orbits. They have also calculated the theoretical values of pressure derivatives obtained from their self-consistent band-structure calculation based on the LMTO method using the local density approximation with BH-XC potential and are found to be in good agreement with the experimental pressure derivatives. Cavalloni et al [48] have reported hydrostatic-pressure dependence of FS of Pt using LMTO

method. They have compared their results with experimental values obtained by converting their uniaxial results. Their results for Γ centred electron are consistent with the measurement of the Vuillemin and Bryant [234] the only avilable data.

Since we have already calculated the Fermi surface areas and masses for Pd [3] and Pt [6] at equlibrium lattice constant, now we perform the similar calculations at the expanded lattice constant. From these two self-consistent calculations of Fermi surface areas, 1/A dA/dP can be obtained using the compressibilities [128] of 5.5×10^{-4} $kbar^{-1}$ for Pd and 3.59×10^{-4} $kbar^{-1}$ for Pt. These calculations are done with 240 $\vec{k}$ points and using angular momentum expansion up to ℓ=2 with different XC potentials. In Xα-XC potential α=0.75 for Pd [3] and α=0.817 for Pt [6] because these gave a good fit to the zero-pressure Fermi surface.

5.5 RESULTS AND DISCUSSIONS

The pressure derivatives for the FS orbits in Pd and Pt using various potentials are given in Tables 5.4 and 5.5. Consider first the case of Pd. There exist three sets of data obtained by Vuillemin and Bryant [234], Skriver et al [197] and Joss and van der Mark [123]. While the first two measured 1/A dA/dP under hydrostatic pressure, the last group deduced 1/A dA/dP from their uniaxial data. Hence the uncertainties are larger. All the data are consistent with each other. Skriver et al have calculated 1/A dA/dP using the LMTO-ASA with the BH-XC potential (including combined correction terms). The differences (large in some orbits) could be due to the tetrahedron technique used by them for calculating pressure derivatives. However our Xα

and VWN XC potentials results are in better agreement with theirs. We find that pressure derivatives of the large Fermi surface orbits are insensitive to the XC potential used, while the small Fermi surface orbits are very sensitive. It would be tempting to decide on the appropriateness of any XC potential based on the experimental 1/A dA/dP. However no single XC potential yields a good agreement with all the Fermi surface orbits. We hope that with data available on more orbits the situation could be more encouraging.

Our results for Pt are given in Table 5.5. Unfortunately, Vuillemin and Bryant [234] have measured the pressure derivative only for the Γ centered Fermi surface. Recenty Cavalloni et al [48] has reported experimental and theoretical volume derivatives of the area of some extremal orbits on the Fermi surface of Pt. They have obtained these experimental volume derivatives by converting the experimental stress derivatives. They have found the biggest discrepancy between theory and experiment occurs for the W-centred α orbit, for which no accurate measurement exists. The large volume dependence of the X-centered hole pocket is an indication of the strong sp-d hybridization. Our pressure derivatives using different XC potentials for Γ-centered orbits are consistent with experimental results of Vuillemin and Bryant [234] and the calculations of Cavalloni et al [48]. For the X-centered orbits, Xα-XC gives better agreement with the experiment as well as the calulations of the Cavalloni et al in comparison to other XC potentials. The pressure derivative for the open hole W-centred α orbit with Xα-XC is more close to the experimental value in comparison to Cavalloni et al's

calculations. So the scarcity of data precludes us from making any more definitive conclusions.

5.6 CONCLUSIONS

Our calculations of 1/A dA/dP for Pd and Pt suggest that the LMTO-ASA method yields values that are in agreement with the minuscule experimental data. We find that the agreement is better for the Γ-centered sheet while it is not so good for the X-centered and L-centered pockets in Pd. Our calculations show that the choice of XC potential does not influence the pressure derivatives of the larger Fermi surface orbits. The pressure derivatives of the smaller Fermi surface orbits are dependent on the XC potential used. Hence one could use the experimental data to determine the best XC potential. However, the lack of sufficient data precludes us from drawing any definitive conclusions. We hope our work will lead to more experiments on the measurement of 1/A dA/dP in Pd and Pt.

III. NICKEL

5.7 INTRODUCTION

Nickel has been a prototype metal for innumerable studies of various physical properties involving itinerant-electron ferromagnetism, d-band electronic structure and transition-metal surfaces. We have seen that the pressure derivative 1/A dA/dP calculated using LMTO method agree with the experimental data for the noble metals and for the transition metals Pd and Pt. In this section we would like to address ourselves to the effect of pressure on the FS of ferromagnetic nickel. The first experimental study of effect of pressure on the FS of nickel was

reported by Anderson et al [20] who measured the pressure derivatives for the "neck" and "elipsoid" orbits using the solid helium high-pressure technique. Around the same time Vinokurova et al group [228 - 230] presented experimental results of measurement of de Haas-van Alphen (dHvA) effect under pressures up to 1 Kbar. Anderson et al [20] found that the experimental derivative of the [001] hole-pocket cross-sectional area of FS is positive in contradiction to the negative value reported by Vinokurova et al [228 - 230]. This was later explained by Gapotchenko et al [86] as due to the pressure derivative for the [001] hole pocket being small and less than the limiting accuracy of the measurements made by Vinokurova et al [228 - 230].

On the theoretical side Anderson et al [19] have studied the effect of a change in lattice spacing on the band structure of nickel using the augmented plane-wave (APW) method. Their calculations for the change in FS and magneton number with pressure shows reasonable agreement with the available experimental measurements. Two authors of Vinokurova et al group [230] have calculated the band structure using a model Hamiltonian technique and have shown that pressure dependence on the FS of ferromagnet comes from two contributions i.e. 'magnetic' contribution and 'potential' contribution where former can be deduced from Stoner theory and later can be obtained by comparing the properties of ferromagnet and paramagnet.

We have used the LMTO-ASA method including the combined correction terms to calculate the FS area of various orbits for magnetic field along [001], [111] and [110] directions. Now the lattice is expanded by 0.1% and the self-consistent parameters

are recalculated. From these two self-consistent calculations at two different lattice spacing and using the value of compressibility 5.38 x 10^{-4} for nickel [128], we obtain 1/A dA/dP. The calculations are done with the von Barth-Hedin (BH), Vosko-Wilk-Nussair (VWN) and Slater Xα XC potentials. In the Xα-XC, α was taken to be 0.715 because this gave a good fit to the zero-pressure FS [7].

5.8 RESULTS AND DISCUSSIONS

The calculated pressure derivatives along with the experimental one are given in Table 5.6. Consider first the majority spin up orbits. For the Neck [111] and Neck [112] our pressure derivatives for VWN-XC and Xα-Xc are in good agreement with the experimental results [20, 228 - 230]] in comparison to Anderson et al [19] calculations and quite fair for BH-XC. For the rest two i.e Neck [110] and large square [001] for which no experimental as well as theoretical value is avialable, our calculations for different XC's are consistent with each other.

Now to the minority spin down case, for the small X-pockets [001] the pressure derivative is positive which is in agreement with experimental results of Anderson et al [20] as well as their calculations [19] but in contradiction to the negative value of Vinokurova et al [228 - 230] who showed that the solid-helium phase-shift measurement for this particular orbit is more reliable. For the pressure derivative of the necks [111] and [112], our calculation for VWN-XC and Xα-XC shows better agreement with the measured values campared to the calculation of Anderson et al [19] while no other calculation is available for the neck [112]. For the rest of the orbits as there

exist no experimental measurement, our results particularly for ellipsoids and small squares centered at Γ are consistent with the calculation [19] for all three XC and for remaining pockets and ellipsoids centered at X, our calculations for different XC are not in agreement with the calculations of Anderson et al [19]. An overall look at Table 6.6 shows that VWN-XC and Xα-XC with α=0.715 give better agreement with measurements [20, 228 - 230] in comparison to BH-XC.

5.9 CONCLUSIONS

Our calculations of 1/A dA/dP for the nickel suggest that the values given by LMTO method are in good agreement with experiment. It shows that the LMTO method is capable to explain the FS topology of the ferromagnetic transition metals as good as for paramagnetic metals. For nickel, there exist a minuscule data, so our calculations in this direction present a way for experimentalist to look further to give more data for the orbits which are untouched till now. Our calculations show that Xα-XC gives the better agreement with the measured orbits. For the small X-pocket <001>, our calculated pressure derivative is positive which is in agreement with Anderson et al [20] measurement which shows that Solid-helium phase shift measurement for this piece is more reliable. For the larger orbits, the pressure derivative with different XC potentials are almost same. This is consistent to our work of the noble metals and transition metals Pd and Pt that the larger orbits are insensitive to choice of the XC-potential used. We have also learned that particular attention must be paid to convergence, in spin polarized calculations to obtain the accuracy required for the computation of FS changes.

TABLE 5. 1

Experimental and calculated values for $A^{-1}dA/dP$ (10^{-4} $kbar^{-1}$) for Copper

	B111	B100	N111	D110
Xα-XC (α=0.77)	4.4	4.5	22.8	3.9
VWN-XC	4.4	4.5	23.6	3.9
BHJ-XC	4.2	4.6	9.4	4.0
BH-XC	2.3	2.8	4.7	4.8
Gavenda et al[a]	4.11	4.66	16.0	3.79
Davis et al[b]	4.4	4.7	15.5	4.1
Shaw et al[c]	4.26	4.57	15.5	4.1
Bosacchi et al[d]	4.25	4.60	18.97	4.01
Expt. value[e]	4.21±0.03	4.42±0.03	19.8±0.5	4.04±0.02
Expt. value[f]	4.25	4.6	18.0	4.0

[a]Reference 87

[b]Reference 70

[c]Reference 189

[d]Reference 39

[e]Reference 221

[f]Reference 181

TABLE 5. 2

Experimental and calculated values for $A^{-1}dA/dP$ ($10^{-4}kbar^{-1}$) for Silver

	B111	B100	N111	D110
Xα-XC (α=0.77)	5.6	6.3	62.2	4.6
VWN-XC	5.6	5.9	90.4	4.6
BHJ-XC	5.7	6.3	41.4	5.7
BH-XC	5.7	6.3	41.4	4.7
Shaw et al[a]	5.18	5.59	61.2	4.76
Bosacchi et al[b]	5.34	5.61	59.81	4.40
Expt. value[c]	5.29±0.03	5.68±0.04	65.0±0.7	4.49±0.03
Expt. value[d]	5.1	5.6	50.0	4.4

[a]Reference 189

[b]Reference 39

[c]Reference 221

[d]Reference 181

TABLE 5. 3

Experimental and calculated values for $A^{-1}dA/dP$ (10^{-4} $kbar^{-1}$) for Gold

	B111	B100	N111	D110
Xα-XC (α=0.693)	3.1	3.8	19.7	2.8
VWN-XC	3.1	3.6	26.2	2.8
BHJ-XC	3.1	3.5	13.1	2.8
BH-XC	2.8	3.6	19.7	2.8
Ramchandani[a]			7.1	
Bosacchi et al[b]	2.90	3.70	22.06	2.75
Expt. value[c]	3.06±0.04	3.58±0.03	20.6±0.5	2.70±0.02
Expt. value[d]	2.8±0.2	3.7±0.3	20.0±1.0	2.7±0.3

[a]Reference 175

[b]Reference 39

[c]Reference 221

[d]Reference 181

TABLE 5. 4

$A^{-1}dA/dP$ (10^{-4}kbar^{-1}) with different XC potential for Pd.

$A^{-1}dA/dP$ → / Field direction ↓	using BH XC	using BHJ XC	using VWN XC	using Xα XC α=0.75	Calculation (a)	Joss & Mark (b)	Expt. Value (a)	Expt. Value (c)
L center								
<111>LKW	-20.3	-17.7	-20.2	-11.6	-30.0	-34.5±10		
<111>	-16.9	-15.3	-12.8	-9.4				
<110>LKΓ	-12.4	-13.1	-12.6	-9.3	-15.6			
<100>	-16.0	-16.6	-15.0	-12.5	-20.0		-17±2.0	
X center								
<010>XWΓ	2.9	2.9	4.6	7.7	6.8	7.0±0.8	6.1±0.7	
<110>XUΓ	5.8	5.7	8.4	7.3	6.9			
<100>XWU	5.4	5.4	8.0	4.6	4.2	10.5±2.0	10.5±.7	
<110>	3.4	3.4	5.3	5.3	5.0			
<111>	3.0	3.0	4.8	4.8				
Γ center						[3.9±1.0		
<111>	4.4	4.4	4.7	4.5		[3.6±0.5		3.9±0.4
<100>	4.6	4.6	4.8	4.7	4.2	3.5±0.5	4.1±0.8	4.0±0.4
<110>	5.0	5.0	5.3	5.1				
Open hole								
<100>α	5.0	4.9	5.1	5.2				
<001>ε	3.8	3.8	3.8	3.8				
<110>β	5.8	5.7	5.7	6.7				
<111>β	4.2	4.2	4.1	4.7				
<110>γ	7.3	6.4	6.4	4.7				

[a]Reference 197

[b]Reference 123

[c]Reference 234

TABLE 5. 5

$A^{-1}dA/dP$ (10^{-4} $kbar^{-1}$) with different XC potential for Pt.

$A^{-1}dA/dP$ → / Field direction ↓	using BH XC	using BHJ XC	using VWN XC	using Xα XC α=0.815	Calculation (a)	Expt. Value
X center						
<010>XWΓ	11.9	10.9	32.3	52.0	45.5	68.0[a]
<110>XUΓ	11.8	11.1	32.0	51.8		
<100>XWU	10.1	9.3	27.8	47.8	41.2	38.0[a]
<110>	10.5	9.8	28.8	49.0		
<111>	10.1	9.4	28.0	48.0		
Γ center						
<111>	3.0	3.0	3.1	3.1	3.0	2.8±0.3[b]
<100>	3.2	3.2	3.3	3.3	3.3	3.2±0.3[b]
<110>	3.3	3.5	3.6	3.6	3.6	
Open hole						
<100>α	3.3	3.2	3.4	3.7	2.8	5.2[a]
<001>ε	2.6	2.6	2.7	2.7	2.6	
<110>β	4.6	4.3	4.8	5.2		

[a] Reference 48

[b] Reference 234

TABLE 5. 6

Experimental and Calculated values of 1/A dA/dP (10^{-4} $Kbar^{-1}$)

ORBIT	Orientation	Center	Band	Experiment value	Calc. (c)	Our calculation		
						BH-XC	VWN-XC	Xα-XC
Neck	[111]	L	$6_{\uparrow}$	6.0[a] (8.0)[b]	2.6	11.0	8.1	7.9
Neck	[110]	L	$6_{\uparrow}$		1.5	9.7	6.8	5.1
Neck	[112]	L	$6_{\uparrow}$	6.6[b]	2.3	10.7	7.8	7.2
Large Square	[001]	Γ	$6_{\uparrow}$			1.9	1.8	1.0
Pockets	[001]	X	$3_{\downarrow}$	1.0[a] (-0.8)[b]	2.6	7.3	2.6	2.8
Pockets	[100]	X	$3_{\downarrow}$		3.1	17.5	7.3	7.3
Pockets	[110]	X	$3_{\downarrow}$		2.6	16.8	7.1	6.5
Pockets	[101]	X	$3_{\downarrow}$		2.5	10.5	4.1	4.0
Pockets	[112]	X	$3_{\downarrow}$	1.5[b]		12.5	5.3	5.0
Pockets	[111]	X	$3_{\downarrow}$	6.6[b]	2.7	14.6	5.8	5.0
Ellipsoids	[001]	X	$4_{\downarrow}$		-0.4	-47.5	12.7	14.1
	[100]	X	$4_{\downarrow}$		1.4	12.3	5.2	6.4
	[110]	X	$4_{\downarrow}$		1.9	10.1	3.9	6.0
	[001]	Γ	$5_{\downarrow}$		4.4	5.6	4.7	4.9
	[110]	Γ	$5_{\downarrow}$		4.5	6.7	5.3	5.7
	[111]	Γ	$5_{\downarrow}$		4.5	6.7	5.1	5.7
Small Square	[001]	Γ	$6_{\downarrow}$		4.3	5.3	4.5	4.7
	[110]	Γ	$6_{\downarrow}$		4.0	5.3	4.6	4.8
	[111]	Γ	$6_{\downarrow}$		4.3	5.3	4.5	4.7

[a]Reference 20

[b]Reference 228

[c]Reference 19

CHAPTER VI

EFFECT OF UNIAXIAL TENSION ON THE FERMI SURFACE OF THE NOBLE METALS

6.1 INTRODUCTION

The Fermi surface(FS) of the noble metals at ambient pressure has been studied in great detail both theoretically as well as experimentally. Accurate de Haas-van Alphen(dHvA) measurments have confirmed the topology predicted by the first principle band structure calculations, and agreement between measured and self-consistently calculated extremal areas is fair [2]. Experimental measurements of pressure dependence of the FS of most of elemental metals have been made in the last decade or so, in order to obtain information about the dependence of energy band-structure on the lattice parameter. The response of the FS to uniaxial strain, which can be determined either directly by applying an external stress to the sample, or indirectly from the oscillatory magnetostriction or sound velocity, has been measured in many metals. The effect of hydrostatic pressure on the FS of noble metals has also been studied both theoretically and experimentally. Once again the theoretical results are in agreement with the experimental data [4]. Since the effect of hydrostatic pressure on the FS provides a more stringent test of band-structure (compared to the FS at ambient pressure), this reflects the accuracy of the band-structure calculations. A more strigent test would be the study of the effect of non-homogeneous strain on the FS. In this chapter we have studied the effect of uniaxial tension on the FS of the noble metals. Our reasons for choosing the noble metals are (i) they have a simple FS topology

consisting of a single sheet (ii) availability of experimental data with which our calculations can be compared and (iii) self-consistent *ab initio* calculations are almost non existent.

Shoenberg and Watts [193] reported the first experimental study of the effect of uniaxial tension on the Fermi surface(FS) of the noble metals normal to <100> and <111> directions by observing the change in the phase of the dHvA oscillations in the persistent mode of a superconducting solenoid. Later Lukhvich [146] measured dHvA oscillations and reported the values of the relative change in the "neck" and other extremal cross-sectional areas of the FS per unit stress by stretching the FS both uniaxially and hydrostatically while Aron [22] obtained the stress derivatives of FS cross-sectional areas for the "neck" of the noble metals by measuring the absolute amplitudes of the oscillatory component of the magnetostriction.

The first detailed theoretical investigation of uniaxial tenson on the electronic structure of the noble metals was made by Davis [69] who has performed the calculations using the Korringa-Kohn -Rostoker(KKR) method. For each combination i.e. in <001> and <111> directions of lattice deformation, over 25,000 points have been calculated on several individual constant energy surfaces in the vicinity of the combination's Fermi energy. The calculations for change in FS with deformations compare very favorably with the results of Shoenberg and Watts [193]. Gray and Gray [91, 92] have used the perturbation technique in connection with modified plane wave method to calculate first order changes in the electronic energy levels under tetragonal and trigonal strain. They have applied this approch to the changes at the

Fermi level of copper and compared with the calculation of Davis by taking the approximate linear combination of hydrostatic and tetragonal (trigonal) results. Gavenda, Theis and Mulvaney [87] have used a straight forward method for finding expansion functions with the symmetry of strained lattice. They have applied this method to copper under hydrostatic and uniaxial strains. Changes in FS cross-sectional areas are computed, based on a fit to energy shifts calculated by Gray and Gray. The dependence of FS extremal cross-sectional areas in copper on uniaxial tension along <001> and <111> direction by calculating $d(\ln A)/d(\ln A_s)$ where A_s is the diametral area of a free electron sphere whose volume remains exactly half that of the Brillouin zone. These calculations are compared with experimental results of Shoenberg and Watts [193] and give good agreement. Based on the strong interaction between the condution electrons and lattice in the noble metals and transition metals, Fawcett et al [79] have given the most successful approach of the phase-shift pseudopotential, in which the lattice potential is approximated by an array of non-overlapping spherically symmetric potentials, each centered on a lattice site. This phase-shift pseudopotential calculations are based on the multiple scattering formalism of KKR. They have calculated the shear dependence of copper for the areas of the principal orbits and deduced their response to uniaxial tension. The results of their calculations are generally in very satisfactory agreement with the experimental data of Shoenberg and Watts [193].

As we have already computed the FS of the noble metals [2] and the effect of hydrostatic pressure on the FS of these

metals [4], it is worth while to calculate the FS for the deformated lattice. Measurements of the way in which the Fermi surface is distorted by the application of hydrostatic or uniaxial tension yield information about the response of the electronic structure to homogeneous lattice strain. The lattice strain is related to the applied stress through the elastic stiffness constants c_{ij} of the metal. Taking the simple case of cubic crystals, the strain may involve the elongation of the basis vector so that the basis vector $x = a\hat{x}$ takes the form $x' = a\hat{x}(1+\varepsilon_{xx})$, here ε_{xx} represent the fractional elongation of the x-axis. The tetragonal shears γ_x, γ_y and γ_z are volume-conserving combinations of the elongations, ε_{xx}, ε_{yy}, and ε_{zz}. For the strains associated with pure tetragonal shear γ_x along x-axis are

$$\varepsilon_{xx} = \gamma_x \; ; \quad \varepsilon_{yy} = \varepsilon_{zz} = -\frac{1}{2}\gamma_x \tag{6.1}$$

The angular shears γ_{xy}, γ_{yz} and γ_{zx} are combination of the axis rotations ε_{xy}, ε_{yx}, ε_{xz}, ε_{zx}, ε_{yz}, ε_{zy}. For γ_{xy}, the angular shear in the x-y plane is given by

$$\gamma_{xy} \equiv \gamma_{yx} \equiv (\varepsilon_{xy} + \varepsilon_{yx}) \tag{6.2}$$

If stress is applied along <001> so that $\gamma_x = \gamma_y = 0$, then tetragonal shear is given by

$$\gamma_z = \frac{2}{3}\left(\frac{\sigma_{001}}{c_{11} - c_{12}}\right) \tag{6.3}$$

where c_{11} and c_{12} are stiffness constants and σ is uniaxial stress. If the stress lies along <111>, all tetragonal shears must vanish by symmetry. Angular shear is intrinsically a volume-conversing shear. If the tension is applied along the <111> direction, the angular shears are

$$\gamma_{xy} = \gamma_{xz} = \gamma_{yz} = \frac{\sigma_{001}}{2c_{44}} \qquad (6.4)$$

To summarize, a tension applied along a general direction produces both tetragonal shears and also angular shears about all three axes.

In the case of hydrostatic pressure, unit cell will be same as at ambient pressure. Hence there is no problem with self-consistency. Now in case of uniaxial strain the unit cell is tetragonal. So the number of $\vec{k}$ points will be different with those at ambient pressure. This will include an unknown input resulting for different levels of self-consistency condition. As a simple approach, the ε is small and we assume that the unit cell will be same as at ambient pressure. The distorted potential parameters which are expected to differ only insignificantly from those the ones at equilibrium, as expected from the theorem of Gray and Gray [92], according to which there are no first order corrections in strain for a potential of the muffin-tin or equivalently of atomic sphere form. The calculation of the extremal areas is done using Stark's area-mass routine in conjunction with Skriver's codes. The extremal FS areas of the undistorted lattice are calculated using the self-consistent potential parameters obtained earlier. Using the same potential, the extremal FS areas are then calculated for distorted structures when the strain is along <001> and <111> directions. From these two calculation i.e. on equlibrium lattice and on distorted lattice and using the values of stiffness constants of these metals [128] ,we obtain the dependence of FS extremal areas $d(\ln A)/d(\ln A_s)$ along <001> and <111> directions. The calculations

are done with the von Barth-Hedin (BH), von Barth-Hedin-Janak (BHJ), Vosko-Wilk-Nussair (VWN) and Slater Xα XC potentials. For Xα-XC the values of α for copper and silver are 0.77 and 0.693 for gold are used.

6.2 RESULTS AND DISCUSSIONS

The $d(lnA)/d(lnA_s)$ calculated for the different FS orbits using various XC potentials are given in Table 6.1 - 6.6 along with the experimental results of Shoenberg and Watts [193]. We now discuss each metal separately.

Table 6.1 shows the values of $d(lnA)/d(lnA_s)$ for copper. When uniaxial tension is along <001> direction, the value of $d(lnA)/d(lnA_s)$ for the B001 orbit is almost in the range of experimental value for all XC's as well as other theoretical calculations. For all other orbits as there exists no other experimental data, so we have compared our results with other existing theoretical calculations. For D110 and B100 orbits our values are close to those obtained by Davis [69] and Gavenda, Theis and Mulvaney [87] but for B100 it is different from that of Gray and Gray [92]. The "neck" which is very sensitive to the choice of the XC potentials, our values for this orbit are close to that of Gray and Gray [92] and Gavenda, Theis and Mulvaney [87] while for the B111 orbit the values for BH and BHJ-XC are close to the values of the latter compared to VWN and Xα-XC.

Table 6.2 shows our results for uniaxial tension along the <111> direction for copper. The results show a very large uniaxial dependence of the neck. The physical interpretation of this result is that under an applied tension, the lattice is

elongated in the <111> direction which decreases the separation between the <111> and <$\bar{1}\bar{1}\bar{1}$> BZ planes, thereby increasing the area of contact with the FS and enlarging the neck orbit. In case of N111 the VWN-XC and Xα-XC give better agreement to experimental results compared to BH and BHJ-XC. For the B111 orbit, our values for all XC's are in agreement with the experimental results. Thus an overall look on Tables 6.1 and 6.2 shows that for the copper, the stress derivatives using Xα-XC and VWN-XC are in good agreement with the experimental data. This is consistent with our conclusions in case of hydrostatic pressure derivatives [4].

Tables 6.3 and 6.4 give our results for silver along with the experimental results for uniaxial tension applied in <001> and <111> directions. Here we do not have any other theoretical calculation, so our results are compared with the data of Shoenberg and Watts [193]. The stress derivative of the B001 orbit for uniaxial tension along <001> direction is consistent with experimental results for all four XC's. But when the tension is along <111>, BH and BHJ-XC give better agreement with experiment then VWN and Xα-XC. The stress derivative of B111 is almost the same for all XC's. Thus the results for silver are in satisfactory agreement with the experimental data.

The $d(\ln A)/d(\ln A_s)$ for gold is given in Tables 6.5 and 6.6. The results for tension along <001> direction is given in Table 6.5. For B001 the stress derivative with VWN-XC is in fair agreement with the experimental result compared to other XC's but our stress derivatives are three times then those of Davis [69]. For N111 our stress derivative is very much smaller than that of

Davis [69]. We think that this is due to their fitting of the Fermi energy. For tension along <111>, the stress derivative for N111 using all XC's except VWN-XC is in range of exerimental value and in better agreement then those of Davis [69]. The B111 is also conistent with experimental result as well as theoretical results of Davis [69]. Thus for the gold the BH-XC and Xα-XC give good agreement with experimental results which is also shown by our previous calculations of the hydrostatic pressure derivatives [4].

6.3 CONCLUSIONS

The stress derivatives $d(\ln A)/d(\ln A_s)$ for the noble metals under uniaxial tension along <001> and <111> directions has demonstrated that the current band structure ground-state formalism is capable of handling such type of calculations. These results also show the versatility of the LMTO method. The difference between our values and the expermental values may be due to the sizeable experimental uncertainties. All the orbits except the N111 (for tension along <111> directions) are not affected by the choice of XC potentials. A look at the noble metals shows that Xα-XC potential gives a good representation to the experimental results which is obvious because we are using an adjustable parameter α. Our results give good agreement with the data. Our calculations are *ab-initio* and self-consistent. In contrast Gray and Gray [92] and Gavenda, Theis and Mulvaney [87] have used perturbation technique and interpolation functions respectively while the calculations of the Davis and Fawcett et al are not self-consistent. In the case of silver, our calculations are the first *ab initio* self-consistent

calculations. It would be beneficial to have more data to check the reliablity of the calculations.

TABLE 6.1

Dependance of Fermi-surface extremal cross-section areas in copper on unaxial tension along [001] [$d(\ln A)/d(\ln A_s)$, where A_s is the diametral area of free-electron sphere whose volume remains exactly half that of Brillouion zone 1.

ORBIT	SW(Expt.) (a)	Davis (b)	GG (c)	Gavenda et al(d)	Fawcett* et al(e)	BH-XC	BHJ-XC	VWN-XC	Xα-XC
B100		-0.3	0.5	-0.52		-0.94	-0.70	-0.33	-0.42
B001	2.4 ± 0.5	3.6	2.7	3.94	2.98	3.13	3.77	2.99	3.05
N111		5.1	2.9	-0.99			1.6	3.2	6.1
B111		-0.6		0.97		0.54	0.94	0.69	0.73
D110		18.0		21.1		20.9		21.8	21.6

[a]Reference 193
[b]Reference 69
[c]Reference 92
[d]Reference 87
[e]Reference 79

TABLE 6. 2

Dependence of Fermi-surface extremal cross-sectional areas in copper on uniaxial tension along [111] [$d(\ln A)/d(\ln A_s)$]

ORBIT	SW(Expt.) (a)	Davis (b)	GG (c)	Gavenda et al(d)	Fawcett et al(e)	BH-XC	BHJ-XC	VWN-XC	Xα-XC
B001		-1.2	1.0	0.98		0.50	0.94	0.90	0.90
N111	-44 ± 10	-28.0	-32	-50.0	-46.2	-27.5	-26.0	-37.2	-34.5
B111	0.6 ± 0.2	1.0		-1.36	-1.02	0.42	0.80	0.85	0.85

[a]Reference 193

[b]Reference 69

[c]Reference 92

[d]Reference 87

[e]Reference 79

TABLE 6. 3

Dependence of Fermi-surface extremal cross-sectional areas insilver on uniaxial tension along [001] [$d(\ln A)/d(\ln A_s)$]

ORBIT	SW(Expt.) (a)	BH-XC	BHJ-XC	VWN-XC	Xα-XC
B100		-0.94	-0.98	-0.61	-0.64
B001	2.2 ± 0.3	3.7	3.7	2.97	3.1
N111		19.4	9.8	21.4	16.4
B111		1.5	1.4	1.1	1.1
D110		24.4	24.5	24.7	24.7

[a]Reference 193

TABLE 6. 4

Dependence of Fermi-surface extremal cross-sectional areas in silver on unaxial tension along [111] [$d(\ln A)/d(\ln A_s)$]

ORBIT	SW(Expt.) (a)	BH-XC	BHJ-XC	VWN-XC	Xα-XC
B001		0.93	0.93	0.86	0.92
N111	-72.0 ± 5.0	-61.0	-61.0	-106.0	-97.0
B111	0.8 ± 0.3	0.86	0.82	0.82	0.82

[a] Reference 193

TABLE 6. 5

Dependence of Fermi-surface extremal cross-sectional areas in gold on uniaxial tension along [001] [$d(\ln A)/d(\ln A_s)$]

ORBIT	SW(Expt.) (a)	Davis (b)	BH-XC	BHJ-XC	VWN-XC	Xα-XC
B100		0.3	-7.6	-7.0	-5.3	-6.8
B001	8.0 ± 1.0	4.0	13.6	14.4	11.4	14.4
N111		72	8.5	6.8	11.5	8.5
B111		-1.8	-0.8	-0.8	-0.43	-0.7
D110		32.0	25.4	26.4	29.5	26.5

[a]Reference 193

[b]Reference 69

TABLE 6. 6

Dependence of Fermi-surface extremal cross-sectional areas in gold on uniaxial tension along [111] [$d(\ln A)/d(\ln A_s)$]

ORBIT	SW(Expt.) (a)	Davis (b)	BH-XC	BHJ-XC	VWN-XC	Xα-XC
B001		-5.5	0.71	0.86	0.90	0.96
N111	-60.0 ± 8.0	-110.0	-74.0	-74.6	-114.0	-73.0
B111	2.6 ± 0.4	0.9	0.6	0.72	0.72	0.7

[a]Reference 193

[b]Reference 69

CHAPTER VII

In this thesis we have used the LMTO-ASA method to calculate the Fermi surface and the effect of pressure on the Fermi surface of the noble metals, transition metals palladium, platinum and ferromagnetic nickel. A knowledge of the electronic band structure is essential for the calculation of these physical properties. Its implications have been brought out in chapter-I where we have shown that the Linear Muffin Tin Orbital (LMTO) method satisfies the requirements of a fast, accurate, physically transparent and flexible method of band structure calculation. The method is discussed in some detail,and its advantages and limitations vis-a-vis other first principles methods have been elaborated. This chapter also gives some discussion on the density functional theory (DFT), different exchange-correlation potentials and a description of some experimental methods that measure the Fermi surface.

In chapter-II, we have discussed the Fermi surface of the noble metals [2]. The band structure and Fermi surface of noble metals is so well established that the experimantalists use it to standardize their apparatus and theoreticians use it to debug their programs. We have calculated the extremal areas for four orbits in the noble metals. Our study shows that the choice of XC-potential plays an important role while other effects such as increase of number of $\vec{k}$ points, inclusion of relativistic effects and angular momentum expansion up to ℓ=3 are not significant. The agreement between the calculated Fermi surface extremal areas and experimentally measured areas is determined by calculating the

shift in the Fermi energy ΔE_F, required to bring the calculated area in agreement with the experiment. The extreme ΔE_F is 4.1 mRyd and 0.9 mRyd for copper and silver respectivly, (with the Slater Xα (α =0.77) XC potential) while for gold the extreme ΔE_F is around 3.5 mRyd (with Slater Xα (α = 0.693) XC potential). We have also studied the suggestion of Jepsen et al [117] that the Fermi surface of noble metals could be characterized by k_N/k_S and A = $k_F[100]/k_F[110]$ where k_N is neck radius and k_S is radius of free electron sphere. Our calculations suggest that these two parameters are not sufficient to charactrize the Fermi surface. The inclusion of the nonlocal exchange-correlation proposed by Langreth and Mehl shows that for the copper results are degraded with experiment in accordance with the calculations of Norman and Koelling [160] and Barbiellini et al [27] but in silver and gold the effect is negligble.

In chapter III, we present our the Fermi surface of the transition metals palladium [3] and platinum [6] calculated using the LMTO method. We have chosen these metals because they have a fairly complicated Fermi surface and will provide a check of the accuracy of the LMTO method. Also their Fermi surface has been accurately measured by a number of workers. The Fermi surface areas for Pd are calculated for four sheet i.e. a Γ-centred electron sheet, two hole sheet centred at X and L and one open hole surface (in Pt there is no L pocket hole). The study of various effect shows that relativistic effects which are negligible in the noble metals, are important here. The extreme ΔE_F for Pd is 4.0 mRyd (with Slater Xα (α = 0.75)-XC) and 2.7

mRyd for Pt(with Slater Xα (α =0.815)-XC). Using the Slater Xα-XC potential we have calculated the Fermi velocities. There are found to closely resemble the experimental and calculated velocties of other authors. The enhancement indicated by our results is also in agreement with earlier calculations. We have also calculated the mass enhancement in Pd and Pt from two other considerations, viz., *from cyclotron masses and from specific* heat data. These calculations yield a mass enhancement $1+\lambda_{\gamma}$ for Pd near 1.68 and 1.19 for Pt.

The development and refinement of certain experimental and theoretical methods in solid state physics in recent year has led to major advances in our understanding of itinerent-electron magnetism in the 3d transition metals. Despite considerable progress, however, a number of formidable long-standing as well as novel problems remain unsolved. Spurred on by the sucess with which the LMTO method gives the Fermi Surface of the paramagnetic metals, we have performed calculations for ferromagnetic nickel [7]. To calculate the FS of ferromagnetic nickel we to have perform self-consistent spin-polarised LMTO calculations. The FS of nickel is complicated by the existence of exchange interaction and spin orbit coupling. The Fermi surface of nickel consists of : spin-up copperlike Γ-centered surface with necks at L, two sets of spin down hole pockets centered at X and two large spin down pieces centered at Γ. We have calculated ΔE_F for various orbits using different XC potentials. Our results give an extreme ΔE_F = 9.0 mRyd (Slater Xα-XC). This is small compared to all previous calculations except the calculation of Prasad et al (Ref),who have used the fitting procedure. So our results show that the

LMTO method gives the correct Fermi surface geometry of ferromagnetic nickel.

Pressure studies of Fermi Surface are of increasing interest in the study of metals, since they provide a valuable check on the reliability of band structure calculations. In fact a band structure method which gives good representation to Fermi surface can fail to account for its pressure variation. Therefore, it turns out to be useful to see whether the LMTO method can give meaningful values of the pressure derivatives of the FS orbits. In chapter V, we have studied the effect of pressure on the FS of noble metals [4] and transition metals palladium, platinum [5] and nickel [8]. The pressure derivatives are obtained from the zero pressure calculation and one at an expanded lattice. Using the areas from these two calculations and the value of compressibility, we have obtained the pressure derivative 1/A dA/dP of the external areas. Our results for the noble metals suggest that the LMTO method gives values that are in good agreement with experiment. We find that the B111, B100and D110 orbits are insensitive to the choice of the XC-potential used while the N111 orbit is greatly affected by the XC-potential. Thus the pressure data can be used to determine the most appropriate XC-potential. For palladium, platinum and nickel LMTO pressure derivatives are in agreement with scanty experimental data. Here again we find that the pressure derivatives of the larger FS orbits are not influenced by the choice of the XC potential. However the lack of sufficient data precludes us from drawing any definitive conclusions. We hope our work will generate more interest and more experiments on the

measurements of 1/A dA/dP.

In chapter VI, we have studied the effect of uniaxial tension on the FS of the noble metals [9]. We think that this is a more stringent test of the accuracy of band structure calculation compared to the case of hydrostatic pressure. We have calculated the dependence of the area $d(\ln A)/d(\ln A_s)$ using different XC-potentials for the uniaxial tension along <001> and <111> directions. The calculations reported by us are self-consistent and we think this is first such type of calculation. Our results for the noble metals are in good agreement with experiment. Lack of the sufficient data does not allow us to make any definitive conclusions.

APPENDIX

PRACTICAL ASPECTS OF THE LMTO METHOD

The LMTO method outlined so far may be applied at many levels of approximation in problems of condensed matter physics. For most applications one must resort to calculations on a large-scale electronic computer, and to that end we now present Skriver's [196] package of computer programs LMTOPACK. This LMTOPACK is a collection of Fortran routines which may be used to calculate the electronic structure of a given crystalline material from the knowledge of the crystal symmetry and the atomic numbers of the constituents involved. As explained in the LMTO formalism, the energy band calculation is separated into two parts, one that depends on the structure and the other that depends on the potential. The structure dependent part calculates the structure constant matrix and this part of the computer program is named STR. The potential dependent section calculates the eigen values and eigen vectors by solving the LMTO secular equation with proper potential parameters and this program is called LMTO. These two programs are considered to be the heart of the calculational procedure. Apart from this other programs namely COR, DDNS and SCFC are needed for the combined correction, density of states calculation and self-consistent energy band calculation. The self-consistent procedure is described in the flow chart given in Figure Ap.1. The function of each program is described below.

The STR program calculates the volume and energy independent structure constants. The inputs required for this

calculation are crystal structure, number of atoms per primitive cell and the positions of the basis. The structure constant calculation is restricted to a certain distance in real and reciprocal space by a proper choice of maximum distances.

The COR program is constructed to calculate those extra structure constants which may be used to correct the ASA for approximate treatment of the region between the sphere and atomic polyhedron, and for the neglect of higher ℓ components. The basis input for COR is the basis vectors giving the positions of the atom in the cell, and the reciprocal-space vectors generated by STR.

The secular equation of the LMTO theory is solved in the LMTO program. The basic input to LMTO is the structure-constant matrices generated by STR, the correction-term structure-constant matrices generated by COR, if the correction to the atomic-sphere approximation is to be included, and the potential parameters. The basic output is the eigen-values and eigen-vectors evaluated for the specified number of $\vec{k}$ points in the irreducible BZ.

The obtained energy values are used in the DDNS program for the calculation of ℓ-projected density of states and the number of electrons. The density of states and the corresponding number of state functions are calculated by means of the tetrahedron technique.

The ground state properties are calculated in the SCFC program which is designed to solve the energy-band problem self -consistently. The program treats only the conduction states, i.e. the outermost s, p, d and f electrons, while the charge

density of the remaining electrons is kept fixed. In this frozen-core approximation the core charge density is obtained from atomic calculations renormalised to the relevant atomic volume. The basic input includes the projected state densities and number-of- states functions generated by DDNS and the atomic charge densities calculated by RHFS (relativstic Hartree-Fock self-consistent procedure) program. The main output is the self-consistent potential parameters. If the potential parameters in original run of LMTO have been suitably chosen, one will have a reasonably converged result after just one execution of SCFC. If this is not the case, one must use the output potential parameters to perform new band-structure and state-density calculations and then repeat SCFC with the new state densities to get new outputs until self- consistency is reached.

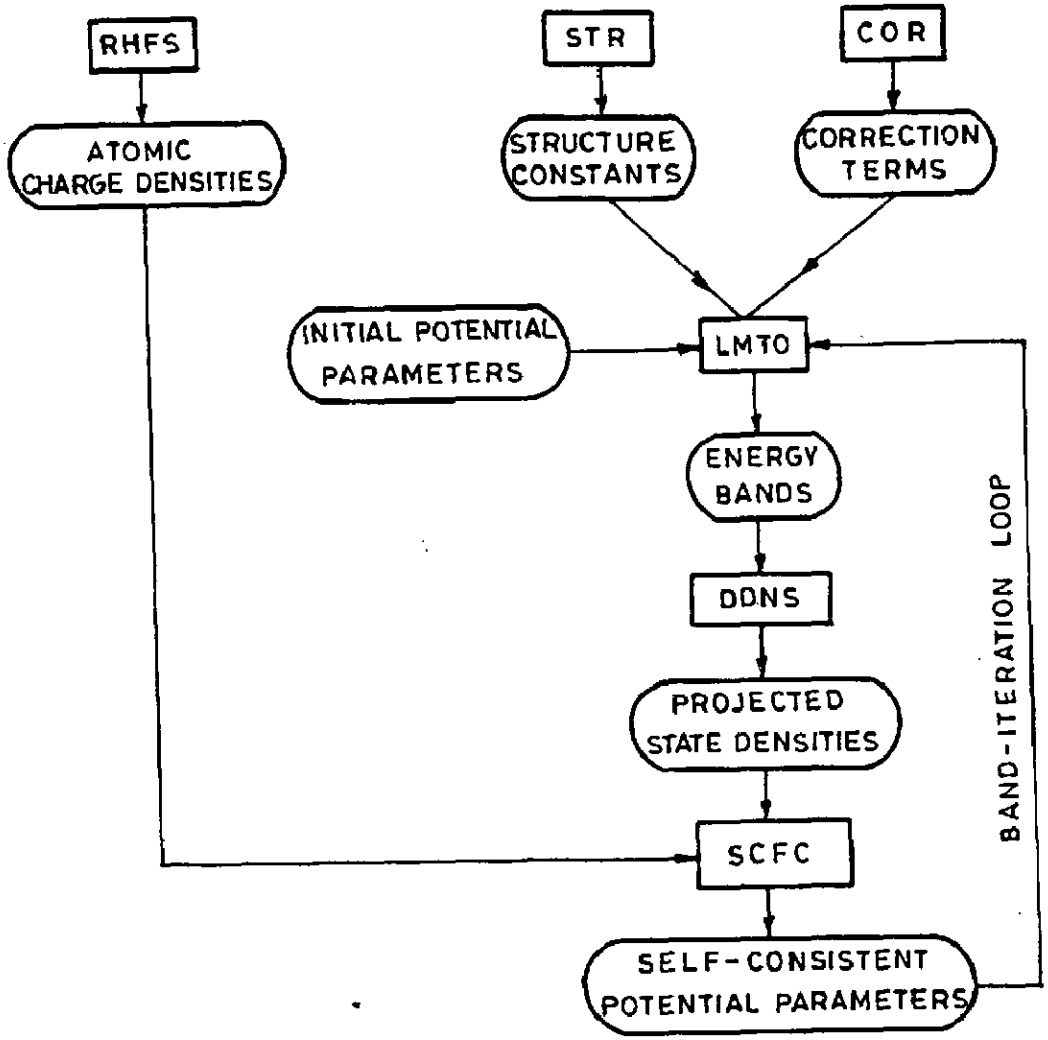

Fig. Ap.1 Flow chart of self-consistent LMTO procedure

REFERENCES

1. Ahuja A.K., *Electronic and optical properties of noble and transition metals*, Ph.D Thesis (University of Roorkee, India, 1982) unpublished.

2. Ahuja Rajeev, Solanki A.K., Nautiyal T. and Auluck S., *Fermi surface of the noble metals*, Pramana -J. Phys. **32**, 831 (1989).

3. Ahuja R., Solanki A.K. and Auluck S., *Effect of pressure on the Fermi surface of the noble metals*, Phys. Rev. B **39**, 9806 (1989).

4. Ahuja R., Solanki A.K. and Auluck S., *Fermi surface characteristics of palladium*, Phys. Stat. Sol. (b) **160**, 549 (1990).

5. Ahuja R., Solanki A.K. and Auluck S., *Effect of hydrostatic pressure on the Fermi surface of Pd and Pt*, Phys. Rev. B **43** 401 (1991).

6. Ahuja R., Solanki A.K. and Auluck S., *Fermi surface properties of Platinum* (communicated).

7. Ahuja R., Solanki A.K. and Auluck S., *Fermi surface of the ferromagnetic Nickel* (communicated).

8. Ahuja R., Solanki A.K. and Auluck S., *Effect of pressure on the Fermi surface of Nickel* (communicated).

9. Ahuja R., Solanki A.K. and Auluck S., *Effect of strain on the Fermi surface of the noble metals* (communicated).

10. Alonso J.A. and Girifalco L.A., *Nonlocal approximation to the exchange potential and kinetic energy of an inhomogeneous electron gas*, Phys. Rev. B **17**, 3735 (1978).

11. Andersen O.K., *Linear methods in band theory*, Phys. Rev. B **12** , 3060 (1975).

12. Andersen O.K., Jepsen O. and Sob M. in '*Electronic band structure and its application*, ed. M. Yussouff, (Springer Verlag, Berlin, 1987), p.1.

13. Andersen O.K., Jepsen O. and Glotzel D., in *Highlights of condensed-Matter Theory*, edited by Bassni F., Fumi F. and Tosi M.P. (North Holland, New York, 1985).

14. Andersen O.K., *New methods for the one-electron problem*, Europhys. News **12**, 5, 1 (1981).

15. Andersen O.K. in *The Electronic Structure of Complex Systems*, ed Teemmerman W. and Phariseau P. (Plenum, New York, 1984).

16. Andersen O.K. and Jepsen O., *Explicit, First principle Tight-Binding Theory*, Phys. Rev. Lett. 53, 2571 (1984).

17. Anderson O.K. and Mackintosh A.R., *Fermi surfaces and effective masses in fcc transition metals*, Solid State Commun. 6, 285 (1968).

18. Anderson O.K., *Electronic structure of the fcc transition metals Ir, Rh, Pt and Pd*, Phys. Rev. B 2 883 (1970).

19. Anderson J.R., Papaconstantopoulous D.A., Boyer L.L. and Schirber J.E., *Spin-polarized band-structure calculations for Ni*, Phys. Rev. B 20, 3172 (1979).

20. Anderson A.R., Heiman P., Schirber J.E. and Stone D.R., AIP Conf. Proc. N. 29, Magnetism and Magnetic Materials, USA (1975), p. 529.

21. Anosen H., Lindroos M., Pessa M and Dahlback N, *Experimental determination of electronic band structure and photoemission of Pd*, Solid State Commun. 35, 69 (1980).

22. Aron Paul R., *Oscillatory Magnetostriction in the Noble Metals*, J. Low Temp. Phys. 9, 67 (1972).

23. Azbel' M.Ya. and Kaner I.M., in *Progress in Low Temperature Physics*, ed. Gorter C.J. (North-Holland Publishing Co., Amsterdam, 1961), Vol. 3.

24. Bagno P., Jepsen O. and Gunnarsson O., *Ground-state properties of third-row elements with nonlocal density functionals*, Phys. Rev. B 40, 1997 (1989).

25. Ballinger R.A. and Marshall C.A.W., *Study of potentials suitable for band structure calculations of the noble metals : I-Copper*, Proc. Phys. Soc. 91, 203 (1967).

26. Ballinger R.A. and Marshall C.A.W., *Study of potentials suitable for band structure calculations of the noble metals. II silver and gold*, J. Phys. C 2, 1822 (1969).

27. Barbiellini B., Moroni E.G. and Jarlborg T., *Effects of gradient corrections on electronic structure in metals*, J. Phys. C 2, 7597 (1990).

28. Barth U von, and Hedin L., *A local exchange-correlation potential for spin polarized case : I*, J. Phys. C. 5, 1629 (1972).

29. Beal-Monod M.T., *Could Pd in confined geometries be a 'p-wave' superconductor or an itinerant ferromagnet ?*, Solid State Commun. 32, 357 (1979).

30. Bearden J.A. and Burr A.F., *Reevaluation of X-ray atomic energy levels*, Rev. Mod. Phys. 39, 125 (1967).

31. Berk N.F. and Schrieffer J.R., *Effect of ferromagnetic spin correlations on superconductivity*, Phys. Rev. Lett. **17**, 433 (1966).

32. Bhatnagar S., *Energy bands for silver by the Augmented-Plane-Wave method*, Phys. Rev. **183**, 657 (1969).

33. Boerstoel B.M., Zwart J.J. and Hansen J., *Specific heat of palladium, platinum, gold and copper below 30 K*, Physica **54**, 442 (1971).

34. Bordoloi A.K., *Electronic properties of palladium and platinum*, Ph.D Thesis (University of Roorkee, India, 1982) unpublished.

35. Bordoloi A.K. and Auluck S, *Electronic structure of palladium*, Phys. Rev. B **27**, 5116 (1983).

36. Bordoloi A.K. and Auluck S., *Electronic structure of platinum*, J. Phys. F **13**, 2101 (1983).

37. Bordoloi A.K. and Auluck S., *Mass enhancement factor for Pd and Pt*, Pramana J. Phys. **30**, 435 (1988).

38. See, for instance, Born M. and Huang K., *Dynamical Theory of Crystal Lattices* (Oxford University Press, London, 1954).

39. Bossachi B., Ketterson J.B. and Windmiller L.R., *Pressure dependence of the Fermi surface of noble metals*, Phys. Rev. B **2**, 3025, (1970).

40. Bosacchi B., Ketterson J.B. and Windmiller L.R., *Measurement and inversion of de Haas-van Alphen data in gold*, Phys. Rev. B **4**, 1197 (1971).

41. Brandt N.B., Itskevich E.S. and Minima N.Y., *Influence of pressure on the Fermi surface of metals*, Soviet Phys. Uspekhi **14**, 438 (1972).

42. Brown C.R., Kalejs J.P., Manchester F.D. and Perz J.M., *Magnetoacoustic evidence for the existence of the L-centred pocket of Fermi surface of palladium*, Phys. Rev. B **6**, 4458 (1972).

43. Burdick G.A., *Energy band structure of copper*, Phys. Rev. **129**, 138 (1963).

44. Butler W.H., *Electron-phonon coupling in the transition metals: Electronic aspects*, Phys. Rev. B **15**, 5267 (1977).

45. Callaway J. and Zhang H.M., *Band structure spin splitting and spin wave effective mass in nickel*, Phys. Rev. B **1**, 305 (1970).

46. Callaway J. and Wang C.S., *Self consistent calculation of energy bands in ferromagnetic Ni*, Phys. Rev. B **7**, 1096 (1973).

47. Caroline D. and Schriber J.E., *Pressure effect on the Fermi surfaces of Ag and Cu*, Phil. Mag. **8**, 71 (1963).

48. Cavalloni C. Joss W., Monnier R. and Jarlborg T., *Fermi surface of Pd and Pt under homogeneous strain*, Phys. Rev. B **31**, 1744 (1985).

49. Causula F. and Herman F., *Generalized muffin-tin orbitals for electronic structure studies of surfaces, interfaces and organic solids*, J. Chem. Phys. **78**, 858 (1983).

50. Chakin P. and Dumoulin L. (unpublished).

51. Chatterjee S. and Sen S.K., *Study of the Fermi surface of silver by orthogonalized plane wave method*, Proc. Roy. Soc. **87**, 779 (1966); ibid. *Theoretical energy band structure of silver by the composite wave variational method*, **91**, 749 (1967); ibid. *Energy band structure of noble metals*, J. Phys. C **1**, 759 (1968).

52. Chen A.B. and Segall B., *Parameterization of the electronic band structure using the Green's function method : Empirical application to Cu to Ag*, Phys. Rev. B **12**, 600 (1975).

53. Chen H., Brener N.E. and Callaway J., *Electronic structure, optical and magnetic properties of fcc palladium*, Phys. Rev. B **40**, 1443 (1989).

54. Chouteau G., Fourneaux R., Gobiecht K. and Tournier R., *Specific heat and susceptibility enhancement in dilute Pd : Ni alloys*, Phys. Rev. Lett. **20**, 193 (1968).

55. Christensen N.E., *High energy band structure of gold*, Phys. Rev. B **13**, 2698 (1976).

56. Christensen N.E., *An APW calculation for silver*, Phys Stat. Sol. **31**, 635 (1969).

57. Christensen N.E., *Primary photoemission spectra of gold and their relation to band structure*, Phys. Stat. Sol. (b) **52**, 241 (1972).

58. Christensen N.E., *The band structure of silver and optical interband transitions*, Phys. Stat. Sol. (b) **54**, 551 (1973).

59. Christensen N.E., *Electronic structure of palladium and its relation to uv spectroscopy*, Phys. Rev. B **14**, 3446 (1976).

60. Christensen N.E. and Seraphin B.O., *Relativistic band calculation and the optical properties of Gold*, Solid State Commun. **8**, 1221 (1970).

61. Christensen N.E. and Seraphin B.O., *Relativistic band calculation and the optical properties of gold*, Phys. Rev. B **4**, 3321 (1971).

62. Coleridge P.T. and Templeten I.M., *High precision de Haas-van Alphen measurement in the noble metals*, J. Phys. F 2, 643 (1972).

63. Condon E.U. and Shortley G.H., *The Theory of Atomic Spectra* (University Press, Cambridge 1951).

64. Connolly J.W.D., *Energy bands in ferromagnetic nickel*, Phys. Rev. **159**, 415 (1967).

65. See, for instance, Cracknell A.P. and Wong K.C., *The Fermi surface* (Claredon Press, Oxford, 1973), p.164.

66. Crangle J. and Scott W.R., *Dilute ferromagnetic alloys*, J. Appl. Phys. **36**, 921 (1965).

67. Dahlbach N., Nilsson P.O. and Pessa M., *Ultraviolet photoemission from Pd (111)*, Phys. Rev. B **19**, 5961 (1979).

68. Dannan H., Heer R. and Meyer A.J.P., *New determinations of the saturation magnetization of nickel and iron*, J. Appl. Phys. **39**, 669 (1968).

69. Davis H.L., *Some effects of hydrostatic pressure and uniaxial tension on the electronic structure of the noble metals*, in Proceedings of Colloque International du C.N.R.S. sur les Proprietes Physiques des Solides sous Pression, Grenoble, 1969 (Editions du Centre National de la Recherche Scientifique, Paris, 1970), p. 123.

70. Davis H.L., Faulkner J.S. and Joy H.W., *Calculation of the band structure for copper as a function of latice spacing*, Phys. Rev. **167**, 601 (1968).

71. See, for instance, Davydov A.S., *Quantum Mechanics* (Pergamon Press, Oxford, 1965).

72. Dimmock J.O.*The calculation of electronic energy bands by the Augmented Plane Wave method* in Solid State Physics (ed. Ehrenreich H., Seitz F. and Turnbull D., Academic Press, New York and London, 1971) **26**, p.104.

73. Doniach S. and Englesberg S., *Low-temperature properties of nearly ferromagnetice Fermi liquids*, Phys. Rev. Lett. **17**, 750 (1966).

74. Dye D.H., Campbell S.A., Crabtree G.W., Ketterson J.B., Sandesara S.A. and Vuillemin J.J.,*Fermi-surface and many-body enhancement in Pd*, Phys. Rev. B **23**, 462 (1981).

75. Dye D.H., Ketterson J.B. and Crabtree G.W., *The Fermi surface of platinum*, J. Low Temp. Phys. **30**, 813 (1978).

76. Ebert H., Strange P. and Gyorffy B.L., *The influence of relativistic effects on the magnetic moments and hyperfine fields of Fe, Co and Ni*, J. Phys. F **18**, L135 (1988).

77. Eckardt H. and Fritsche L., *The effect of electron correlations and finite temperatures on the electronic structure of ferromagnetic nickel*, J. Phys. F **17**, 925 (1987).

78. Faulkner J.S., Davis H.L. and Joy H.W., *Calculation of consistent energy surfaces for copper by the Korringa-Khon -Rostoker method*, Phys. Rev. **161**, 656 (1967); ibid. *Calculation of the band structure for copper as function of lattice spacing*, **167**, 601 (1968).

79. Fawcett E., Griessen R., Joss W., Lee M.J.G. and Perz J.M., *The effect of strain on the Fermi surface*, in Electrons at the Fermi surface, ed. Springford M. (Cambridge University Press, Cambridge, 1980) p. 278.

80. Fernando G.W., Cooper B.R., Ramana M.V.. Krakauer H. and Ma C.Q., *Practical method for highly accurate large scale surface calculations*. Phys. Rev. Lett. **56**, 2299 (1986).

81. Freeman A.J., Dimmock J.O. and Furdyna A.M., *Electronic band structure, Fermi surface and magnetic properties of palladium metal*, J. Appl. Phys. **37**, 1256 (1966).

82. See, e.g., Friedel J., in *The Physics of Metals*, ed. Ziman J.M. (Cambridge University Press, London, 1969), Vol. I, p. 340.

83. Friedel J., Lenglart P. and Leman G., *Etude du couplage spin-orbite dans les metaux de transition. Application au platine*, J. Phys. Chem. Solids **25**, 781 (1964).

84. Fritsche L., Noffke J. and Eckardt H., *A relativistic treatment of interacting spin-aligned electron systems : application to ferromagnetic iron, nickel and palladium metal*, J. Phys. F **17**, 943 (1987).

85. Fujiwara T., *LMTO method with the most localised orbitals for surface electronic structures*, J. Phys. F **16**, 869 (1986).

86. Gapotchenko A.G., Itskevich E.S. and Kulatov E.T. in *The Magnetic and Electron Structure of Transition Metals and Alloys*, ed. Veselago V.G. and Vinokurova L.I. (Nova, New York, 1988), p.150.

87. Gavenda J.D. Theis W.M. and Mulvaney B., *Interpolation functions fo Fermi surfaces in strained metals*, Phys. Rev. B **21**, 2096 (1980).

88. Gersdorf R., *Experimental evidence for the X_2^+ hole pocket in the Fermi surface of Ni from magnetic crystalline anisotropy*, Phys. Rev. Lett. **40**, 344 (1978).

89. Gold A.V., *Solid State Physics*, ed. Cochran J.F. and Haering R.R. (Gordon and Breach, New York, 1978), p. 39.

90. Gold A.V., *Fermi surface of the ferromagnetic transition metals*, J. Low Temp. Phys. **16**, 3 (1974).

91. Gray A.M., Gray D.M. and Brown E., *Band-structure perturbations in strained crystals*, Phys. Rev. B **11**, 1475 (1975).

92. Gray D.M. and Gray A.M., *Band-structure perturbations in strained crystal. II. Shifts at the Fermi surface of Cu*, Phys. Rev. B **14**, 669 (1976).

93. Gunnarsson O., Jepsen O. and Andersen O.K., *Self-consistent impurity calculations in the atomic-spheres approximation*, Phys Rev B **27**, 7144 (1983).

94. Gunnarsson O., Johnson M. and Lundqvist B.I., *Exchange and correlation in atoms, molecules and solids*, Phys. Lett. **59A**, 177 (1976).

95. Gunnarsson O., Johnson M. and Lundqvist B.I., *Exchange and correlation in inhomogeneous electron systems*, Solid State Commun. **24**, 765 (1977).

96. Gunnarsson O., Johnson M. and Lundqvist B.I., *Descriptions of exchange and correlation effects in inhomogeneous electron systems*, Phys. Rev. B **20**, 3136 (1979).

97. Gunnarsson O. and Jones R.O., *Density functional calculations for atom, molecules and clusters*, Phys. Scri. **21**, 394 (1980).

98. Halse M.R., *The Fermi surfaces of the noble metals*, Phil. Trans. Roy. Soc. (London) A **265**, 507 (1969).

99. Hanus J.G., MIT Solid State and Molecular Theory Group Quarterly Progress Report, 1962 (unpublished).

100. Harris J., in *The Electronic Structure of Complex Systems*, ed. Temmerman W. and Phariseau P. (Plenum, New York, 1984); and references therein.

101. Hedin L. and Lundqvist B.I., *Explicit local exchange-correlation potentials*, J. Phys. C **4**, 2064 (1971).

102. Hochest H., Hufner S. and Goldmann A., *XPS-valance bands of iron, cobalt, palladium and platinum*, Phys. Lett. A **57**, 265 (1976).

103. Hodges L., Stone D.R. and Gold A.V., *Field-induced changes in the band structure and Fermi surface of nickel*, Phys. Rev. Lett. **19**, 655 (1967).

104. Hodges L., Ehrenreich H. and Lang N.D., *Interpolation scheme for band structure of noble and transition metals : Ferromagnetism and neutron diffraction in Ni*, Phys. Rev. **152**, 505 (1966).

105. Hohenberg P. and Kohn W., *Inhomogeneous electron gas*, Phys. Rev. **136**, B864 (1964).

106. Hoare F.E. and Yates B., *The low temperature (2 to 4.2 K) specific heats of palladium-silver alloys*, Proc. Roy. Soc. **A240**, 42 (1957).

107. Hu C.D. and Langreth D.C., *A spin dependent version of the Langreth-Mehl exchange-correlation functional*, Phys. Scr. **32**, 391 (1985).

108. Hufner S. and Wertheim G.K., *Core-line asymmetries in the X-ray photoemission spectra of metals*, Phys.Rev. B **11**, 678 (1975).

109. Hufner S., Wertheim G.K. and Buchanan D.N.E., *X-ray photoemission spectra of palladium*, Chem. Phys. Lett. **24**, 527 (1974).

110. Jacobs R.L., *The electronic structure of noble metals. I. The energy bands*, J. Phys. C **1**, 1296 (1968).

111. Jan J.P. and Templeton I.M., *Precsion measurement of (111) de Haas-van Alphen effect frequencies in copper, silver and gold*, Phys. Rev. **161**, 556 (1967).

112. Janak J.F., Moruzzi V.L. and Willams A.R., *Ground state thermomechanical properties of some cubic elements in local density formalism*, Phys. Rev. B **12**, 1257 (1975).

113. Janak J.F., Eastman D.E. and Williams A.R., *Direct transition analysis of photoemission from Pd*, Natl. Bur. Std., Washington D.C., 181 (1971) (NBS-SP-323, N72-21723).

114. Janak J.F., Williams A.R. and Moruzzi V.L., *Local exchange -correlation potentials and Fermi surface of copper*, Phys. Rev. B **6**, 4367 (1972).

115. Janak J.F., Williams A.R. and Moruzzi V.L., *Self-consistent band theory of the Fermi surface, optical and photoemission properties of copper*, Phys. Rev. B **11**, 1522 (1975).

116. See, for instance, Jensen M.A. and Andres K., *Superconductivity, susceptibility and specific heat in the noble transition elements and alloys. II. Comparison with theory*, Phys. Rev. **165**, 545 (1968) and references contained therein.

117. Jepsen O., Glotzel D. and Mackintosh A.R., *Potentials, band structures, and Fermi surfaces in the noble metals*, Phys. Rev. B **23**, 2684 (1981).

118. John W., Lenham G. and Ziesche P., *The Korringa-Kohn-Rostoker augmented plane wave method for non-sperically symmetric muffin-tin potentials*, Phys Stat. Sol. (b) **53**, 287 (1972).

119. Joseph A.S. and Thorsen A.C., *de Haas-van Alphen effect and Fermi surface in Rhenium*, Phys. Rev. **133**, A1546 (1964); ibid. *Low field de Haas-van Alphen effect in Ag*, **138**, A1159 (1965).

120. Joseph A.S., Thorsen A.C. and Blum F.A., *Low field de Haas-van Alphen effect in gold*, Phys. Rev. **140**, A2046 (1965).

121. Joseph A.S., Thorsen A.C., Gertner E. and Valby L.E., *Low field de Haas-van Alphen effect in copper*, Phys. Rev. **148**, 569 (1966).

122. Joseph A.S. and Thorsen A.C., *de Hass-van Alphen effect and Fermi surface in nickel*, Phys. Rev. Lett. **11**, 554 (1963).

123. Joss W. and van der Mark W. in *Proceedings of the International Conference on the Physics of Transition Metals, Toronto*, 1977, ed. Lee M.J.G., Perz J.M. and Fawcett E. (IOP, London, 1978), p.74.

124. Ketterson J.B., Koelling D.D., Shaw D.D. and Windmiller L.R., *Parametrization of transition metal Fermi-surface data*, Phys. Rev. B **11**, 1447 (1975).

125. Ketterson J.B., Priestly M.G. and Vuillemin J.J., *de Haas-van Alphen effect from both s and d bands in platinium*, Phys. Lett. (Netherlands) **20**, 452 (1966).

126. Ketterson J.B. and Windmiller L.R., *The de Haas-van Alphen effect in noble and transition metals*, Comments Sol. St. Phys. (G.B.) **5**, 9 (1972).

127. Ketterson J.B. and Windmiller L.R., *Inversion of de Haas-van Alphen data on nearly ellipsoidal surfaces Application to As an Sb*, Phys. Rev. B **1**, 463 (1970).

128. Kittel C., *Introduction to Solid State Physics*, 4th edition (Wiley, New York, 1971).

129. Knapp G.S. and Jones R.W., *Determination of the electron-phonon enhancement factor from specific heat data*, Phys. Rev. B **6**, 1761 (1972).

130. Koenig C., Stefanou N. and Koch J.M., *Point defects in ordered metallic compounds. I. Electronic-structure calculation by the linear-muffin-tin -orbital method.* Phys. Rev. B 33, 5307 (1986).

131. Kohn W. and Hanke W., *Centre Europeene de Calculs Atomiques et Moleculaires Report oo workshop on Ab Initio One Electron Potentials*, University of Paris, Orsay (1976) (unpublished).

132. Kohn W., and Sham L.J., *Self consistent equations including exchange and correlation effects*, Phys. Rev. **140**, A1130 (1965).

133. Krutzen B.C.H. and Springelkamp F., *Spin-polarised relativistic electronic structure calculations*, J. Phys. C 1, 8369 (1989).

134. Kupratukula S. and Fletcher G.C., *Electron band structure of gold*, J. Phys. C 2, 1886 (1969).

135. Lambrecht W.R.L. and Andersen O.K., *Minimal basis sets in linear muffin-tin orbital method: Application to the diamond-structure Crystal C, Si and Ge*, Phys. Rev. B 34, 2439 (1986).

136. Langlinais J. and Callaway J., *Energy bands of ferromagnetic nickel*, Phys. Rev. B 5, 124 (1972).

137. Langreth D.C. and Mehl M.J., *Easily implementable nonlocal exchange-correlation energy functional*, Phys. Rev. Lett. **47**, 446 (1981).

138. Langreth D.C. and Mehl M.J., *Beyond the local-density approximation in the calculations of ground-state electronic properties*, Phys. Rev. B 28, 1809 (1983).

139. Langreth D.C. and Perdew J.P., *The exchange-correlation energy of a metallic surface*, Solid State Commun. 17, 1425 (1975).

140. Langreth D.C. and Perdew J.P., *Exchange-correlation energy of a metallic surface : Wave-vector analysis*, Phys. Rev. B 15, 2884 (1977).

141. Langreth D.C. and Perdew J.P., *The gradient approximation to the exchange-correlation energy functional : A generalization that works*, Solid State Commun. 31, 567 (1979).

142. Langreth D.C. and Perdew J.P., *Theory of nonuniform electronic systems. I. Analysis of the gradient approximation and a generalization that works*, Phys. Rev B 21, 5469 (1980).

143. Lonzarich G.G., *Fermi surface studies of ground-state and magnetic excitions in itinerant electron ferromagnets*, in Electron at the Fermi surface, edited by Springford M. (Cambridge University Press, Cambridge, 1980) p. 225.

144. Lee M.J.G., *Electron-Ion interaction and Fermi surface of the alkali metals*, Phys. Rev. **178**, 953 (1969); ibid *Phase -shfit analysis of the Fermi surface of copper*, **187**, 901 (1969).

145. Lee M.J.G., *Dynamical properties of quasiparticle excitation in metallic copper*, Phys. Rev. B **2**, 250 (1970).

146. Lukhivich A.A., *Influence of elastic deformation on the Fermi surface of noble metals*, Sov. Phys. JETP **4**, 857 (1969).

147. MacDonald A.H., Daams J.M., Vosko S.H. and Koelling D.D., *Influence of relativistic contributions to the effective potential on the electroni structure of Pd and Pt*, Phys. Rev. B **23**, 6377 (1981).

148. Mackliet C.A. and Schindler A.I., *Heat capacity of Ni-Pd alloys*, J. Phys. Chem. Solids **24**, 1639 (1963).

149. Mali S.J., Singru R.M., Singh V.A. and Kanhere D.G., *Calculation of electronic properties of some solids using the non-local density approximation*, J. Phys. F **18**, L201 (1988).

150. Mattheiss L.F., *Energy bands for the iron transition series*, Phys. Rev. **134**, A970 (1964).

151. Miller R.J. and Satterthwaite C.B., *Electronic model for the reverse isotope effect in superconducting Pd-H(D)*, Phys. Rev. Lett. **34**, 144 (1975).

152. Mitzutani U., Massalski T.B. and Bevk J., *Low temperature specific heats in dilute Pd-H alloys*, J. Phys. F **6**, 1 (1976).

153. Moruzzi V.L., Janak J.F. and Williams A.R., *Calculated electronic properites of metals* (Pergamon Press Inc., New York, 1978).

154. Mueller F.M., *New inversion scheme for obtaining Fermi-surface radii from de Haas-van Alphen areas*, Phys. Rev. **148**, 636 (1966).

155. Mueller F.M., *Combined interpolation scheme for transition and noble metal*, Phys. Rev. **153**, 659 (1967).

156. Mueller F.M. and Priestly M.G., *Inversion of cubic de Haas van Alphen data, with an application to palladium*, Phys. Rev. **148**, 638 (1966).

157. Mueller F.M., Freeman A.J., Dimmock J.O. and Furdyna A.M., *Electronic structure of palladium*, Phys. Rev. B 1, 4617 (1970).

158. Mueller F.M., Freeman A.J. and Koelling D.D., *Anisotropic g factors of nickel, palladium and platinum*, J. Appl. Phys. 41, 1229 (1970).

159. Nesbet R.K., *Linearized atomic-cell orbital method for energy band calculations*, Phys. Rev B 33, 8027 (1986).

160. Norman M. and Koelling D.D., *Effect of Langreth-Mehl gradient correction on transition-metal band structures : Copper and vanadium*, Phys. Rev. B 28, 4357 (1983).

161. Papaconstantopoulos D.A., Boyer L.L., Klein B.M., Williams A.R., Murruzzi V.L. and Janak J.F., *Calculation of the superconducting properties of 32 metals with $Z \leq 49$*, Phys. Rev.B 15, 4221 (1977).

162. Perdew J.P.,*Orbital functional for exchange and correlation : self-interaction correction to the local density approximation*, Chem. Phys. Lett. 64, 127 (1979).

163. Perdew J.P., *Density-functional approximation for the correlation energy of the inhomogeneous electron gas*, Phys. Rev. B 33, 8822 (1986).

164. Perdew J.P. and Wang Y., *Accurate and simple density functional for the electronic exchange energy : Generalized gradient approximation*, Phys. Rev. B 33, 8800 (1986).

165. Perdew J.P. and Zunger A., *Self-interaction correction to density-functional approximations for many-electron systems*, Phys. Rev B 23, 5048 (1981).

166. Peuckert V., *Green function theory of an electron gas with surface : HL exchange and correlation effects*, J. Phys. C 9, 4173 (1976).

167. Pinski F.J., Allen P.B. and Butler W.H., *Electron-phonon contribution to electrical resistivity and superconducting 'p-wave' transition temperature of Pd*, Phys. Rev. Lett. 41, 431 (1978).

168. Pipppard A.B., *An experimental determination of the Fermi surface in copper*, Phil. Trans. Roy. Soc. (London) A 250, 325 (1957).

169. Podloucky R., Lasser R., Wimmer E. and Weinberger P., *Electronic structure Pd: Compton scattering, soft X-ray emission and X-ray photoemission spectra*, Phys. Rev. B 19, 4999 (1979).

170. Pollak R.A., Kowalczyk S., Ley L. and Shirley D.A., *Evolution of core states from enrgy bands in the 4d5s5p region from Pd to Xe*, Phys. Rev. lett. 29, 274 (1972).

171. Poole R.T., Kemeny P.C., Liesegang J., Jenkin J.G. and Leckey R.C.G., *High resolution photoemission studies of the d bands of some metals*, J. Phys. F 3, L46 (1973).

172. Prasad R., Joshi S.K. and Auluck S., *Fermi surface and band structure of ferromagnetic nickel*, Phys. Rev. B 16, 1765 (1977).

173. See, for instance, Raimes S., *Wave Mechanics of Electrons in Metals* (North-Holland Publishing Co., Amsterdam, 1961).

174. Ramchandani M.G., *Energy band Structure of gold*, J. Phys. C. Metal. Phys. Suppl. 3, S1 (1970).

175. Ramchandani M.G., *Effect of pressure on the Fermi surface of gold*, J. Phys. F: Metal Phys. 2, 297 (1972).

176. Rasolt M., Malmstrom D. and Geldart D.J.W, *Wave-vector analysis of metallic surface energy*, Phys. Rev B 20, 3012 (1979).

177. Rasolt M. and Geldart D.J.W., *Role of gradient corrections in interpolation formulae for surface energies*, Phys. Lett. 73A, 401 (1979).

178. Rasolt M. and Geldart D.J.W., *Wave-vector decomposition of the exchange and correlation contributions to a metallic surface energy*, Phys. Rev B 21, 3158 (1980).

179. Rayne J.A., *Heat capacity of palladium below 4.2 K*, Phys. Rev. 107, 669 (1957).

180. Roaf D.J., *The Fermi surface of copper silver and gold. II. Calculation of the Fermi surfaces*, Phil. Trans. Roy. Soc. (London) A 255, 135 (1962).

181. Schirber J.E. and O'Sullivan W.J. in *Les Proprietes Physiques des Solides Sous Pression* (Centre National de la Recherche scientifique, Grenoble, Paris, 1970), p.113.

182. Schirber J.E., *Experimental studies of the Fermi surface under pressure* in Honda Memorial Series on Material Science No. 2 (Maruzen Co., Tokyo, 1974), p. 141.

183. Schmidt B. and Mrosan E., *Effective cyclotron masses and many body effects in Pd*, Solid State Commun. 40, 329 (1982).

184. Schrieffer J.R., *Effect of virtual spin waves on the properties of strongly paramagnetic metals*, J. Appl. Phys. 39, 642 (1968).

185. Segall B., *Fermi surface and energy bands of copper*, Phys. Rev. 125, 109 (1962).

186. Segall B., *General Electric Res. Rep. No.* 61-RL-(2785G) (1961).

187. Seitz F., *Modern Theory of Solids*, (McGraw Hill Book Co., Inc., New York and London, 1940).

188. Shaw J.C., Ketterson J.B. and Windmiller L.R., *Phase shift inversion of Fermi surface data for some transition metals*, Int. J. Quan. Chem. 6, 395 (1972).

189. Shaw J.C., Ketterson J.B. and Windmiller L.R., *Inversion of Fermi-surface data using partial-wave phase shifts and their derivatives : An application to the noble metals*, Phys. Rev. B 5, 3894 (1972).

190. Shoenberg D., in *Progress in Low Temperature Physics*, ed. Gorter C.J. (North-Holland Publishing Co., Amsterdam, 1957),Vol. 2, p. 226.

191. Shoenberg D., *The Fermi surfaces of copper, silver and gold. I. The de Haas-van Alphen effect*, Phil. Trans. Roy. Soc. (London) A 255, 85 (1962).

192. See, e.g., Shoenberg D., in *The Physics of Metals*, ed. Ziman J.M. (Cambridge University Press, London, 1969), Vol. I, p. 62.

193. Shoenberg D. and Watts B.R. *The effect of tension on the Fermi surfaces of the noble metals*, Phil. Mag. 15, 1275 (1967).

194. Singh G.S., Prasad R, Auluck S. and Joshi S.K. (unpublished).

195. Singwi K.S., Sjolander A., Tosi M.P. and Land R.H., *Electron correlations at metallic densities. IV*, Phys. Rev. B 1, 1044 (1970).

196. Skriver H.L., *The LMTO method*, (Springer Verlag, Berlin, 1984).

197. Skriver H., Venema W., Walker E. and Griessen R., *Effect of hydrostatic pressure on the electronic states in palladium*, J. Phys. F: Metal Phys. 8, 2313 (1978).

198. Slater J.C., *Treatment of exchange in Atomic, Molecular and Solid State Theory*, Int. J. Quantum Chem. 5S, 403 (1971).

199. Smith N.V., *High derivative photoemission spectra and the relativistic band structure of gold*, Phys. Rev. B 5, 1192 (1972).

200. Smith N.V. and Mattheiss L.F., *Photoemission spectra and band structures of d-band metals. I. Practical aspects of the fcc interpolation schemes*, Phys. Rev. B 9, 1341 (1974).

201. Smith N.V. and Chiang S. *Photoemission spectra and band structures of d-band metals. VI. Spin polarization of bulk photoemission from ferrmagnetic Ni*, Phys. Rev. B **19**, 5013 (1979).

202. Smith N.V., *Photoemission spectra and band structures of d-band metals. III. Model band calculations on Rh, Pd, Ag, Ir, Pt and Au*, Phys. Rev. B **9** 1365 (1974).

203. Smith N.V., Wertheim G.K., Hufner S. and Traum M.M., *Photoemission spectra and band structure of d-band metal. IV. X-ray photoemission spectra and density of states in Rh, Pd, Ag, Ir, Pt and Au*, Phys. Rev. B **10**, 3197 (1974).

204. Smith N.V., *Photoemisssion spectra and band structures of d-band metals. VII. Extensions of the combined interpolation scheme*, Phys. Rev. B **19**, 5019 (1979).

205. Smith T.F., Gardner W.E. and Montgomery H.J., *A study of spin-wave excitations in dilute Pd-Fe alloys*, J. Phys. C Suppl. **3**, 370 (1970).

206. Snow E.C., *Self-consistent energy bands of silver by an Augmented-Plane-Wave method*, Phys. Rev. **172**, 708 (1968).

207. Snow E.C. and Waber J.T., *Self-consistent energy bands of metallic copper by the Augmented-Plane-Wave method*, Phys. Rev. **157**, 570 (1967); Snow E.C., ibid. *Self-consistent energy bands of metallic copper by the Augmented-Plane-Wave method. II*, **171**, 785 (1968).

208. Springborg M. and Andersen O.K., *Method for calculating the electronic structure of large molecules; helical polymers*, J. Chem. Phys. **87**, 7125 (1987).

209. Springborg M. and Jones R.O., *Energy surfaces of polymeric sulfur: structure and electronic properties*, Phys. Rev. Lett. **57**, 1145 (1986).

210. Springford M. and Stockton J.R., *Improved method for the calibration of field measuring magnetoresistor*, J. Phys. E **3**, 55 (1970).

211. Stafleu M.D. and de Vroomen A.R., *The de Haas-van Alphen effect in platinum*, Phys. Lett. A **19**, 81 (1965).

212. Stark R.W. (Private Communication).

213. Stark R.W. (Private Communication); Some of the results of Stark's experiment are reported in Ref. 237.

214. Stark R.W. and Tsui D.C., *The de Haas-van Alphen effect in Ferromagnetic Nickel*, J. Appl. Phys. **39**, 1056 (1968).

215. Stritzker B., *Superconductivity in irradiated palladium*, Phys. Rev. Lett. **42**, 1769 (1979).

216. O'Sullivan W.J. and Schirber J.E., *Experimental determination of the effect of hydrostatic pressure on the Fermi surface of copper*, Phys. Rev. **170**, 667 (1968).

217. O'Sullivan W.J. and Schirber J.E., *Experimental determination of the effect of hydrostatic pressure on the Fermi surface of copper*, Phys. Rev. **170**, 667 (1968); ibid. *Addendam to experimental determination of the effect of hydrostatic pressure on the Fermi surface of copper: zero pressure de Haas-van Alphen frequencies*, **181**, 1367 (1969).

218. O'Sullivan W.J., Switendick A.C. and Schirber J.E., *Fermi surface parameters and band structure for the noble metals. I. normal volume results and Herman-Skillman potentials*, Phys. Rev. B **1**, 1443 (1970).

219. Svechkarev I.V. and Panfilov A.S., *Effects of pressure on the electronic structure of transition d-metals*, Phys. Stat. Solidi (b) **63**, 11 (1974).

220. Templeton I.M., *The effect of hydrostatic pressure on the Fermi surfaces of copper, silver and gold*, Proc. Roy. Soc. (London) **A292**, 413 (1966).

221. Templeton I.M., *The effect of hydrostatic pressure on the Fermi surfaces of copper, silver and gold. II. High precision studies*, Can. J. Phys. **52**, 1628 (1974).

222. Traum M.M. and Smith N.V., *Photoemission spectra and band structures of d-band metals. II. Experiments on Rh, Ir, Ni, Pd and Pt*, Phys. Rev. B **9**, 1353 (1974).

223. Tsui D.C., *de Haas-van Alphen effect and electronic band structure of nickel*, Phys. Rev. **164**, 669 (1967).

224. Tsui D.C. and Stark R.W., *de Haas-van Alphen effect in ferromagnetic nickel*, Phys. Rev. Lett. **17**, 871 (1966).

225. Van Attekum P.M.Th.M. and Trooster J.M., *An X-ray photoelectron spectroscopy of PdSb, PtBi and AuSn*, J. Phys. F **9**, 2287 (1979).

226. Veal B.W. and Rayne J.A., *Heat capacity of palladium and dilute palladium : iron alloys from 1.4 to 100 K*, Phys. Rev. **135A**, 442 (1964).

227. Venema W.J., Skriver H., Walker E. and Griessen R., *Volume dependence of the Fermi surface of Pd*, J. Phys. (Paris) Colloq. **39**, C6-1099 (1978).

228. Vinokurova L.I., Gaputchenko A.G. and Itskevich E.F., *Effect of pressure on the de Haas-van Alphen effect in nickel*, Pis,ma Zh. Eksp. Teor. Fiz. **26**, 443 (1977) [JETP Lett. **26**, 317 (1977)].

229. Vinokurova L.I., Gapotchenko A.G., Itskevich E.S., Kulatov E.T., *Effect of pressure on the electronic structure of ferromagnetic nickel and iron*, Sov. Phys. JETP **49**, 834 (1979).

230. Vinokurova L.I., Kulatov E., Gapotchenko A., Itskevich E. and Kulikov N., *Band structure of magnetic transition metals under pressure*, J. Magn. Magn. Materials **15-18**, 1205 (1980).

231. Vosko S.H., Wilk L. and Nusair M., *Accurate spin-dependent electron liquid correlation energies for local spin density calculations : a critical analysis*, Can. J. Phys. **58**, 1200 (1980).

232. Vuillemin J.J., and Priestly M.G., *de Haas-van Alphen effect and Fermi surface in palladium*, Phys. Rev. Lett. **14**, 307 (1965).

233. Vuillemin J.J., *de Haas-van Alphen effect and Fermi surface in palladium*, Phys. Rev. **144**, 396 (1966).

234. Vuillemin J.J. and Bryant H.J., *Effect of hydrostatic pressure on the electron Fermi surfaces in Pd and Pt*, Phys. Rev. Lett. 23, 914 (1969).

235. Wakoh S., *Band structure of metallic copper and nickel by self-consistent procedure*, J. Phys. Soc. (Japan) **20**, 1894 (1965).

236. Wakoh S. and Yamashita J., *Fermi surface of nickel*, J. Phys. Soc. Japan **19**, 1342 (1964).

237. Wang C.S. and Callaway J., *Band structure of nickel: spin orbit coupling, the Fermi surface and optical conductivity*, Phys. Rev. B 9, 4897 (1974).

238. Watson-Yang T.J., Freeman A.J. and Koelling D.D., *Magnetic field induced conduction electron polarization, magnetization density and neutron magnetic form factor of Pt metal*, J. Magnetism Magnetic Materials 5, 277 (1977).

239. Webb R.A., Ketterson J.B., Halperin W.P., Vuillemin J.J. and Sandeesara N.B., *Very low temperature search for supercoductivity in Pd, Pt, and Rh*, J. Low Temp. Phys. 32, 659 (1978).

240. Williams A.R., Janak J.F. and Moruzzi V.L., *Relating theory to experiment: The optical properties of copper*, J. de Physique (Suppl. 5-6), 131 (1972).

241. Williams A.R., Kubler J. and Gelatt C.D., *Cohesive properties of metallic compounds: Augmented-spherical-wave calculations*, Phys. Rev. B **19**, 6094 (1979).

242. Williams A.R. and von Barth U., in *Theory of the Inhomogeneous Electron Gas*, Physics of Solids and Liquids Series, edited by Lundqvist S. and March N.H. (Plenum, New York, 1983).

243. Windmiller L.R., Ketterson J.B. and Hornfeldt S., *de Haas-van Alphen effect in palladium*, Phys. Rev. B **3**, 4213 (1971).

244. Yamashita J., Fukuchi M. and Wakoh S., *Energy band structure of Nickel*, J. Phys. Soc. Japan **18**, 999 (1963).

245. See, e.g., Ziman J.M., *Principlees of the Theory of Solids* (Cambridge University Press, London, 1964), p. 250.

246. Zornberg E.I., *Band structure and Fermi surface of ferromagnetic nickel*, Phys. Rev. B **1**, 244 (1970).

247. Zornberg E.I. and Mueller F.M., *Fermi surface of copper*, Phys. Rev. **151**, 557 (1966).

248. Zunger A., Perdew J.P. and Oliver G.L., *A self-interaction corrected approach to many-electron systems : Beyond the local spin density approximation*, Solid State Commun. **34**, 933 (1980).